ASSOCIATION OF THE REST CO-REPRESSORS RCOR1 AND RCOR2 WITH THE TRANSCRIPTIONAL REPRESSOR INSM1 REGULATES THE BALANCE OF PROLIFERATION AND DIFFERENTIATION IN THE DEVELOPING BRAIN

By

Caitlin Monaghan

A DISSERTATION

Presented to the Neuroscience Graduate Program

and the Oregon Health & Science University

School of Medicine

in partial fulfillment of the requirements for the degree of

Doctor of Philosophy

November 2016

School of Medicine

Oregon Health & Science University

CERTIFICATE OF APPROVAL

This is to certify that the Ph.D. dissertation of

Caitlin Monaghan

has been approved

Gail Mandel, Ph.D.; Mentor/Advisor

John Adelman, Ph.D.; Chair

Philip Copenhaver, Ph.D.; Member

Richard Goodman, M.D., Ph.D.; Member

John Rubenstein, M.D., Ph.D.; Member

TABLE OF CONTENTS

LIST OF FIGURES

LIST OF TABLES

LIST OF ABBREVIATIONS

AIP, aryl hydrocarbon receptor interacting protein

AOD, amine oxidase domain

ASCL1, achaete-scute family basic helix-loop-helix transcription factor 1

BCL11B, B-cell CLL/lymphoma 11B

bp, base pairs

BrdU, 5-bromo-2'-deoxyuridine

CDS, coding sequence

CELSR3, cadherin EGF LAG seven-pass G-type receptor 3

ChIP, chromatin immunoprecipitation

ChIP-chip, chromatin immunoprecipitation followed by microarray chip

ChIP-seq, chromatin immunoprecipitation followed by next-generation sequencing

CHRNB2, neuronal acetylcholine receptor subunit beta-2

CGE, caudal ganglionic eminence

CXXC1, CXXC finger 1

DAPI, 4',6-diamidino-2-phenylindole (ultraviolet DNA dye)

DRAQ5, deep red anthraquinone 5 (far red DNA dye)

E(#), embryonic day (#)

ESC, embryonic stem cell

ELM2, EGL-27 and MTA1 homology 2

FAM65B, family with sequence similarity 65, member B

Fl, floxed

FOXP1, forkhead box P1

GAD2, glutamate decarboxylase 2

GFAP, glial fibrillary acidic protein

GFP, green fluorescent protein

HDAC, histone deacetylase

IGS, interganglionic sulcus

INSM1, insulinoma-associated 1

kb, kilobases

kDa, kilodaltons

KO, knockout

NES, nestin

KDM1A, lysine-specific demethylase 1A

LGE, lateral ganglionic eminence

MAP2, microtubule associated protein 2

MGE, medial ganglionic eminence

miRNA, microRNA

MKI67, marker of proliferation Ki-67

NKX2-1, NK2 homeobox 1

P(#), postnatal day (#)

PBS, phosphate buffered saline

PROX1, prospero homeobox protein 1

OLIG2, oligodendrocyte lineage transcription factor 2

RCOR, REST corepressor

REST, repressor 1 element silencing transcription factor

RN45S, 45S pre-ribosomal RNA

RNAi, RNA interference

RPS20, ribosomal protein S20

SANT, SWI3 (switching-defective protein 3)/ADA2 (adaptor 2)/NCOR (nuclear receptor co-repressor)/TFIIIB (transcription factor IIIB)

SCN2A, sodium voltage-gated channel alpha subunit 2

SHH, sonic hedgehog

shRNA, short hairpin RNA

SSC, saline sodium citrate

SCRT1, transcriptional repressor scratch 1

SMARCE1, SWI/SNF related, matrix associated, actin dependent regulator of chromatin, subfamily E, member 1

SNAG, SNAI1 (snail1)/GFI1 (growth factor independence 1)

STMN2, stathmin 2

SWIRM domain, SWI3p, Rsc8p, Moira domain

TGIF1, transforming growth factor beta induced factor homeobox 1

TSS, transcription start site

TUBB3, tubulin beta 3 class III

UNC13A, unc-13 homolog A

UTR, untranslated region

ACKNOWLEDGEMENTS

I thank my thesis advisor, Dr. Gail Mandel, for her guidance, attention, support, and patience. I am very fortunate to have been in her lab. I thank her for the example she set, and for the enormous amount of work she put into teaching me how to be a scientist.

I also would like to thank Dr. Paul Brehm, for pushing me to make science my top priority and for encouraging me.

I thank my coauthors Dr. Tamilla Nechiporuk, Dr. Jianxun Wang, Dr. Michael Rosenfeld, Dr. Shannon McWeeney, and Sophia Jeng. Without their help, this work would not have been possible. In particular, I thank Tamilla for helping me design experiments and interpret results.

I am grateful to the past and present members of the Mandel laboratory. I thank Dr. Huilan Yao for her work laying the foundations for my project. I am grateful to Dr. Daniel Lioy, Glen Corson, and Dr. Michael Linhoff, each of whom went out of his way to mentor me. Thanks also to Susan Kim for her hours of meticulous cell counting. Thanks to Dr. Francesca Cargnin, Dr. Edmund Nesti, Dr. James McGann, Dr. Saurabh Garg, Dr. Jon Oyer, Dr. John Sinnamon, and Christine Schmidt for being insightful, helpful, and supportive.

I would like to thank Dr. Gary Banker, Dr. Gary Westbrook, and Dr. Paul Brehm for hosting me in their labs for rotations.

I am grateful to Dr. John Adelman, Dr. Philip Copenhaver, and Dr. Richard Goodman for their many insights through the years they have served on my

dissertation advisory committee. Thanks also to Dr. John Rubenstein for serving as an ad hoc committee member.

I am grateful to the Neuroscience Graduate Program, particularly to Dr. Gary Westbrook and Liz Lawson-Weber.

I thank my classmates, Gabe Knoll, Dr. Maria Purice, Dr. Courtney Williams, Dr. Madalynn Erb, Dr. Anne Logan, Dr. Jeannie Hunnicutt, Dr. Guhkan Kim, and Dr. Hsin-Wei Lu, for their friendship. I am especially thankful to Maria, for being a very dear friend, and to Gabe, for being my dearest friend of all.

Finally, I thank all of my family, and especially my darling sister, Sarah Monaghan, and my endlessly loving and wonderful parents, Carrie Dean and Dr. Daniel Monaghan.

ABSTRACT

The transcriptional events that lead to the cessation of neural proliferation, and therefore enable the production of proper numbers of differentiated neurons and glia, are still largely uncharacterized. Here, we report that the transcription factor INSM1 forms complexes with co-repressors RCOR1 and RCOR2 in progenitors in embryonic mouse brain. Mice lacking both RCOR1 and RCOR2 in developing brain die perinatally and generate an abnormally high number of neural progenitors at the expense of differentiated neurons and oligodendrocyte precursor cells. In addition, *Rcor1/2* deletion detrimentally affects complex morphological processes such as closure of the interganglionic sulcus. We find that Insulinoma-associated 1 (INSM1), a transcription factor that induces cell cycle arrest, is co-expressed with RCOR1/2 in a subset of neural progenitors, and forms complexes with RCOR1/2 in embryonic brain. Further, the *Insm1*$^{-/-}$ mouse phenocopies predominant brain phenotypes of the *Rcor1/2* knockout. A large number of genes are concordantly mis-regulated in both knockout genotypes, and a majority of the down-regulated genes are targets of RE1 Silencing Transcription factor (REST). *Rest* transcripts are up-regulated in both knockouts, and reducing transcripts to wild-type levels in the *Rcor1/2* knockout partially rescues the defect in interganglionic sulcus closure. Our findings indicate that an INSM1/RCOR1/2 complex controls the balance of proliferation and differentiation during brain development.

CHAPTER 1: INTRODUCTION

1.1 Brain development

1.1.1 Investigating the role of chromatin-modifying complexes in brain development

The development of the nervous system is an intricately orchestrated series of events beginning with formation of neuroepithelia. Progenitors that emerge from neuroepithelial stem cells undergo several proliferative transitions before ceasing to divide and terminally differentiating into neurons and glia. There is a large gap in our knowledge of the general mechanisms that determine when a neural progenitor exits the cell cycle and then differentiates. An understanding of this process is crucial for understanding the formation of the nervous system, but it also has ramifications for understanding other contexts in which proliferation/differentiation balance is upset, for example, in cancer.

Recent studies indicate that chromatin-modifying complexes are key players in the transition from neural progenitor to neuron or glial cell. However, in most of these cases the complexes were identified biochemically, and the roles of the complexes, and of individual members of the complexes, *in vivo* are poorly understood. Further, the transcription factors that recruit particular chromatin-modifying complexes often remain unknown. In this dissertation, I will describe my work studying how two members of chromatin-modifying complexes, *RE*1 *s*ilencing *t*ranscription factor (REST) *co-r*epressors 1 and 2 (RCOR1 and RCOR2, or RCOR1/2) contribute to the development of the brain. My work reveals a surprising new function for RCOR1/2: they promote the production of neurons and glia in developing brain. In addition, and importantly, I identify *ins*ulino*m*a-

associated 1 (INSM1) as the repressor that mediates these functions by recruiting RCOR1/2 to specific genes.

1.1.2 The subpallium

I have focused on the part of the brain known as the ventral telencephalon, also referred to as the subpallium. The subpallium is primarily responsible for the production of GABAergic (inhibitory) neurons (reviewed in Achim et al., 2014). It produces the projection neurons of the striatum and globus pallidus (Corbin and Butt, 2011). The striatum is important for motivation (reviewed in Yager et al., 2015), motor activity (Vink et al., 2005), and executive function (reviewed in Monchi et al., 2006), while the globus pallidus regulates voluntary movement (reviewed in Hegeman, 2016). In addition, the subpallium produces most or all of the interneurons in the brain (reviewed in Corbin and Butt, 2011). Understanding the origins of striatal neurons and interneurons could lead to therapies to treat Huntington's disease, a devastating neurological disorder resulting from degeneration of striatal neurons (reviewed in Walker, 2007), and epilepsy, one of several disorders associated with dysfunction of cortical interneurons (Hunt and Baraban, 2015), based on the generation of neurons from induced pluripotent stem cells or fibroblasts and transplantation of these neurons into patients. The subpallium also produces oligodendrocyte precursor cells (OPCs). Insight into OPC production could contribute to the development of treatments for diseases associated with loss of white matter, such as adrenoleukodystrophy (Kemp et al., 2010) and multiple sclerosis (Tognatta and Miller, 2016).

The developing subpallium contains several progenitor regions. In this work, I focus almost exclusively on the lateral, medial, and caudal ganglionic eminences (LGE, MGE, and CGE, respectively), which together with the preoptic area make up the lateral subpallium (Flames et al., 2007). That is, these structures are the part of the telencephalon lateral to the lateral and third ventricles. The LGE is the anterior, dorsal, and lateral protuberance in the ventral subpallium. By E11, it can be distinguished from a separate protuberance, the MGE, lying ventral and medial to it (Fig. 1.1; Bhide, 1996). At caudal levels, the two protuberances merge to form the CGE.

1.1.3 Balance between neural proliferation and differentiation

The production of mature neurons and glia requires neural progenitors to progress through a series of stages. Prior to the onset of neurogenesis, the central nervous system consists of a hollow tube of progenitor cells called neuroepithelial cells. Neuroepithelial cells undergo symmetrical cell division to self-renew (Fig. 1.2). At the onset of neurogenesis, neuroepithelial cells transform into radial glia (Farkas and Huttner, 2008). Radial glia also self-renew, but they do so asymmetrically, so that each cell division also produces a different cell type. The identity of the second cell type changes through development. When neurogenesis begins, at ~E9.5 in the mouse, radial glia most frequently produce neurons (Martynoga et al., 2012). The neurons migrate to the basal (exterior) side of the neural tube. At this point, the neural tube is composed of two compartments: the ventricular zone, or VZ, which consists of radial glia, and the mantle, which consists of neurons. At ~E11.5, some radial glia switch to

producing intermediate progenitor cells instead of neurons (Kriegstein and Alvarez-Buylla, 2009). These cells are still progenitors, but have much more limited proliferative potential. Intermediate progenitors undergo symmetric cell division to produce two neurons, two OPCs, two astrocytes, or, less commonly, two more intermediate progenitors (Farkas and Huttner, 2008; Sessa et al., 2008). The intermediate progenitors take up residence in between the VZ and the mantle, forming a layer called the subventricular zone (SVZ; Kriegstein and Alvarez-Buylla, 2009).

Much progress has been made toward understanding how progenitors produce differentiated cells of a given type, cell specification. These decisions are initiated by the expression of morphogens such as sonic hedgehog (SHH), bone morphogenetic proteins (BMPs), Wnts (related to *w*ingless and *int*egration-1), and fibroblast growth factors (FGFs; reviewed in Sanes et al., 2006). The signaling molecules are expressed in spatial gradients in the developing brain. The concentration of a morphogen to which a cell is exposed is permissive for the expression of certain so-called patterning transcription factors, and repressive of others (reviewed in Dessaud et al., 2008). The complement of patterning transcription factors expressed in a progenitor refines its identity cell-autonomously (reviewed in Sanes et al., 2006).

In this dissertation, however, I am addressing a somewhat broader question: how do neural progenitors decide when to proliferate and when to differentiate? There are several levels at which this regulation occurs. I will briefly

describe two examples that illustrate how cell-cell signaling and noncanonical cyclin activity each regulate the balance between proliferation and differentiation.

Cells can influence whether their neighbors decide to proliferate or differentiate through a process called lateral inhibition (reviewed in Shimojo et al., 2011). Proneural transcription factors like ASCL1 (achaete-scute family bHLH transcription factor 1) initiate this process by up-regulating Notch ligands such as DLL1 (delta-like ligand 1) and JAG1 (jagged 1), which activate the Notch receptors expressed by neighboring cells (Castro et al., 2006). This triggers the release of the Notch intracellular domain (NICD) from the plasma membrane. The NICD enters the nucleus, where it activates the transcription factor RBPJ, which in turn induces the transcription of genes such as *Hey1*. HEY1 and several other Notch targets are transcription factors that repress the transcription of proneural genes and Notch ligands (Sakamoto et al., 2003). In this way, both progenitors preparing to undergo neuronal differentiation and neurons can, by expressing Notch ligands, prevent their neighbors from differentiating prematurely.

The balance between proliferation and differentiation is also regulated by differential expression of cyclins. The D cyclins are best known for stimulating cell cycle progression by interacting with the cyclin-dependent kinases CKD4 and CDK6 (Alberts et al., 2008). When bound by D cyclins, CDK4 and CKD6 phosphorylate retinoblastoma-1 (RB1), which causes it to detach from the activating transcription factors of the E2F family, allowing them to up-regulate genes associated with cell cycle progression (Coqueret et al., 2002). However, in

addition to regulating cell cycle progression, cyclins may also influence whether a given cell division is produces neurons or progenitors. For instance, loss of cyclin D1 in the developing chick spinal cord (CCND1) shifts the proliferation/differentiation balance toward proliferative cell division, while overexpression of CCND1 promotes neuronogenic cell division (Lukaszewicz et al., 2011). CCND1 promotes neuronogenesis by up-regulating the transcription factor HES6. Further, a point mutant of CCND1 that is unable to interact with cyclin-dependent kinases also promotes neuronogenesis. In contrast, cyclin D2 did not promote neurogenesis, and did not alter *Hes6* expression (Lukaszewicz et al., 2011).

Superficially, Notch-mediated maintenance of progenitor proliferation and CCND1-mediated neuronogenesis seem like two of innumerable ways to shift the proliferation/differentiation balance. However, these mechanisms have in common with each other–and with all other mechanisms affecting the balance between proliferation and differentiation–that they both ultimately function by changing gene expression.

1.2 Chromatin regulation of gene expression

In eukaryotes, genomic DNA can be transcribed (gene expression) or silent. The genetic elements responsible for regulating transcription are promoters and enhancers. Promoters are small sequences located very close to the transcriptional start sites (TSS), within a few hundred base pairs, while enhancers, also small sequences, can be located tens of thousands of base pairs from the TSS. Promoters confer basal transcriptional levels while

enhancers are responsible for up- or down-regulation of transcription. Promoters and enhancers function through the activities of transcription factors that bind DNA directly. However, the scenario is complicated by the fact that genomic DNA in eukaryotes is not naked in the nucleus. It is packaged into chromatin by protein and RNA. (Cutter et al., 2015). The packaging compacts the genomic DNA and organizes it into fundamental structural units called nucleosomes. Nucleosomes are responsible for the beads on a string image from electron microscopy studies performed some four decades ago (Olins and Olins, 1973). The succeeding years have provided much more knowledge about the molecular structure and function of nucleosomes. For example, we now know nucleosomes are composed of four core histone proteins–H2A, H2B, H3, and H4–which assemble into an octameric complex containing two peptides corresponding to each type of histone (Luger et al., 1997). The octamer serves as a spool, around which a length of DNA consisting of 145-147 base pairs is wrapped ~1.65 times (Luger et al., 1997) Within the octamer, the amino-terminus of each histone maintains a flexible conformation in which it is accessible to enzymes that modify the termini by post-translational modifications including phosphorylation, methylation, ubiquitylation, and sumoylation (Cutter et al., 2015). The myriad covalent modifications have been termed a histone code (Jenuwein and Allis, 2001) to describe their effects on gene expression.

Covalent modifications are proposed to directly alter the nature of the interaction between the DNA and the nucleosome. For example, acetylation of a lysine residue on the histone tail is proposed to neutralize the positive charge of

the lysine, and thus weaken the interaction between the histone tail and the inter-nucleosomal DNA (Kouzarides, 2007). This is associated with gene activation. In contrast, deacetylation of histones by histone deacetylases is proposed to condense chromatin and is thus associated with gene repression (reviewed in Allis and Jenuwein, 2016). Additionally, covalent modifications create binding sites for proteins with functional domains that recognize particular histone modifications. For example, many proteins have conserved domains that specifically recognize particular histone modifications such as acetylated lysines (Josling et al., 2012).

Histone-modifying enzymes do not work alone. They are in large mega-dalton complexes with other proteins that serve complementary functions. The complexes also include chromatin-remodeling proteins that shift nucleosomes relative to the DNA and DNA methyltransferases that covalently modify cytosine residues. Therefore, chromatin-modifying complexes can regulate gene expression in many different ways, depending on the intrinsic enzymatic activities within the complexes. For example, some complexes partially disassemble or entirely remove the histone octamer, while others remove histones to allow their replacement by other histone variants. Each of these changes alters transcription by altering the accessibility of the DNA to proteins and RNAs. Partial disassembly of nucleosomes is necessary for the transcriptional machinery to bind the DNA (Li et al., 2012). Replacement of one histone variant with another can also alter the probability of transcription. For instance, because the H2A variant HIST1H2BD (H2A.B) has a truncated carboxy terminus relative to the

canonical variant, its incorporation renders nucleosomes less stable, which leads to reduced chromatin compaction, and therefore promotes transcription (Weber et al., 2014). Repositioning a nucleosome alters the accessibility of DNA to proteins and RNAs. In addition to covalent modification of histones, DNA itself can be modified, which also changes its affinity for chromatin regulatory proteins. For instance, proteins such as methyl CpG-binding protein 2 (MeCP2) and methyl binding domain 2 (MBD2), which contain methyl-binding domains, specifically bind and repress methylated DNA (Nan et al., 1997).

To summarize, the components of chromatin-modifying complexes can be divided into three categories: transcription factors, enzymes, and adaptors. Transcription factors bind to DNA in a sequence-specific manner, while also binding to enzymes and adaptors, and thereby anchor the complex to specific genomic loci. Enzymes directly interact with DNA or histones to catalyze modifications. The third category of protein, the adaptors, is defined negatively: these are components of chromatin-modifying complexes that neither interact with DNA in a sequence-specific manner nor have intrinsic enzymatic activity. Adaptors serve as bridges between proteins, coupling enzymes and transcription factors (Ballas et al., 2001). Adaptors can also competitively or allosterically inhibit inclusion of a different protein into the complex (Upadhyay et al., 2014). Some interact with DNA in a non-sequence-specific manner to stabilize the interaction of the complex with the chromatin (Yang et al., 2006). Theoretically, adaptors could also stabilize their binding partners in a given conformation.

1.3 REST co-repressors 1 and 2 (RCOR1/2)

1.3.1 Introduction to the REST co-repressors 1/2

In my thesis work, I have focused on a pair of adaptor proteins likely to have roles in regulating the balance between proliferation and differentiation: the *R*estriction *E*lement 1 *s*ilencing *t*ranscription factor (REST) *co*repressors 1 and 2 (RCOR1 and RCOR2). RCOR1 was identified originally as a direct binding partner for the master transcriptional regulator of neural genes, REST (Ballas et al., 2005; Otto et al., 2007; Su et al., 2004). Like many other adaptor proteins in transcriptional complexes, RCOR1 does not have intrinsic enzymatic activity but, rather, binds directly to chromatin-modifying enzymes including histone deacetylases 1 and 2 (HDAC1/2) and the histone demethylase KDM1A (LSD1) (Hakimi et al., 2002; Shi et al., 2004; You et al., 2001). A related protein, RCOR2, shares ~90% homology with RCOR1 in the ELM2 and SANT functional domains (UniProt; UniProt) and is also found in complexes with KDM1A and HDAC1/2 (Barrios et al., 2014). Furthermore, RCOR2 is recruited by some of the same RCOR1-associated transcription factors, including REST, GFI1B, and ZMYND8 (Tables 1.1 and 1.2; Saleque et al., 2007; Zeng et al., 2010). A large number of studies, which investigated either the RCOR proteins themselves or the enzymes and transcription factors with which they are associated, strongly suggest that RCOR1 and RCOR2 play important roles in regulating the balance between neural proliferation and differentiation. However, because most of this work was done *in vitro*, the importance of RCOR1/2 in brain development had not been established definitively.

Before I describe the work I did to address that gap in knowledge, I will first summarize background information concerning the RCOR genes, the structures of the proteins they encode, and the expression of RCOR proteins. Then I will discuss the work that has been done to clarify the role of the RCORs and their binding partners during neural differentiation.

1.3.2 RCOR genes, transcripts, and proteins

Mammals have three *Rcor* genes, *Rcor1-3*, located on chromosomes 12, 19, and 1, respectively. Throughout the text, I will use the sequences shown in Fig. 1.3 as the reference sequences for the three RCOR proteins. My numeration therefore differs slightly from those in the literature, as most papers refer to human sequences. Given the high degree of homology between human and mouse sequences (92% identity and 98% similarity between the reference murine RCOR1 sequence and the human sequence Q9UKL0 [UniProt]; 98% identity and 99% similarity between the reference murine RCOR2 sequence and the human sequence Q8IZ40), I expect most observations made in one mammalian species to hold true in others.

The 477-amino acid murine RCOR1 reference sequence consists of Q8CFE3 (from UniProt) with two Xs substituted with As on the basis of the genomic sequence (*i.e.* chr12:111039738-111039741 and 111039777-111039779 in mm10). This protein sequence differs from that of uc007pck.1, the only UCSC Rcor1 transcript, in having a longer amino terminus. My reasons for preferring the longer amino terminus are as follows. First, my RNA-seq experiments verify the presence of cDNA corresponding to sequence upstream

of and containing the 5' end of the extended amino terminus. Second, dating from its characterization in 1999 (Andrés et al., 1999), human RCOR1 has been thought to contain amino acids homologous to this extended amino terminus (the mouse extended RCOR1 amino terminus is 78% identical [79 of 101 amino acids] and 94% similar [95 of 101 amino acids] to this region). It is worth noting that since then, annotations have further extended the amino terminus of the human protein to include an additional three amino acids (MPA) at the extreme amino terminus in some databases (ENST00000262241.6/uc001ymb.5, in the UCSC Genome Browser) but not others (Q9UKL0, in UniProt). The corresponding sequence in the mouse, if translated, would also encode "MPA." Third, an antibody made against the first sixteen amino acids in the original human RCOR1 sequence (Q9UKL0, in UniProt) recognizes both overexpressed human RCOR1 and an endogenous mouse protein of a similar size (Yao, 2014).

The RCOR2 sequence is Q8C796. This is uncontroversial–both of the UCSC transcripts, uc008gkn.2 and uc008gko.2, are thought to encode the same 523-amino acid protein.

The UCSC Genome Browser lists five Rcor3 transcripts, each encoding a distinct protein. Variant 4 is depicted in Fig. 1.3 because it has the highest amount of homology to RCOR1 and RCOR2.

1.3.3 RCOR protein structures

All three RCORs consist of an ELM2 domain and two SANT domains (Fig. 1.3). (Note, however, that variant 4 of RCOR3 is the only RCOR3 isoform to have the classic ELM2-SANT1-linker-SANT2 structure of the other RCORs; the other

variants lack the SANT2 domain.) The ELM2 (EGL-27 and MTA1 homology 2) domain and SANT1 domain of RCOR1 are together responsible for binding to REST (Ballas et al., 2001; Fig 1.4). Given that RCOR2 also interacts with REST (Zeng et al., 2010; McGann et al., 2014), it is likely that it, too, does so using the ELM2 and SANT1 domains. Whether RCOR3 interacts with REST is not known. The ELM2 and SANT1 domains also mediate interactions with the histone deacetylases HDAC1 and HDAC2 (Barrios et al., 2014). Further, the ELM2 and SANT domains of RCOR1 and RCOR3 interact with HDAC1/2 much more efficiently than do those of RCOR2 (Barrios et al., 2014). As a result, RCOR2 complexes have greatly diminished deacetylase activity relative to RCOR1 and RCOR3 complexes (Barrios et al., 2014). The linker between the two SANT domains mediates interactions between each of the three RCOR proteins and the lysine specific demethylase KDM1A (Yang et al., 2006; Tortorici et al., 2013; Barrios et al., 2014). The SANT2 domain of RCOR1 interacts with DNA (Yang et al., 2006). However, whether this interaction is at all dependent upon DNA sequence remains unknown. The inter-SANT linker and SANT2 domains are also responsible for interactions with SMARCE1/BAF1 (SWI/SNF related, matrix associated, actin dependent regulator of chromatin, subfamily E, member 1; Battaglioli et al., 2002). SMARCE1 is a component of the BAF (mammalian SWI/SNF) complex, which is one of the four kinds of mammalian ATPase-dependent chromatin remodeling complexes (Hargreaves and Crabtree, 2011).

1.3.4 Expression of RCORs in the brain

RCOR1. Characterizations of *Rcor1* expression in the nervous system show that it is expressed in every major neural cell type. RCOR1 was detected in neurons and astrocytes by immunohistochemistry (Yao, 2014; Sáez et al., 2015). By Western blotting, RCOR1 was detected in the cortex, hippocampus, midbrain, and parabrachial nucleus of adult rat brain (Sáez et al., 2015). Transcriptional profiling detected *Rcor1* in all cell types examined (Cahoy et al., 2008; Zhang et al., 2014b), including neurons, astrocytes, OPCs, oligodendrocytes, microglia, and endothelial cells. However, immunohistochemistry suggests that while RCOR1 is expressed in all major cell types, a minority of cells in the striatum, hippocampus, and cortex in the adult rat express little or no RCOR1 (Sáez et al., 2015).

Despite its broad expression pattern, RCOR1 protein levels do appear to be dynamically regulated. RCOR1 protein levels are downregulated in PC12 cells (adrenal gland pheochromocytoma cells) that have undergone a differentiation protocol (Sáez et al., 2015). Similarly, cultured rat cortical cells expressed lower levels of RCOR1 after undergoing differentiation. In contrast, differentiation did not change the levels of *Rcor1* transcript (Sáez et al., 2015). Western blot analysis of RCOR1 protein in the neocortex showed that RCOR1 was present at each of five timepoints ranging from E14.5 to adult, but was higher at P0 and P15 than at embryonic or adult stages (Fuentes et al., 2012). These studies suggest that *Rcor1* transcript is expressed in most, if not all, neural cells, but that post-transcriptional regulation likely limits protein levels in some cells.

RCOR2. Several studies have examined *Rcor2* transcript or protein levels during neural development. By Northern blot, transcript levels in the brain diminished progressively between E12 and P0. Protein levels of RCOR2 protein in the brain also diminished between E11.5 and E17.5 (Wang et al., 2016). Consistent with these findings, levels of *Rcor2* transcripts in both PC12 cells and rat cortical cultures were reduced after cells underwent *in vitro* differentiation (Sáez et al., 2015). However, Sáez et al. did not see reduced transcript levels at E18.5 relative to E14.5 in rats. Tontsch et al. (2001) and Sáez et al. (2015) show that *Rcor2* transcript levels in mice and rats, respectively, were reduced in adult brain relative to embryonic brain. Tontsch et al. (2001) show that in E12.5 telencephalon, the cells with the highest *Rcor2* transcript levels are at the border between the ventricular zone and mantle. In contrast, the *in situ* hybridizations of Wang et al. (2016) give the impression of ubiquitous Rcor2 expression, with elevated levels in the cortex. Their immunohistochemistry of E13.5 cortex shows that the cortical plate also has higher levels of RCOR2 protein than the VZ/SVZ. With regards to the cell-type specificity of RCOR2 expression, RCOR2 protein was detected in both neurons and astrocytes (Sáez et al., 2015). Like RCOR1, it was detected in the nuclei of most, but not all, cells in the striatum, hippocampus, and cortex of adult rat. *Rcor2* transcripts were expressed in neurons, astrocytes, OPCs, and oligodendrocytes, but there was very little expression in microglia or endothelial cells (Zhang et al., 2014b). These findings demonstrate that RCOR2 has a more limited expression pattern than RCOR1. However, it suggests that

RCOR1 and RCOR2 are similar in being down-regulated when neural progenitors differentiate.

RCOR3. Relatively little is known about the expression of RCOR3. RCOR3 protein could not be detected in E13.5 brain (Yao, 2014). However, *Rcor3* transcripts were expressed in PC12 cells and cortical rat cells. In contrast to *Rcor1* and *Rcor2* transcript, levels of *Rcor3* did not diminish in either of these cell types as they differentiated. Transcript levels in rat brains did not change noticeably between E14.5, E18.5, and adulthood. RCOR3 protein was detected in the several parts of the adult rat brain by Western blotting (Sáez et al., 2015). One transcriptional profiling study detected transcripts in all brain cells assayed (Cahoy et al., 2008), and another found it to be more highly expressed in astrocytes, neurons, and OPCs than in endothelial cells, myelinating oligodendrocytes, or microglia (Zhang et al., 2014b). While these results demonstrate that *Rcor3* transcript is present in the developing nervous system, they suggest that there is little to no RCOR3 protein in the developing brain. In contrast, both transcript and protein are present in the adult brain.

1.4 Role of RCORs and RCOR-associated proteins in brain development

1.4.1 Overview

In order to summarize what is known about the roles of RCOR proteins in the brain, I will first describe work concerning REST, the first transcription factor shown to recruit RCOR1. The role of REST in neural development has been studied extensively, and has heavily influenced perceptions of the role of the REST co-repressors. I will then describe studies directly investigating RCOR1/2.

RCOR3 is not discussed because the function of RCOR3 in the brain has not been investigated. Then I will describe work concerning two RCOR-interacting proteins, KDM1A and INSM1, which, as I will show, I believe to be essential for RCOR1/2 function in the brain.

1.4.2 REST

REST was originally characterized as a master silencer/repressor of neuronal genes in non-neuronal cells. It was first identified by the Mandel and Anderson laboratories, which sought mechanisms to explain how neuronal gene expression was limited to neurons (Chong et al., 1995; Schoenherr and Anderson, 1995). While the original studies indicated only that REST regulated the voltage-dependent sodium channel subunit *Scn2a* and stathmin 2 (*Stmn2*, also known as *Scg10*) genes, later studies indicated that REST binds to a consensus sequence located in over 1000 loci, the majority of which are associated with neuronal genes (Otto et al., 2007; Johnson et al., 2008; McGann et al., 2014). To these sites, REST recruits co-repressors using one or both of two independent repressor domains (Tapia-Ramírez et al., 1997). The N-terminal repressor domain recruits the co-repressors SIN3A or SIN3B (Huang et al., 1999; Naruse et al., 1999), while the C-terminal domain recruits RCOR1 (Andrés et al., 1999) and RCOR2 (Zeng et al., 2010). REST can also directly recruit the co-repressor CDYL (Mulligan et al., 2008), although which domain it uses to do this is not known. Which co-repressors REST recruits varies depending upon the gene target (Greenway et al., 2007), and presumably also depending upon the

cell type (Ballas et al., 2005; Mulligan et al., 2008). The co-repressors recruit chromatin-modifying complexes including HDAC1/2 and KDM1A.

Rest transcript is expressed in a majority of non-neural tissues, and at lower levels in neural progenitors, consistent with its role in restricting neuronal gene expression to neurons (Chong et al., 1995; Schoenherr and Anderson, 1995). By recruiting different complements of histone-modifying enzymes in these two contexts, it represses neuronal genes in differentiated non-neuronal tissues, and keeps targets in a largely-repressed but poised state in neural stem cells (Ballas et al., 2005). In culture, REST levels diminish when neuronal differentiation is induced. Interestingly, REST is nevertheless highly expressed in certain neurons, such as hippocampal pyramidal cells (Palm et al., 1998), and may be a transcriptional activator in these cells (Kuwabara et al., 2004). Why REST is lost from some differentiating neurons, but remains present in others, is still an open question. Whether RCOR1/2 are associated with REST in neurons has not been investigated.

1.4.3 RCOR1

Only one study has examined RCOR1 brain function i*n vivo* (Fuentes et al., 2012). In this study, an shRNA targeting *Rcor1* was electroporated *in utero* into the E14.5 cortices of mice. By E17.5, few *Rcor1* shRNA-electroporated cells had migrated to the cortical plate, although many of their control shRNA-electroporated counterparts had. However, by P7, all electroporated cells under either condition had reached the cortical plate. At E17.5, larger numbers of electroporated cells expressed the progenitor markers SOX2 and EOMES2

(TBR2) in the *Rcor1* shRNA condition than in the control shRNA condition, suggesting that the defect in migration be a secondary effect of neural progenitors failing to differentiate. In addition, neurons in brains treated with *Rcor1* shRNAs exhibited abnormal morphologies. By comparing these results with the effects of shRNAs targeting *Kdm1a*, the authors demonstrated that the migration deficit phenotype–which was phenocopied by the Kdm1a shRNA-electroporated cells–was caused by mechanisms distinct from those causing the neuronal morphology phenotype, which was not phenocopied by the *Kdm1a* knockdown.

The role of RCOR1 in neural cells was also investigated in a series of three papers that characterized the binding of RCOR1 to chromatin in several subtypes of cultured neurons, glia, and neural stem cells using ChIP-chip (Abrajano et al., 2009a; Abrajano et al., 2009b; Abrajano et al., 2010). By doing ChIP-chip on cultured glial cells at progressive stages of differentiation, Dr. Mark Mehler's laboratory found that the binding of RCOR1 to chromatin is dynamically regulated at every successive step–that is, RCOR1 binds different targets in every cell. Further, most of the binding sites identified in glial cells were not also bound by RCOR1 in neurons (and conversely). Similarly, most loci targeted by RCOR1 in one neuronal cell type were not targeted by RCOR1 in the other neuronal cell types. In short, there was little to unify the chromatin-binding profiles of RCOR1 between one cell type and the next. Further, the Mehler lab also analyzed REST using ChIP-chip, and found that while REST and RCOR1 had many shared binding sites, each also had many independent binding sites.

The fact that RCOR1 is bound to many sites not bound by REST provides a potential explanation for why knockdown of *Rcor1 in utero* produced such different results from knockdown of *Rest*: clearly REST is not the only factor targeting RCOR1 to the chromatin. In fact, given that each cell type had a different binding profile, it seems likely that many different transcription factors recruit RCOR1.

In an *in vitro* study examined the effects of knocking down *Rcor1* in cultured neural stem/progenitor cells (Covey et al., 2012). After three days of differentiation, *Rcor1* shRNA had increased the number of neurons expressing the immature neuronal marker TUBB3/TUJ1, or tubulin beta 3 class III, and the mature neuronal marker MAP2, or microtubule associated protein 2. The shRNAs also decreased the number of nestin-expressing progenitors. Furthermore, neurons derived from Rcor1 shRNA-treated sometimes had structures similar to growth cones, which were not seen in control shRNA-treated cells. After 10 days of differentiation, the numbers of astrocytes and oligodendrocytes were assessed, but neither was abnormal. Comparison of these results with those described above, regarding shRNA-targeting of *Rest*, suggests that REST recruits RCOR1 to prevent premature neuronal differentiation, but regulates oligodendroglial and astrocyte differentiation in an RCOR1-independent manner. This work shows that RCOR1 supports the maintenance of the progenitor state in cultured neural progenitors. These results contrast with those observed after knockdown of *Rcor1 in utero*, which suggested that RCOR1 promotes neuronal migration.

1.4.4 RCOR2

The role of RCOR2 in the brain was studied with conditional *Rcor2* KO mice and *in utero* electroporation of shRNAs (Wang et al., 2016). A brain-targeted *Rcor2* KO made from floxed *Rcor2* and Cre driven by the nestin promoter resulted in mice with very small brains. This is probably primarily the result of premature cell cycle exit. Consistent with this interpretation, analysis of MKI67 expression 24 or 48 hours after 5-bromo-2'-deoxyruridine (BrdU) incorporation at E13.5 showed that more progenitors had left the cell cycle between E13.5 and either E14.5 or E15.5 in the *Rcor2* KO than in controls. Furthermore, E13.5 *Rcor2* KOs had fewer cortical progenitors expressing the proliferation marker MKI67, the apical progenitor marker SOX2, or the basal progenitor marker EOMES/TBR2. Surprisingly, *Rcor2* KOs still had normal numbers of mitotic cells at E13.5, as assessed using an antibody recognizing phosphorylation of histone H3 serine 10. Another factor contributing to decreased brain size was apoptosis. *In utero* electroporation of shRNAs against *Rcor2* resulted in apoptosis of the newborn daughter cells of radial glia. Consistent with this finding, *Rcor2* KOs had more apoptotic cells (assessed with cleaved caspase 3 antibody) at E15.5 than did controls. *Rcor2* KOs also had fewer neurons. This is unsurprising given the shortage of progenitors and excessive apoptosis. Another possible explanation for the decrease in neuronal numbers in the *Rcor2* KO is that RCOR2 diminished the ability of progenitors to differentiate. This hypothesis is supported by the observation that shRNAs targeting *Rcor2* at E13.5 prevented electroporated cells from migrating out of the VZ/SVZ by E16.5. This

phenotype resembles that of the *Rest* KO mouse, insofar as both are associated with reductions in cortical progenitors, premature cell cycle exit, reduced numbers of neurons, and excessive apoptosis. Further, the *Rcor2* KO phenotype contrasts with that observed in *Rcor1* knockdown experiments, in which progenitor numbers increased.

To investigate RCOR2 targets in the brain, Wang et al. (2016) performed ChIP-seq on E13.5 cortex using FLAG-tagged RCOR2 expressed from the endogenous locus. Nearly 2000 RCOR2 binding sites were identified. RCOR2 binding sites were enriched for an AG-rich motif. Characterization of genes near binding sites revealed significant enrichment of gene ontology terms pertaining to sonic hedgehog (SHH) signaling, transcription, cell fate commitment, cell migration, and synaptic organization. Importantly, some of the RCOR2 binding sites near SHH genes were also bound by KDM1A in control mice, with reduced binding to KDM1A in *Rcor2* KO mice. Further, these sites were also associated with elevated H3K4me1 in the *Rcor2* KO relative to the control.

RNA transcript profiling analysis of control and *Rcor2* KO E13.5 cortex showed that knockouts had many more up-regulated than down-regulated genes, which suggests that RCOR2 functions primarily as a repressor in this tissue. Importantly, some of the SHH-pathway genes identified by RCOR2 ChIP-seq were among the up-regulated genes. Many down-regulated genes were involved in neuronal differentiation. RT-qPCR confirmed up-regulation of several SHH-related genes identified by transcript profiling analysis, and the up-regulation of three of these genes–*Shh*, *Ptch1*, *Dlx2*–were corroborated on the protein level by

both immunohistochemistry and Western blotting. Further, diminishing SHH signaling using either shRNA against Shh or pharmacological inhibitors partially rescued the migration defects caused by shRNA against *Rcor2*.

1.4.5 KDM1A

Lysine demethylase 1A (KDM1A) is an RCOR-interacting enzyme with essential roles in nervous system development. KDM1A demethylates mono- and di-methylated histone 3 lysine 4 (H3K4), histone 4 lysine 20 (H4K20), and histone 3 lysine 9 (H3K9; Shi et al., 2004; Wang et al., 2015; Laurent et al., 2015). Most studies found that the ubiquitously-expressed isoforms of KDM1A that demethylate H3K4 repressed transcription (*e.g.* Shi et al., 2005; Sun et al., 2010; Hirano and Namihira, 2016; but see Zhang et al., 2014a). In contrast, the isoforms responsible for demethylating H4K20 and H3K9, which are primarily expressed in neurons, promote transcription (Wang et al., 2015; Laurent et al., 2015). To demethylate nucleosomal H3K4 or H4K20, KDM1A requires an RCOR protein as a cofactor (Shi et al., 2005; Lee et al., 2005; Wang et al., 2015). KDM1A-mediated demethylation of H3K9 also requires cofactors (Laurent et al., 2015), but whether it specifically requires RCOR proteins is not yet known.

Because RCORs are essential for all or some types of KDM1A activity, analyses of KDM1A may provide insights into the functions of RCORs in neural development. Supporting this hypothesis, multiple experiments suggest that loss of KDM1A recapitulates phenotypes associated with loss of RCOR1. Fuentes et al. (2012), who showed that using shRNA to knock down *Rcor1* in the E14.5 mouse cortex drastically reduced the number of electroporated cells that had

migrated to the cortical plate by E17.5 (described above), obtained similar results when they instead electroporated an shRNA targeting *Kdm1a*. The *in vitro* experiments of Zhang et al. (2014a) show that loss of KDM1A increases the number of neurons, and decreases the number of neural progenitors, that are present after two days in culture. Similarly, the *in vitro* experiments of Sun et al. (2010) show that loss of KDM1A reduced neural stem cell proliferation. These *in vitro* results resemble those observed by Covey et al. (2012) when they assessed the effects of *Rcor1* knockdown. The similarities between studies of RCOR1 and studies of KDM1A imply that KDM1A is required for some of RCOR1's functions in the brain.

1.5 INSM1

1.5.1 Functions of INSM1

In the course of conducting my thesis work, I came across several lines of evidence implicating the transcription factor Insulinoma-associated 1 (INSM1) in RCOR-mediated gene repression. I will now review evidence that delineates several functions of INSM1, explains how INSM1 associates with RCOR1/2, and illustrates the role of INSM1 in the developing nervous system.

Several lines of evidence suggest that INSM1 functions as a traditional transcriptional repressor. It binds to DNA in a sequence-specific manner (Breslin et al., 2002) using the second and third of its five zinc fingers. An INSM1-GAL4 DNA binding domain fusion protein represses reporter transcription (Breslin et al., 2002). Reporter assays suggest that INSM1 binds its own promoter (Breslin et al., 2002), as well as those of *Neurod1* (Breslin et al., 2002; Liu et al., 2006), *Ins1*

(insulin-1 preproprotein; Zhang et al., 2009), and *Ins2* (insulin-2 preproprotein; Wang et al., 2008). INSM1-mediated repression was enhanced by coexpression of HDAC3 (Wang et al., 2008), which suggests that HDAC3 may be an INSM1 co-repressor. Supporting this interpretation, HDAC3 is present at the *Ins2* promoter (Wang et al., 2008) and the *Neurod1* promoter (Liu et al., 2006). Most importantly, there is also evidence that INSM1 recruits RCOR1, RCOR2, and KDM1A. This data will be discussed in a subsequent section.

Surprisingly, transcriptional profiling experiments in *Insm1* KOs show larger numbers of down-regulated than up-regulated genes in embryonic pancreas, neocortex, and adrenal and pituitary glands (Gierl et al., 2006; Osipovich et al., 2014; Farkas et al., 2008; Wildner et al., 2008; Welcker et al., 2013). One possible explanation for these results is that INSM1 represses a small number of repressor genes, which each repress many targets. Alternatively, INSM1 may be transcriptional activator in some contexts. Supporting this hypothesis, ChIP-qPCR revealed that INSM1 was bound to both up-regulated genes in *Insm1*$^{-/-}$ pancreas, and down-regulated genes. Interestingly, *Ins2* was downregulated in the *Insm1*$^{-/-}$ pancreas relative to the *Insm1*$^{+/-}$ (Osipovich et al., 2014), which emphasizes the fact that activity toward a reporter *in vitro* does not always reflect how a protein expression of endogenous transcripts (see also Otto et al., 2007, for an example of this in the context of REST).

INSM1 has functions independent of direct transcriptional regulation. INSM1 arrests the cell cycle by sequestering CCND1 (cyclin D1), and thereby preventing cell cycle progression (Zhang et al., 2009). However, the INSM1-

CCND1 interaction may also support direct chromatin regulation. CCND1 regulates transcription independent of cyclin-dependent kinases (Coqueret et al., 2002). Co-transfection experiments show that CCND1 contributes to repression of a reporter with the promoter of *Neurod1* (Coqueret et al., 2002). Further, CCND1 mutants unable to bind CDK4 or RB1 also repress this promoter. CCND1 interacts with HDAC3 (Lin et al., 2002), which suggests that it may provide the means by which INSM1 associates with HDAC3. Supporting this possibility, yeast two-hybrid assays suggest that the interaction between HDAC3 and INSM1 is not direct (Zhang et al., 2009).

While CCND1 may contribute to INSM1-mediated transcriptional repression in some circumstances, it is not required for all INSM1-mediated repression. Amino acids 1-168 of INSM1 (human) are sufficient to interact with CCND1 (Zhang et al., 2009), but an INSM1 construct consisting of amino acids 1-167 fused to the GAL4 DNA binding domain was unable to induce repression of a reporter (Breslin et al., 2002). In contrast, amino acids 168-263 of INSM1 did induce repression. In addition, mutant INSM1 incapable of binding to CCND1 had only slightly less repressor activity than wild-type INSM1. Further, as discussed below, the SNAG domain of INSM1 is able to recruit an RCOR/KDM1A complex.

1.5.2 INSM1 is associated with RCOR1/2

In mouse and rat pituitary cell lines, INSM1 complexes contain RCOR1 and RCOR2, as well as several RCOR-associated proteins including KDM1A (Welcker et al., 2013). However, a version of INSM1 lacking its first seven amino acids was unable to immunoprecipitate either RCOR1 or KDM1A (Welcker et al.,

2013). These amino acids make up the SNAG domain, which is named for *Sna*i1 and *G*fi1, two transcription factors that possess it. Notably, both of these transcription factors are also found in complexes with RCOR1 and KDM1A. Analysis of mice in which the SNAG domain of INSM1 was selectively deleted demonstrate that genes mis-regulated in the *Insm1* KO were similarly mis-regulated in a mouse with one null and one SNAG-deleted *Insm1* allele. Both the *Insm1*$^{-/-}$ mouse and the SNAG-deleted mouse had deficits in pituitary cell differentiation, which shows that an INSM1/RCOR complex is likely involved in this process.

Crystal structures of the ternary complex of INSM1, KDM1A, and RCOR1 show that INSM1 and RCOR1 are connected by KDM1A (Fig. 1.5; Tortorici et al., 2013). Structures show that the SNAG domain of INSM1 fits into the catalytic pocket of KDM1A in a manner comparable to that in which the N-terminus of histone H3 does. This structure has interesting implications for the function of the complex, because KDM1A cannot bind histone H3 (its substrate) while penetrated by INSM1. In fact, it was proposed that isolated SNAG domains could be used as a starting point from which to develop KDM1A inhibitors to be used as therapeutic agents (Tortorici et al., 2013). Perhaps the INSM1-KDM1A interaction is used to recruit the KDM1A/RCOR complex to a given chromatin locus, where it is then held in place by other mechanisms, such as the binding of RCOR1 to DNA.

1.5.3 INSM1 expression in the brain

Characterization of *Insm1* expression in the murine nervous system

revealed transcript in all neurogenic areas examined, including the embryonic CNS, embryonic PNS, postnatal external granule layer of the cerebellum, and adult neurogenic structures (Duggan et al., 2008). *Insm1* was expressed in a band of abventricular (basal) cells surrounding the ventricular system in the CNS (Duggan et al., 2008; Farkas et al., 2008). In contrast, a majority of periventricular (apical) cells did not express *Insm1* (Duggan et al., 2008; Farkas et al., 2008). This spatial pattern suggests that INSM1 is expressed in intermediate progenitors, which are expected to undergo only one or two additional cell divisions, and/or in newborn neurons that have not yet migrated away from the progenitor zone (Duggan et al., 2008). Comparison of *Insm1* expression with BrdU incorporation or MKI67 expression showed that many, but not all, actively dividing progenitors expressed *Insm1*, and that not all *Insm1*-expressing cells were proliferating (Duggan et al., 2008). In cortex, most *Insm1*-expressing cells also expressed EOMES/TBR2, a basal progenitor marker, and conversely, which further confirmed that most *Insm1*+ cells were intermediate progenitors. Similarly, most cells expressing the intermediate progenitor marker TIS21 expressed *Insm1*, and conversely (Farkas et al., 2008). Comparison of the expression domain of *Insm1* with that of the early neuronal marker DCX showed almost no overlap between these domains (Duggan et al., 2008). Further, there was no evidence for maintenance of *Insm1* in neurons after migration to their target destinations (Duggan et al., 2008). In cultures of dissociated cerebellar cells, only ~15% of TUBB3+ cells expressed *Insm1* (Duggan et al., 2008). These results collectively suggest that *Insm1* is expressed in both progenitors–

specifically intermediate progenitors–and in newborn neurons, but not in mature neurons.

1.5.4 Developmental roles of INSM1

Insulinoma-associated 1 (INSM1) is required for the differentiation of a variety of endocrine and neural cells (Gierl et al., 2006; Wildner et al., 2008; Farkas et al., 2008; Jacob et al., 2009; Rosenbaum et al., 2011; Ramachandran et al., 2012; Welcker et al., 2013; Forbes-Osborne et al., 2013; Osipovich et al., 2014; Jia et al., 2015; Lorenzen et al., 2015). It promotes differentiation several different ways. In the nervous system, it facilitates the transition from apical to basal progenitors (Farkas et al., 2008; Rosenbaum et al., 2011), increases cell division in basal progenitors (Farkas et al., 2008; Rosenbaum et al., 2011; Lorenzen et al., 2015), and is required for serotonergic and noradrenergic neurons to acquire their neurotransmitter phenotypes (Jacob et al., 2009).

The first clues to the function of INSM1 in the brain came from *C. elegans*. The *C. elegans* homolog of *Insm1*, *egl-46*, was identified in a screen for mutants with defects in hermaphrodite-specific neurons (Desai and Horvitz, 1989). *Egl-46* is expressed in progenitors of the Q lineage. In wild-type worms, Q progenitors express *egl-46* shortly before undergoing terminal cell division, and turn it off soon thereafter (Wu et al., 2001). In *egl-46* mutants, cells failed to exit the cell cycle, and instead underwent an additional round of cell division (Desai and Horvitz, 1989). This suggests that *egl-46* promotes cell cycle exit in neurons.

Two studies directly investigated the role of INSM1 in the mouse brain: Farkas et al. (2008) studied the cortical phenotype associated with either global

KO or cortical overexpression of Insm1, and Jacob et al. (2009) investigated the effect of loss of *Insm1* on specific neurons in the hindbrain (Table 1.3). Three additional studies, focused on the peripheral nervous system, reinforce the conclusions drawn from the brain studies (Table 1.3).

Analysis of the cortical phenotype of a global *Insm1*$^{-/-}$ mouse suggests that *Insm1* promotes the production of basal progenitors from apical progenitors, and possibly also their proliferation (Farkas et al., 2008). *Insm1*$^{-/-}$ cortices were slightly thinner than those of heterozygotes at E13.5-E14.5, a phenotype that worsened by E16.5. The thinning of the cortex was a reflection of reduced numbers of neurons. KOs had fewer TBR1 (deep-layer) and BRN1 (upper-layer) cortical neurons. There was no evidence of excessive apoptosis in *Insm1*$^{-/-}$ cortex. While both the CP and the SVZ were thinner, the VZ was thicker. This suggests that INSM1 promotes the transition of apical progenitors into basal progenitors. Consistent with this interpretation, there were fewer mitotic basal progenitors in the *Insm1*$^{-/-}$ cortex at E13.5 and E14.5. Loss of *Insm1* may also reduce proliferation among basal progenitors. At E14.5, there were ~30% fewer interphase EOMES/TBR2+ cells in the KO than in the control (Farkas et al., 2008). However, at E13.5, there was a ~60% reduction in basal mitoses in the KO. This suggests that even those EOMES/TBR2 cells that were still generated in the KO underwent mitosis less frequently than their control counterparts.

In the ventral telencephalon, as in the cortex, *Insm1*$^{-/-}$ mice had fewer neurons (Farkas et al., 2008). The progenitor zones in the subpallium were expanded, suggesting excessive progenitor self-renewal (Farkas et al., 2008).

Theoretically, this could indicate that the apical/primary progenitor population is increased to a greater degree than the basal/intermediate progenitor population is reduced. Given that the total VZ/SVZ was not dramatically expanded in the cortex but was in the subpallium, it seems probable that these two phenotypes are regulated by independent mechanisms.

In contrast to the above, investigation of the hindbrain phenotype of the *Insm1*$^{-/-}$ mouse emphasizes the role of INSM1 in neurons, not progenitors (Jacob et al., 2009). At E10.5, few of the hindbrain cells that had incorporated BrdU in a 45-minute pulse expressed INSM1, suggesting that cells in this region rarely turn on INSM1 before G2 of their final cell cycle, at the earliest. At E11.5, no overlap was observed between MKI67 and INSM1. These findings contrast with those of Duggan et al., 2008, which found BrdU/*Insm1* double-labeled cells in E12.5 hindbrain after 30 minutes of BrdU incorporation. In the *Insm1*$^{-/-}$ hindbrain, TUBB3 staining was normal, but several markers of serotonin neurons, including serotonin itself, were reduced (Jacob et al., 2009). These findings suggest that INSM1 is not required for production of serotonergic neurons, but does promote their serotonergic cell identity. Further, there was a transient reduction in the expression of tyrosine hydroxylase in the noradrenergic neurons of the locus coeruleus at E12.5. However, other markers associated with noradrenergic fate were not affected, suggesting that INSM1 is required for the functioning, but not the specification, of noradrenergic neurons.

The above studies suggest that in the brain, INSM1 may play a role in production of basal progenitors from apical progenitors, cell cycle dynamics of

basal progenitors, and acquisition of a mature neuronal phenotype. Several studies of INSM1 in the peripheral nervous system provide additional evidence for these three roles of INSM1 (summarized in Table 1.3). The discrepancy between the *Insm1*$^{-/-}$ phenotype in the cortex and that in the subpallium suggests that even within the telencephalon, INSM1 may have multiple independent functions. This discrepancy should caution us against drawing conclusions about the functions of repressive complexes in the subpallium on the basis of neocortical function.

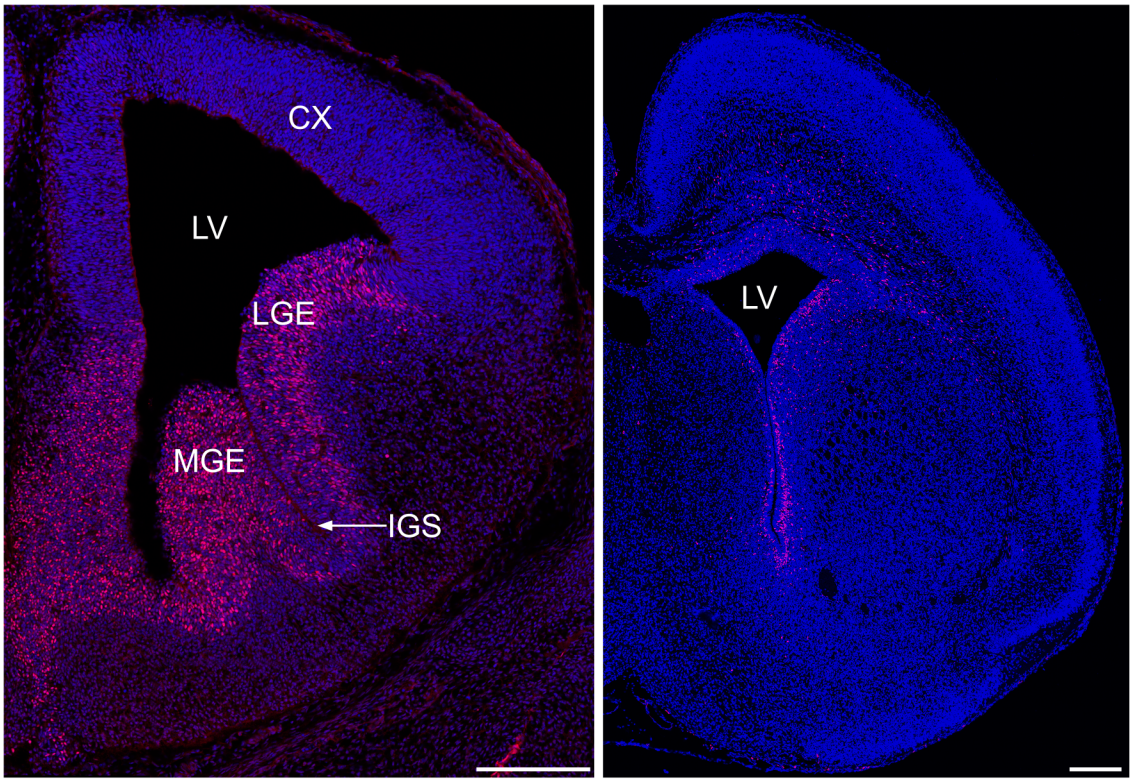

Figure 1.1. The subpallial ventricular and subventricular zones. Coronal hemisections of E13.5 (*left*) and E18.5 (*right*) brains stained for ASCL1 (red), a transcription factor expressed in a subset of subpallial progenitors (Horton et al., 1999), and counterstained with DAPI to mark nuclei. The lateral and medial ganglionic eminences are separated by the interganglionic sulcus. Scale bars, 200 μm. CX, neocortex; IGS, interganglionic sulcus; LGE, lateral ganglionic eminence; LV, lateral ventricle; MGE, medial ganglionic eminence.

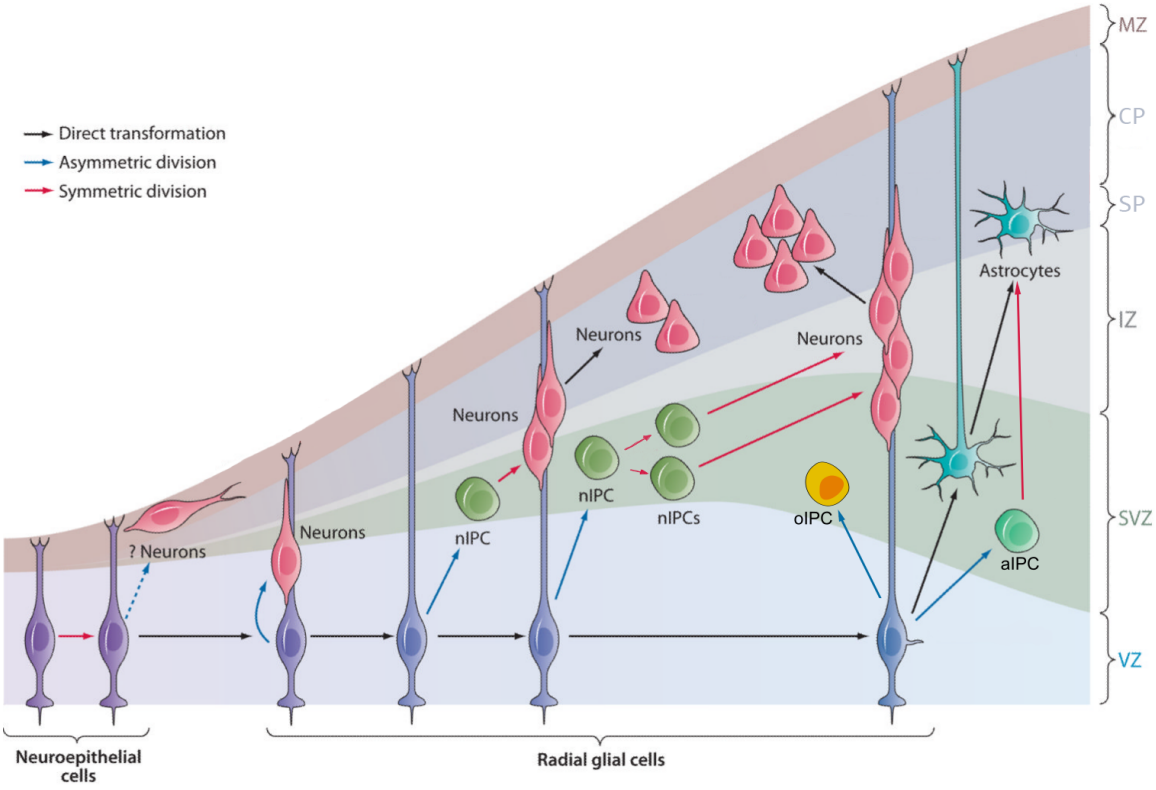

Figure 1.2. Neurogenesis. Neuroepithelial cells divide symmetrically to self-renew. At the onset of neurogenesis, neuroepithelial cells convert into radial glia. Radial glia typically divide asymmetrically, self-renewing and producing either a neuron or an intermediate progenitor cell (IPC). IPCs usually divide symmetrically to produce neurons, oligodendrocyte precursor cells, astrocytes, or more IPCs. During embryonic stages, most IPCs (nIPCs) produce neurons; after birth, some IPCs (oIPCs) produce oligodendrocyte precursor cells and others (aIPCs) produce astrocytes. Astrocytes are also produced by direct conversion from radial glia. VZ, ventricular zone; SVZ, subventricular zone; IZ, intermediate zone; SP, subplate; CP, cortical plate; MZ, marginal zone. Figure was adapted from Kriegstein and Alvarez-Buylla, 2009.

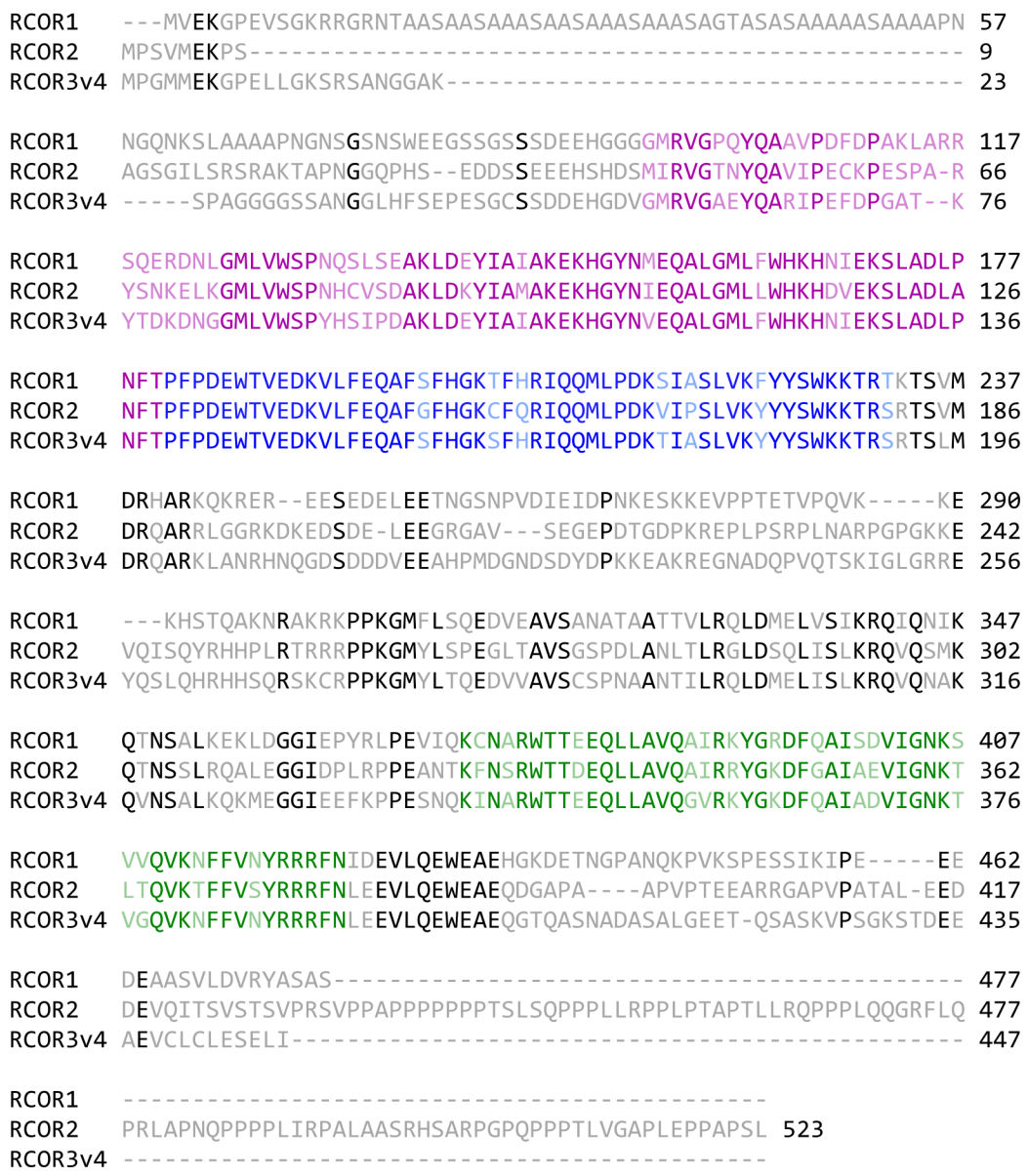

Figure 1.3. Alignment of murine RCOR1, RCOR2, and RCOR3 variant 4. The RCOR proteins share homology in three domains. The ELM2 domain is shown in magenta, the first SANT (SANT1) domain in blue, and the second SANT (SANT2) domain in green. Amino acids shared by all three proteins are shown in dark lettering, and unshared amino acids, in light lettering. Variant 4 was chosen to represent RCOR3 because it shares more amino acids with RCOR1 and RCOR2 than the other isoforms do.

Figure 1.4. Functional domains and binding partners of murine RCOR1. Amino acids that interact with other proteins are depicted on top. Either amino acids 96-189 or amino acids 162-224 were sufficient to interact with REST; amino acids 96-224 are shown for simplicity (Ballas et al., 2001). The ELM2 domain and Ser216 interact with HDAC2 (and presumably also HDAC1; Barrios et al., 2014); it is not known whether this interaction is direct. Amino acids 287-375 interact with KDM1A (Shi et al., 2005). Amino acids 287-436 interact with SMARCE1 (BAF57; Battaglioli et al., 2002). Domain structure is depicted in the middle. The ELM2 domain, shown in magenta, occupies amino acids 94-180. The SANT1 domain, in blue, consists of amino acids 181-232. The SANT2 domain, in green, consists of amino acids 372-423.

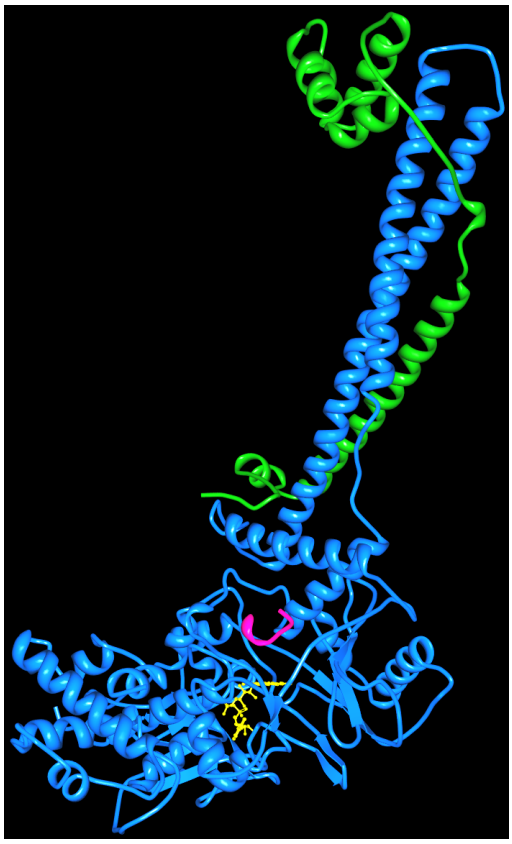

Figure 1.5. Crystal structure of the RCOR1/KDM1A/INSM1 complex.

Structure of a complex consisting of the C-terminus of human RCOR1 (green), the C-terminus of human KDM1A (blue), and the N-terminus of human INSM (pink), with flavin adenine dinucleotide (yellow). Image is from RCSB Protein Data Bank (PBD ID: 3ZMS); deposited by Tortorici et al., 2013.

Transcription factor	Full name	Key functional domain	RCOR with which interaction was proposed	Report the presence of HDAC1/2 and KDM1A?	Brain expression	Reference for interaction with RCOR proteins	Reference for brain expression
NACC1	Nucleus accumbens associated 1	zinc finger (POZ/BTB)	RCOR1	not investigated	yes	Korutla et al., 2007	Cha et al., 1997
NR4A2/ NURR1	Nuclear receptor subfamily 4, group A, member 2	nuclear receptor	RCOR1	interaction not investigated; effects of HDAC1 knockdown suggest it interacts with NR4A2 and RCOR1	yes	Saijo et al., 2009	Saijo et al., 2009
REST	Repressor element 1 silencing transcription factor	zinc finger	RCOR1, RCOR2	KDM1A, HDAC1, HDAC2	yes	Andrés et al., 1999; Zeng et al., 2010; McGann et al., 2014	Palm et al., 1998
BCL11A/ CTIP1	B-cell CLL/lymphoma 11A	zinc finger	RCOR1	KDM1A, HDAC1, HDAC2	yes	Xu et al., 2013	Leid et al., 2004
ESRRB	Estrogen Related Receptor Beta	nuclear receptor	RCOR1	not investigated	?	Liu and Mandel, unpublished	-
FOXK2	Forkhead box K2	fork head DNA binding domain	RCOR1	HDAC1, HDAC2	yes	Shan et al., 2016	Fujii and Nakamura, 2010
GFI1	Growth factor independence 1	zinc finger	RCOR1	KDM1A, HDAC1, HDAC2	yes	Saleque et al., 2007	Wilson et al., 2010
GFI1B	Growth factor independence 1b	zinc finger	RCOR1, RCOR2, RCOR3	KDM1A, HDAC1, HDAC2	yes	Saleque et al., 2007	-
INSM1/IA1	Insulinoma-associated 1	zinc finger	RCOR1, RCOR2, RCOR3	KDM1A, HDAC1, HDAC2	yes	Welcker et al., 2013	Duggan et al., 2008
KLF4	Krüppel-like factor 4	zinc finger	RCOR1	KDM1A not present	yes	Boxer et al., 2014	Qin and Zhang, 2012
MECP2	Methyl-CpG binding protein 2	methyl CpG binding	RCOR1	others not investigated	yes	Lunyak et al., 2002	Meehan et al., 1992
MYT1	Myelin transcription factor 1	zinc finger	RCOR1	KDM1A, HDAC1, HDAC2	yes	Yokoyama et al., 2014	Kim et al., 1997
NR2E1/TLX	Nuclear receptor subfamily 2, group E, member 1	nuclear receptor	RCOR1	KDM1A, HDAC1, HDAC2	yes	Yokoyama et al., 2008	Roy et al., 2004
NR2E3/PNR	Nuclear receptor subfamily 2, group E, member 3	nuclear receptor	RCOR1	KDM1A, HDAC1 (HDAC2 not investigated)	?	Yokoyama et al., 2008	Kitambi et al., 2006
NR4A1/ NURR77	Nuclear receptor subfamily 4, group A, member 1	nuclear receptor	RCOR1	KDM1A, HDAC1 (HDAC2 not investigated)	yes	Palumbo-Zerr et al., 2015	McNulty et al., 2012

Table 1.1. Transcription factors found in complexes with RCOR proteins. Page 1 of 2.

Transcription factor	Full name	Key functional domain	RCOR with which interaction was proposed	Report the presence of HDAC1/2 and KDM1A?	Brain expression	Reference for interaction with RCOR proteins	Reference for brain expression
POU5F1/ OCT4	POU class 5 homeobox 1	POU	RCOR2	KDM1A, HDAC1 (HDAC2 found in both test and control)	yes	Pardo et al., 2010	Sachewsky et al., 2014
RREB1	Ras-responsive element-binding protein 1	zinc finger	RCOR1, RCOR3	KDM1A, HDAC1, HDAC2	?	Shi et al., 2005; Liu and Mandel, unpublished	-
SALL1	Spalt-like transcription factor 1	zinc finger	RCOR1	KDM1A, HDAC2	yes	Liu and Mandel, unpublished	Buck et al., 2001
SALL4	Spalt-like transcription factor 4	zinc finger	RCOR1	KDM1A, HDAC2	yes	Liu and Mandel, unpublished	Sakaki-Yumoto et al., 2006
SNAI1	Snail family zinc finger 1	zinc finger	RCOR1	KDM1A (HDACs not investigated)	yes	Lin et al. 2010	Zander et al., 2014
TAL1	T-cell acute lymphocytic leukemia 1	basic helix-loop-helix	RCOR1	KDM1A, HDAC1, HDAC2	yes	Hu et al., 2009	Achim et al., 2013
ZFP217	Zinc finger protein 217	zinc finger	RCOR1	KDM1A, HDAC2	?	You et al., 2001; Liu and Mandel, unpublished	-
ZFP219	Zinc finger protein 219	zinc finger	RCOR1	KDM1A, HDAC2	?	Liu and Mandel, unpublished	-
ZFP281	Zinc finger protein 281	zinc finger	RCOR1	KDM1A, HDAC2	yes	Liu and Mandel, unpublished	Wang et al., 2008
ZMYM2/ ZNF198/FIM	Zinc finger MYM-type containing 2	zinc finger (MYM)	RCOR1	KDM1A, HDAC1, HDAC2	yes	Gocke and Yu, 2008	Xiao et al., 1998
ZMYND8	Zinc finger MYND-type containing 8	zinc finger (MYND)	RCOR1, RCOR2	not investigated	yes	Zeng et al., 2010	Zeng et al., 2010
ZNF750	Zinc finger protein 750	zinc finger	RCOR1	KDM1A, HDAC1	?	Boxer et al., 2014	-
CTCF	CCCTC-binding factor	zinc finger	RCOR2, RCOR3	not investigated	yes	Yu et al., 2011	Hirayama et al., 2012
PGR	Progesterone receptor	nuclear receptor	RCOR1	KDM1A, HDAC1, HDAC2	yes	Vicent et al., 2013	Brinton et al., 2008
RAR	Retinoic acid receptor (a, b, or g)	nuclear receptor	RCOR1	HDAC1 (others not investigated)	yes	Ballas et al., 2005	Gofflot et al., 2007
ZEB1/ ZFHX1A	Zinc finger E-box binding homeobox 1	zinc finger	RCOR1, RCOR3	KDM1A (HDAC1/2 implied in ChIPs but not pursued)	yes	Shi et al., 2005; Wang et al., 2007	Singh et al., 2016
ZMYM3/ ZNF261/XFIM	Zinc finger MYM-type containing 3	zinc finger (MYM)	RCOR1	KDM1A, HDAC1, HDAC2	yes	Hakimi et al., 2003; Gocke and Yu, 2008	Scheer et al., 2000; Philips et al., 2014

Table 1.1. Transcription factors found in complexes with RCOR proteins. Page 2 of 2.

	Transcription factor	Evidence
Bind RCORs directly	NACC1	Mammalian two-hybrid assays in N2A and HEK293T cells showed that NACC1 and RCOR1 interact. GST pull downs showed that *in vitro*-translated RCOR1 interacts with GST-tagged NACC1. Reciprocal IPs in several brain regions confirmed the interaction.
	NR4A2/ NURR1	After lipopolysaccharide administration, RCOR1 IP'd NR4A2 in BV2 cells. GST-NR4A2 bound to RCOR. GST-RCOR1 bound to NR4A2.
	REST	Yeast two-hybrid assay using a HeLa cell library showed that RCOR1 interacts with REST. GST-RCOR1 bound REST. RCOR1 coimmunoprecipitated REST (Andrés et al., 1999). Overexpressed *Xenopus* Rcor2 coimmunoprecipitated overexpressed Rest in HEK293T cells (Zeng et al., 2010). Mass spec following IP of tagged, overexpressed REST in ESCs showed that REST complexes contain RCOR1 and RCOR2 (McGann et al., 2014).
Present in complexes with RCORs, but whether they directly bind RCORs is unknown	BCL11A/ CTIP1	RCOR1 was identified by mass spec following purification of biotinylated proteins after coexpression of FLAG-tagged BCL11A tagged with BirA recognition motif and BirA in MEL cells and in K562 cells. BCL11A coimmunoprecipitated RCOR1 in primary human erythroid cells.
	ESRRB	Mass spec following IP of overexpressed human RCOR1 in murine ESCs identified ESRRB.
	FOXK2	Mass spec following affinity purification of complex associated with tagged FOXK2 in human breast adenocarcinoma MCF-7 cells identified RCOR1. ChIP/re-ChIP on MCF-7 cells with FOXK2/RCOR1 showed that both are associated with HSP90AA1.
	GFI1	RCOR1was identified by WB after GFI1 IP in HEK293T cells expressing tagged proteins.
	GFI1B	Mass spec following purification of complexes containing recombinant, tagged GFI1B expressed in MEL identified RCOR1-3. Mass spec following purification of complexes containing recombinant, tagged GFI1B expressed in L8057 cells identified RCOR1. RCOR1 was identified by WB after GFI1B IP in HEK293T cells expressing tagged proteins.
	INSM1/IA1	Mass spec following IP of tagged INSM1 identified RCOR1-3 in AtT-20 cells. INSM1 immunoprecipitated RCOR1 in AtT-20 and GH3 cells.
	KLF4	RCOR1 was identified by WB following KLF4 IP, and reciprocally. ChIP confirmed colocalization of KLF4 and RCOR1 on some genomic sites.
	MECP2	MECP2 was coimmunoprecipitated by RCOR1.
	MYT1	MYT1 and RCOR1 were identified by mass spec following isolation of complexes containing tagged KDM1A from Neuro2a cells. WB confirmed that both MYT1 and RCOR1 were coimmunoprecipitated by tagged KDM1A in Neuro2a cells. Analysis following use of a glycerol gradient to separate KDM1A-containing complexes (from Neuro2a extracts) of different sizes suggested that the fraction containing MYT1 probably contains RCOR1.
	NR2E1/TLX	When Y79 retinoblastoma extracts were probed with a tagged NR2E1-truncation mutant, and the NR2E1-interacting proteins were subjected to mass spec, RCOR1 was identified. WBs produced in the same way verified the presence of RCOR1. Further analyses of NR2E1 complexes using glycerol gradients confirmed that NR2E1, KDM1A, RCOR1, and HDAC2 appeared in the same fractions. By WB, RCOR1 coimmunoprecipitated with NR2E1 in Y79 cells.
	NR2E3/PNR	NR2E3 coimmunoprecipitated RCOR1 in Y79 cells.
	NR4A1/ NURR77	NR4A1 coimmunoprecipitated RCOR1 in human fibroblasts overexpressing NR4A1.
	POU5F1/ OCT4	Mass spec following tagged POU5F1 IP in ESCs identified RCOR2.
	RREB1	Mass spec following isolation of complexes containing recombinant tagged CTBP1 in HeLa cells identified RCOR1, RCOR3, and RREB1. Mass spec following IP with recombinant, tagged RCOR1 in ESCs identified RREB1.
	SALL1	SALL1 was identified by mass spec following IP with recombinant, tagged RCOR1 in ESCs.
	SALL4	SALL4 was identified by mass spec following IP with recombinant, tagged RCOR1 in ESCs.

Table 1.2. Evidence demonstrating interactions between transcription factors and RCOR proteins. Page 1 of 2.

For references, see Table 1.1.

	Transcription factor	Evidence
Present in complexes with RCORs, but whether they directly bind RCORs is unknown	SNAI1	Expressing SNAI1 and KDM1A in HEK293 cells, the authors found that MG132 improved the stability of each of these; if they also coexpressed RCOR1, this stabilized SNAI1 and KDM1A comparably to how much MG132 does. Not only did RCOR1 come down in a KDM1A IP along with SNAI1 (both proteins being overexpressed in HEK293 cells), but more SNAI1 came down if RCOR1 was overexpressed than if only SNAI1 and KDM1A were overexpressed. Knocking down endogenous RCOR1 in HCT116 and PC3 cells reduced the level of SNAI1 and KDM1A detectable by WB (they say this was true for a third cell line, but the blot is not convincing). Rcor1 siRNA diminished the amount of SNAI1 pulled down in a KDM1A IP.
	TAL1	Mass spec following TAL1 IP in K562 cells expressing tagged TAL1 identified RCOR1. Mass spec following TAL1 IP in Jurkat cells expressing tagged TAL1 identified RCOR1. Gel filtration analysis shows comigration of TAL1 with RCOR1.
	ZFP217	Mass spec following IP of RCOR1 in HeLa cells identified ZNF217 (You et al., 2001). Mass spec following IP with recombinant, tagged RCOR1 in ESCs identified ZNF217 (Liu and Mandel, unpublished).
	ZFP219	Mass spec following IP with recombinant, tagged RCOR1 in ESCs identified ZNF219.
	ZFP281	Mass spec following IP with recombinant, tagged RCOR1 in ESCs identified ZNF281.
	ZMYM2/ ZNF198/FIM	Mass spec following IP of ZNF198 in HEK293 and HeLa cells identified RCOR1.
	ZMYND8	Yeast two-hybrid with *Xenopus rcor2* identified *zmynd8*. Overexpressed Rcor1 and Rcor2 each immunoprecipitated overexpressed Zmynd8 in HEK293T cells.
	ZNF750	TAP of ZNF750 complexes from differentiated keratinocytes, followed by mass spec, identified RCOR1. RCOR1 was identified by WB following ZNF750 IP, and reciprocally. Comparison of ChIP-seq data for ZNF750 and RCOR1 showed binding at some KDM1A+ and KLF4- sites as well as some KDM1A- and KLF4+ sites. Gene expression analysis after knocking down ZNF750, RCOR1, or other complex members showed that RCOR1 was associated with activating some ZNF750 targets and repressing others.
Possibly present in complexes with RCORs	CTCF	Some RCOR2 ChIP sites and RCOR3 ChIP sites colocalized with CTCF sites.
	PGR	CBX3 (HP1 gamma) coimmunoprecipitated RCOR1, KDM1A, and REST. KDM1A coimmunoprecipitated RCOR1, HDAC1, HDAC2, and CBX3. Application of a progestin analog reduced binding of RCOR1, KDM1A, CBX3 (HP1 gamma), HDAC1, and PGR, to the mouse mammary tumor virus promoter in T47D-MTVL cells. ChIP showed some colocalization of KDM1A and CBX3. In a previous study, there were 25,000 genomic PGR sites post-stimulation, but 6000+ PGR sites pre-stimulation. Hormone stimulation reduced some KDM1A and CBX3 peaks associated with unliganded PGR binding sites. However, at some sites, CBX3 is recruited after hormone application.
	RAR	ChIP indicated that both the retinoic acid receptor and RCOR1 interacted with the *Rest* genomic locus.
	ZEB1/ ZFHX1A	Mass spec following IP with recombinant tagged CTBP1 in HeLa cells identified RCOR1, RCOR3, and ZEB1 (Shi et al., 2003). Tagged ZEB1 came down in an IP for tagged KDM1A in HEK293 cells. Endogenous ZEB1 and endogenous KDM1A both came down in an IP for CTBP in MMQ pituitary cells. RCOR1 came down in a KDM1A IP in MMQ pituitary cells (Wang et al., 2007).
	ZMYM3/ ZNF261/ XFIM	Mass spec following IP of ZNF198 in HEK293 and HeLa cells pulled down both ZNF261 and RCOR1 (Gocke and Yu, 2008). Mass spec following KDM1A IP identified ZNF261 (Hakimi et al., 2003). Mass spec following HDAC2 IP identified ZNF261 (Hakimi et al., 2003).

Table 1.2. Evidence demonstrating interactions between transcription factors and RCOR proteins. Page 2 of 2.

For references, see Table 1.1.

	Transition from apical to basal progenitor	Proliferation among neural progenitors	Cell cycle exit	Differentiation among specified neurons	Acquisition of mature traits in specified neurons	Prevention of excessive apoptosis	Experiment type	Reference
Neocortex	yes	yes	-	-	-	no	KO	Farkas et al., 2008
Neocortex	ambiguous	yes	-	-	-	-	overexpression	Farkas et al., 2008
Hindbrain serotonergic neurons	-	-	-	yes	-	-	KO	Jacob et al., 2009
Hindbrain noradrenergic neurons	-	-	-	no	yes	-	KO	Jacob et al., 2009
Olfactory epithelium	yes	-	yes	-	-	yes	KO	Rosenbaum et al., 2011
Otic vesicle	-	yes	-	-	-	-	KO	Lorenzen et al., 2015
Sympatho-adrenal lineage	-	yes	-	yes	-	yes	KO	Wildner et al., 2008

Table 1.3. Roles of INSM1 in the developing nervous system.

CHAPTER 2: MATERIALS AND METHODS

2.1 Mice

Rcor1$^{fl/fl}$, Nes-Cre, and *Rest*$^{GTi/GTi}$ mice have been described previously (Yao et al., 2014; Tronche et al., 1999; Nechiporuk et al., 2016). The *Insm1*$^{-/-}$ mice (Osipovich et al., 2014) were acquired from the MMRRC. The generation of *Rcor2*$^{fl/fl}$ mice is described below. All of the mice used for experiments were backcrossed onto a C57BL/6J background for at least ten generations unless stated otherwise. In crosses involving Nes-Cre, this transgene was transmitted paternally exclusively. Nes-Cre-negative pups from such crosses were tested for recombination of *Rcor1*^{fl}, *Rcor2*^{fl}, and *Rest*^{GTi} alleles, so that the minority of pups that received recombined alleles as a result of germ-line Nes-Cre activity were excluded from further study.

Insm1$^{+/-}$ mice (Osipovich et al., 2014) were acquired on a mixed genetic background. When backcrossed onto a C57BL/6J background for five generations, *Insm1*$^{-/-}$ pups died before E18.5 (0/28 live pups at E18.5). This is consistent with the observations of Gierl et al. (2006), who reported that in a different *Insm1*$^{-}$ mouse line on mixed-background (129/Ola-C57BL/6), *Insm1*$^{-/-}$ pups ceased to appear at Mendelian ratios after E12.5. Gierl et al. also found that crossing their *Insm1*$^{+/-}$ mice to the CD-1 outbred strain increased the number of *Insm1*$^{-/-}$ pups surviving to E18.5. I therefore outcrossed the founders that I received from the MMRRC to CD-1 mice for one generation. Because CD-1 mice are outbred, continuing to outcross the *Insm1*$^{+/-}$ line to CD-1 mice would not increase the genetic homogeneity of the population. For this reason, the offspring from these first crosses were crossed with one another for one to four

generations to produce the pups used in experiments. In this mixed background, approximately half of the *Insm1*$^{-/-}$ pups survived to E18.5 (16/129 live pups).

Pregnancies were timed on the basis of observation of a coital plug, with the morning that the plug was observed defined as E0.5. Genotyping was performed with the primers listed in Table 2.1.

2.2 Generation of the *Rcor2*^{fl} mouse line

The floxed *Rcor2* mouse line was generated by Dr.Jianxun Wang in Dr, Michael G. Rosenfeld's laboratory at the University of California, San Diego (Fig. 2.1). In this mouse, Cre-mediated excision removes *Rcor2* exons 5-9. The excision prevents expression of all but the first 88 amino acids, which contain part (the first 45 of 86 amino acids) of the ELM2 domain but lacks both SANT domains. Using standard techniques, Dr. Wang generated these mice with the targeting vector described in Fig. 2.1. Dr. Wang confirmed correct targeting by Southern blotting with 5' and 3' external probes (data not shown). Further, PCR analysis of brain genomic DNA confirmed the expected excision events in the *Rcor1*$^{fl/fl}$; *Rcor2*$^{fl/fl}$; Nes-Cre mice (data not shown), and loss of RCOR2 protein was confirmed by Western blotting and immunohistochemistry (Fig. 3.4-3.6).

2.3 Transcardial perfusion for histochemistry

A syringe of room-temperature PBS and a syringe of ice-cold 4% formaldehyde in PBS were fitted with a three-way stopcock fitted with a 30 gauge needle so that the two syringes have alternating access to the needle. The pregnant mother was injected intraperitoneally with 1 ml of 2% Avertin (2,2,2-tribromoethanol), an anesthetic. When she was unresponsive, and did not

respond to pinching, she was placed on a heating pad set on its lowest setting. At the level of the uterine horns, an incision just large enough to pull out one embryo was made into the mother's abdomen. The first embryo was removed in such a way as to prevent disturbing the embryonic sac of neighboring embryos. The embryo was removed from its associated tissues and placed on ice for > 1 minute. Before the perfusion, the end of the tail was removed for DNA extraction. The pup was placed on its back in a cruciform posture on a piece of styrofoam and pinned to the styrofoam with a needle through each forepaw. The styrofoam was placed on the stage of a dissecting microscope. Just below the level of the diaphragm, a lateral incision was made across the ventral surface of the body. Posterior-anterior incisions were then made along each side of the body, running from the first incision to the top of the rib cage. The ribs at this point formed a flap over the front of the animal; this was gently pulled upward, and then cut off. The heart was adjusted, when necessary, so that the ventricle was exposed. The right aorta was snipped. The needle was inserted into the left ventricle from the posterior side. The pup was perfused with approximately 2.5 ml of PBS. The switch on the stopcock was then flipped, and the pup was perfused with 2.5 ml 4% formaldehyde in PBS. The pup was decapitated and stored in PBS or in 4% formaldehyde in PBS until the rest of the litter was finished.

2.4 Antibodies

Primary antibodies used for immunohistochemistry are listed in Table 2.2. Secondary antibodies used for immunohistochemistry, and all antibodies used for immunoprecipitation or Western blotting are listed in Table 2.3. Antibodies were

either stored at 4˚C, or were diluted by 50% with glycerol and stored at -20˚ (for short-term storage) or -80˚ (for long-term storage).

2.5 Nuclear extracts

Nuclear extracts intended for direct analysis by Western blotting were prepared according to a protocol modified from Tuoc et al., 2013. Brains were dissected from E13.5 mice, and the meninges removed, in ice-cold PBS. Each brain was then transferred to a 2 ml dounce homogenizer containing 250 μl of 1.3 M sucrose tissue cracking buffer (0.3 M sucrose; 10 mM HEPES, pH 7.6; 25 mM KCl; 10% glycerol; 1 mM dithiothreitol; Roche complete protease inhibitors with EDTA; adapted from Tuoc et al. 2013). Each sample was disrupted with five strokes with a loosely-fitting pestle (pestle A included with Kimble Kontes dounce tissue grinder, cat. #K885300-0002), followed five minutes later by ten strokes with a tightly-fitting pestle (pestle B). Next, 250 μl of 2 M sucrose tissue cracking buffer was mixed into the sample. The sample was layered onto a 1-ml cushion of 2 M sucrose tissue cracking buffer in a 1.7 ml tube. The samples were spun at 25,000 x g at 4˚C for 1 hour. The supernatant was removed, and the pellet was rinsed three times with nuclear buffer (10 mM HEPES, pH 7.6; 100 mM KCl; 10% glycerol; 1 mM dithiothreitol; Roche complete protease inhibitors without EDTA; adapted from Tuoc et al., 2013). The pellet was resuspended in 40 ul RIPA buffer (25 mM Tris HCl, pH 7.6; 150 mM NaCl; 1% NP-40; 1% sodium deoxycholate; 0.1% SDS; 1 mM beta-mercaptoethanol; Roche complete protease inhibitors without EDTA), vortexed, and stored at -80˚C.

Benzonase (250 U/μl) was diluted 1:12 in 50 mM $MgCl_2$. Samples were

thawed, treated with Benzonase/$MgCl_2$, and incubated at room temperature for 30 minutes. During the incubation, each sample was homogenized for 1 minute with a motorized pestle. Samples were centrifuged at 25000 x g at 4˚C for 20 minutes, and the supernatant was transferred to a new tube. Protein concentration was quantified using a Pierce BCA Protein Assay Kit.

Nuclear extracts for co-immunoprecipitation analysis were prepared from whole brain by dounce homogenization in tissue cracking buffer, centrifugation to collect a nuclear pellet, and washing of the pellet in nuclear buffer. These steps were performed as described above, except that phosphatase inhibitors (Millipore 524628) and 1 mM phenylmethylsulfonyl fluoride were included in the tissue cracking and nuclear buffers, and only pestle B was used for tissue disruption. After washing the pellet with nuclear buffer, each pellet was resuspended in 150 μl of lysis buffer (50 mM Tris, pH 7.4; 140 mM NaCl; 1% Triton X-100; 2 mM MgCl2; protease inhibitors without EDTA [Roche]; phosphatase inhibitors [Millipore Calbiochem Phosphatase Inhibitor Cocktail Set IV Cat. #524628]; 1 mM sodium orthovanadate; adapted from Welcker et al., 2013). Samples were homogenized with a motorized pestle and frozen at -80˚C.

Nuclear samples were pooled with others of the same genotype and treated with Benzonase at room temperature for 30 minutes. Lysates were then spun at 25,000 x g for 20 minutes at 4˚, and the supernatants were retained. Lysates were quantified using the BioRad DC Protein Assay II (BioRad 500-0112).

2.6 Western blotting

Protein samples were run on either a NuPAGE Novex 4-12% Bis-Tris gel or a 3-8% NuPAGE Novex Tris-Acetate Gel. Proteins were transferred onto a nitrocellulose membrane at 100 V for 2 h at 4˚C in transfer buffer (Towbin et al., 1979; 192 mM glycine, 25 mM Tris, 20% methanol). Membranes were blocked ≥ 1 hour in blocking solution (5% powdered nonfat milk; 150 mM NaCl; 20 mM Tris, pH 8.0; 0.05% Tween-20) and incubated for either 4 hours at room temperature or overnight at 4˚C with antibody diluted in blocking solution. The membranes were rinsed six times with wash solution (150 mM NaCl; 20 mM Tris, pH 8.0; 0.1% Tween-20) and incubated for one hour with secondary antibodies diluted in block solution. Membranes were rinsed six more times in wash solution. Fluorescently labeled membranes were imaged with a LI-COR Odyssey CLx using AutoScan. Background-subtracted signal intensity was quantified using Image Studio 4.0 software. For each sample, the levels of protein signals were normalized to the level of histone H3 signal. Membranes labeled with secondary antibodies conjugated to horseradish peroxidase were treated with SuperSignal West Pico Chemiluminescent Substrate (Thermo Scientific cat. #34080), and exposed to X-ray film.

2.7 Tissue preparation for histochemistry

Pups were perfused transcardially with 4% formaldehyde in PBS. For E18.5 pups, the brain was dissected, and in some cases postfixed at 4˚C overnight, before being rinsed with PBS and incubated in 30% sucrose in PBS at 4˚C overnight. For E13.5 pups, the head was removed, rinsed with PBS, and

incubated in 30% sucrose in PBS at 4˚C overnight. Heads and brains were incubated in a 50:50 mixture of 30% sucrose in PBS and Tissue Freezing Medium, and then embedded in Tissue Freezing Medium, frozen, and stored at -80˚C until they were sectioned. Tissue was cut into 14 or 20 μm sections at -25˚C, mounted on slides, and stored at -20˚.

2.8 Immunohistochemistry

Slides were dried at 65˚C for 1-2 hours before staining. Sections were prepared for blocking in one of three ways, depending upon the antibody. The blocking method used for each antibody is indicated in Table 2.2). Blocking and antibody labeling were performed with either a mouse-on-mouse kit (Vector Labs cat. #BMK-2202) or 5% normal serum and 0.125% bovine serum albumin in PBS-Triton. All slides were blocked for one hour at room temperature and labeled with primary antibody at 4˚ overnight and then at 37˚C for two hours (with the exception of MAP2 and TUBB3 antibodies, with which the 37˚ step was omitted). Slides were then rinsed three times with PBS containing TritonX-100, treated with secondary antibodies and a DNA dye (either DAPI [4',6-diamidino-2-phenylindole] or DRAQ5 [Deep Red Anthraquinone 5]) at room temperature for 1-2 hours, rinsed four times with PBS-Triton, rinsed once with PBS, and coverslipped after application of Prolong Gold Antifade Mountant (Thermo Fisher Scientific P36930).

2.9 Hematoxylin and eosin (H&E) staining

Twenty-micron sections were prepared from E18.5 brains as described above (section 2.7), with the overnight 4˚ post-fixation step included. Sections

were dried at 65˚C for 1-2 hours before staining. The sections were fixed with 4% formaldehyde in PBS for 15 minutes, then dehydrated through successive incubations in 50%, 80%, and 95% ethanol for 2 minutes, 2 minutes, and 5 minutes, respectively. Sections were incubated in tap water for 30 s and in hematoxylin for 45 s (filtered Harris Modified Hematoxylin without acetic acid [Fisher cat. #SH30-500D] to which 1/50 volume of glacial acetic acid [Fisher cat. #A38-212] was added). Sections were rinsed with several changes of tap water and then dipped briefly in acid alcohol solution (0.25% hydrochloric acid [Fisher cat. #HXO603-3] in 70% ethanol). Sections were rinsed with two changes of tap water and incubated in ammonia water for one minute (0.25% ammonium hydroxide in tap water). Sections were incubated in tap water for 20 s, 80% ethanol for 45 s, and eosin for two minutes (~0.5% eosin and ~0.5% glacial acetic acid in 40% ethanol). Sections were destained with two sequential 45 s washes in 95% ethanol, dehydrated with two one-minute washes in 100% ethanol, treated with xylenes (Fisher cat. #X5-500) with three washes of three minutes each, and coverslipped using Permount (Fisher cat. #SP15-500).

2.10 Image analysis

Immunofluorescent images were acquired using a Zeiss LSM 710 confocal microscope. Images intended to be compared with one another were acquired under the same conditions and processed identically. For quantifications, matching sections from each of five animals per genotype were used. In general, analyses were performed on 4-8 section per mouse. Images were processed using ImageJ and Photoshop CS4. Length and area

measurements were made using ImageJ. Cell counts were determined by eye. Measurements of the width of the MKI67+ region in the septum were made objectively using image thresholding. Before analyzing images, I renamed images arbitrarily in order to be blinded to genotype.

2.11 *In situ* hybridization

In situ hybridization for Dlx2 and Lhx6 were performed using the plasmids described in Porteus et al., 1991 and Grigoriou et al., 1998, respectively. The Dlx2 plasmid was restricted with HindIII to generate the template for the antisense probe, or NotI to generate the template for the sense probe. The Lhx6 plasmid was restricted with NotI to make the template for the antisense probe, or XhoI to make the template for the sense probe. Linearized plasmids were purified with phenol/chloroform/isoamyl alcohol and used as templates for *in vitro* transcription incorporating digoxigenin-11-UTP. T3 polymerase was used to transcribe each antisense probe and T7 polymerase was used for each sense probe. Probes were treated with DNaseI to remove the template, and purified with either a QIAGEN RNeasy Mini Kit or a PureLink RNA Mini Kit. Probes were diluted to 1 μg/ml with prehybridization solution (50% formamide; 5x SSC, pH 4.5; 50 μg/ml yeast tRNA; 1% SDS; 50 μg/ml heparin), and in situ hybridization was performed based on the protocol of Sciavolino et al., 1997.

Brain sections were prepared in the same way as described for the H & E staining. Slides were dried at 37˚ overnight. Slides were hybridized with probe as previously described (Sciavolino et al., 1997). After hybridization, slides were washed three times at 70° with wash solution 1 (50% formamide; 4x SSC, pH

4.5; 1% SDS), three times at 65° C with wash solution 2 (50% formamide; 2x SSC, pH 4.5), and three times at room temperature with TBST (50 mM Tris, 150 mM NaCl, 0.1% Tween-20). Sections were then blocked for one hour with 5% normal sheep serum in TBST. Sections were incubated overnight at 4˚ with anti-digoxigenin Fab fragments conjugated to alkaline phosphatase (Roche 11093274910) that had been pre-adsorbed with powdered mouse embryo and diluted to 1:2000 in 1% normal sheep serum. Next, sections were washed four times with TBST and washed three times with coloration buffer (100 mM Tris HCl, pH 9.5; 100 mM NaCl; 0.1% Tween-20). They were then developed using NBT/BCIP Stock Solution (Roche 11681451001) as per the manufacturer's instructions until the signal was sufficiently dark (245 minutes, Dlx2; 145 minutes, Lhx6). Finally, sections were fixed with 4% PFA and 0.1% glutaraldehyde in PBS, progressively dehydrated with 50%, 75%, 95%, and 100% ethanol, infiltrated with xylenes, dabbed with Permount (Fisher Scientific SP15), and coverslipped.

2.12 Co-immunoprecipitation

Immunoprecipitations were performed using 10 μg of antibody and 65 μg of Protein A Dynabeads for every 1.5 mg protein lysate (~20 brains). First, antibodies were incubated with Protein A Dynabeads in PBS containing 0.02% Tween-20 at 4˚C for several hours.

Samples corresponding to individual embryos were pooled with others of the same genotype and treated with Benzonase at room temperature for 30 minutes. Lysates were then spun at 25,000 x g for 20 minutes at 4˚, and the supernatant was retained. Lysates were quantified using the BioRad DC Protein

Assay II (BioRad 500-0112). Next, lysates were precleared by incubation with Dynabeads pre-conjugated to the appropriate control IgG or serum, and a fraction of each lysate was set aside as input. The rest of each lysate was split in half, and incubated at 4˚ overnight with either a specific antibody or the appropriate negative control antibody. Beads were then rinsed four times with lysis buffer lacking protease/phoshatase inhibitors, and once with pre-elution buffer (5 mM Tris, pH 7.4; 140 mM NaCl). Immunoprecipitated antibodies were eluted with 100 mM glycine, pH 2.6, which was then neutralized with 1 M Tris (3/10 volume of Tris per volume of glycine). After proteins had been eluted from the beads with glycine, residual proteins were eluted by boiling in NuPAGE LDS Sample Buffer containing 300 mM DTT, and the eluates combined.
Each input lane was loaded with 15 μg of lysate, and each IP lane was loaded with the amount of immunoprecipitate corresponding to 200 μg of protein lysate. Each immunoprecipitation was performed at least twice.

2.13 RNA profiling

Brains were dissected from E13.5 embryos, embedded in Tissue Freezing Medium, frozen, cut into 10-μm coronal sections at -25˚, and loaded onto poly-L-lysine-coated PEN-membrane slides (Zeiss 415190-9041-000). Immediately after sectioning, slides were stained with an abbreviated hematoxylin staining protocol. Slides were sequentially dipped in 70% ethanol, water, hematoxylin, Scott's tap water substitute (0.2% sodium bicarbonate, 2% magnesium sulfate heptahydrate), 70% ethanol, and 100% ethanol. Slides were air-dried and stored in airtight containers at -80˚ C. A cell-dense region equivalent to the VZ/SVZ of

the MGE was isolated using laser capture microdissection (LCM) with a Zeiss PALM MicroBeam. Tissue was pooled to make samples of three pups each. RNA was extracted using a QIAGEN RNeasy Micro Kit in accordance with the manufacturer's instructions, except that each sample was incubated in Buffer RLT containing 0.1% β-mercaptoethanol for 30 minutes at room temperature before starting.

cDNA Libraries were made by the OHSU Massively Parallel Sequencing Shared Resource. A BioAnalyzer 2100 confirmed that all samples had RNA integrity numbers ≥ 9.3. Each cDNA library was made from 300-500 ng (RNA using the Illumina TruSeq RNA Prep Kit v2). Knockout-control pairs were made with the same amount of RNA. Library quality was assessed using a TapeStation 2200, and libraries were quantified by qPCR using a KAPA Library Quantification Kit. Libraries were sequenced using 100-cycle single-read runs on a HiSeq 2500.

RNA-seq analysis was performed by Sophia Jeng and Dr. Shannon McWeeney in the department of Department of Medical Informatics and Clinical Epidemiology at OHSU. Sample quality was assessed using Fastqc (v0.11.3). To address technical artifacts due to biased amplicon amplification during cDNA library preparation, they trimmed 3 base pairs (bp) from the 5 prime end and 1 bp from the 3 prime end. This removes the bases most likely to not represent the original sequence of the transcript from which the amplicon was derived. They aligned each sample to the mm10 genome (i.e. the Dec. 2011 *Mus musculus* assembly) using Subread (Liao et al., 2013) and aggregated transcript counts using featureCounts (Liao et al., 2014). Transcript counts were

aggregated at the gene level to perform gene level differential expression analysis. Differential Expression Analysis was conducted using edgeR (Robinson et al., 2010). Data were normalized using TMM (Trimmed Mean of M-Values). P-values were adjusted for multiple comparisons using the Benjamini-Hochberg correction (Benjamini and Hochberg, 1995). Putative differential expression was based on FDR-adjusted p-value < 0.05.

To test whether the number of concordantly up-regulated genes was significant, Sophia performed a simulation of the amount of overlap achieved if 451 (number of genes up-regulated in the *Rcor1/2* KO) and 100 (number of genes up-regulated in the *Insm1*$^{-/-}$) genes were sampled randomly and independently from the total pool of 30737 genes. She performed the sampling 10^6 times to determine the distribution of possible overlaps. She performed a comparable simulation, sampling 300 and 197 genes, to determine whether the number of concordantly down-regulated genes was significant. The 99th percentile of the random sampling was 5 for the up-regulated genes and 6 for the down-regulated genes, compared to the observed values of 21 and 105, respectively. To be conservative, we report this result as p<<0.01 (calculations with hypergeometric distribution re p < 1.389e-18 and p < 3.639e-163 respectively).

2.14 RT-qPCR

RT-qPCR was performed on manually microdissected medial ganglionic eminences. Tissue was stored in RNALater Stabilization Solution (Thermo Fisher AM7020) at 4˚C overnight and then transferred to -80˚C until RNA extraction.

Samples were stored up to five weeks before RNA purification. Tissue was homogenized in 1 ml TRIzol (Thermo Fisher 15596026) with a motorized pestle. RNA extraction was performed with the PureLink RNA Mini Kit (Thermo Fisher 12183025), including on-column DNase treatment (Thermo Fisher 12185010). After extraction, RNA was precipitated with sodium acetate and ethanol, resuspended in water, and quantified with a NanoDrop 2000. Samples had A260/A280 ratios between 1.79 and 2.02, and A260/A230 ratios of 1.26 to 2.27. Samples of 600 ng RNA were reverse transcribed with the SuperScript III First Strand Synthesis System (Thermo Fisher 18080-051) using random hexamers. RT-qPCR was performed on a QuantStudio 6 Flex Real-Time PCR System using Power SYBR Green PCR Master Mix (Applied Biosystems #4367659) and 300 nM of each primer (with the exception of the *Prox1* primers, which were used at 900 nM each). RT-qPCR primers are listed in Table 2.4.

2.15 Statistical analysis

T tests were used for comparisons between two groups, unless the F statistic indicated that the variances of the two groups were unequal. In this case, either t tests with Welch's correction were used. For comparison of more than two groups, I used one-way ANOVA followed by Tukey's multiple comparison test. RT-qPCR data was $\log_2$-transformed prior to statistical analysis, so that groups compared using ANOVA would have equal variances. Throughout the text, experimental results are expressed as mean ± standard deviation.

Figure 2.1. Schematic diagram of *Rcor2* gene targeting strategy. Mice with conditional *Rcor2* alleles (floxed) were generated by inserting LoxP sites flanking exons 5-9. Exons are depicted as black rectangles, and LoxP sites as white diamonds. HSVTK, herpes simplex virus thymidine kinase; PGKNEO, neomycin resistance gene driven by the phosphoglycerine kinase promoter.

Target (amplicon length in base pairs)	Forward primer	Reverse primer
Cre (646)	GCTAAACATGCTTCATCGTCGG	GATCTCCGGTATTGAAACTCCAGC
Rcor1^{fl} (481) vs. *Rcor1*$^{+}$ (390)	GTAGTTGTCTTCAGACACTCCAGA	GGGAAGCTCATCTATAGGCAA
Rcor1^{fl} (1199) or *Rcor1*$^{+}$ (1006) vs. *Rcor1*^{rec} (336)	ATTTGTGTCATGTGTCATGTA	GGGAAGCTCATCTATAGGCAA
Rcor2^{fl} (315) vs. *Rcor2*$^{+}$ (143)	TCCGAGGTCTTGACTCACAGC	CAGGCTTGACACTGCACCATT
Rcor2^{rec} (365)	AATTCTGCTCATCCTTTCAGA	CAGGCTTGACACTGCACCATT
Insm1$^{-/-}$ (~550) vs. *Insm1*$^{+/+}$ (447)	CCTTGTACAACCGACAGCTCT	GTGCCCTGTATCTGCTGTGC
Rest^{+} (478)	TGGATGTTGAGGTCCGTTGTG	GGCTACGGATCCCTTCTTCCC
Rest^{GTi} (782)	CTCCGCCTCCTCTTCCTCCAT	TTTGAGGGGACGACGACAGTA
Rest^{GTreinv} (518)	CTCCGCCTCCTCTTCCTCCAT	CCTCCCCCGTGCCTTCCTTGA

Table 2.1. Genotyping primers.

Antigen	Manufacturer and catalog number	Concentration	Postfix	Protocol
ASCL1/MASH1	BD Pharmingen 556604	1:1000	none	A
BCL11B/CTIP2	Abcam ab28448	1:500	no	A
Cleaved caspase 3	Cell Signaling 9664	1:500	none	C
CNTN2/TAG1	DSHB 4D7/TAG1	1:50	2 hours	B
DCX	Cell Signaling 4604	1:500	2 hrs or O/N	C
FOXP1	Abcam ab16645	1:2000	no	A
GFAP	Dako Z 0334	1:500	none	A
INSM1	Birchmeier lab guinea pig serum	1:20,000	none	A
KDM1A/LSD1	Abcam ab17721	1:200	none	A
L1CAM	Chemicon MAB5272	1:1000	2 hours	B
MAP2	Millipore MAB3418	1:500	O/N	A
MKI67/Ki67	Abcam ab16667	1:100	O/N	C
NKX2-1	Santa Cruz Biotechnology sc-13040	1:500	none	B
OLIG2	Chemicon AB9610	1:500	either	C
PCNA	Mouse antibody	1:400	O/N	C
Phospho-histone H3 S10	Cell Signaling 3377	1:500	O/N	C
RCOR1	Neuromab clone K72/8	1:200	none	C
RCOR2	Rosenfeld lab rabbit serum	1:10,000	none	A
REST	Mandel lab "095" serum	1:2500	O/N	A
TUBB3/TUJ1	Covance MMS-435P	1:500	O/N	A

Table 2.2. Primary antibodies used for immunohistochemistry. Slides were prepared for blocking in one of three ways. In protocol A, sections were incubated with PBS containing 0.1% TritonX-100 (PBS-Triton) for 30 minutes. In protocol B, slides were incubated in -20˚C acetone for 10 minutes, dipped in deionized water, and incubated in PBS for 5 minutes. Protocol C consisted of protocol B followed by treatment with 10 mM sodium citrate tribasic dihydrate containing 0.1% Tween-20, pH 6.0, for 40 minutes in an Aroma kitchen steamer. O/N, overnight.

Antibody	Company and catalog number	Concentration	Application
CF647 goat α-mouse IgG (H+L)	Biotium 20281	1:2000	IHC, 2˚
Alexa Fluor 568 donkey α-rabbit IgG (H+L)	Thermo Fisher Scientific A10042	1:2000	IHC, 2˚
CF647 goat α-mouse IgG1	Biotium 20252	1:2000	IHC, 2˚
Alexa Fluor 555 goat α-mouse IgG (H+L)	Thermo Fisher Scientific A21424	1:2000	IHC, 2˚
Alexa Fluor 555 goat α-rabbit IgG (H+L)	Thermo Fisher Scientific A21429	1:2000	IHC, 2˚
Alexa Fluor 568 goat α-rabbit IgG (H+L)	Thermo Fisher Scientific A11011	1:2000	IHC, 2˚
Alexa Fluor 488 goat α-rabbit IgG (H+L)	Thermo Fisher Scientific A11034	1:2000	IHC, 2˚
Alexa Fluor 647 goat α-Guinea Pig IgG (H+L)	Thermo Fisher Scientific A21450	1:2000	IHC, 2˚
Alexa Fluor 555 goat α-mouse IgG2a	Thermo Fisher Scientific A21137	1:2000	IHC, 2˚
Rabbit α-human N-terminal RCOR1	Dr. Gail Mandel laboratory	10 ul/rxn	IP
Normal rabbit IgG	Jackson ImmunoResearch 011-000-002	1 ul/rxn	IP
Guinea pig α-INSM1	Gift from Dr. Carmen Birchmeier	1 ul/rxn	IP
Normal guinea pig serum	Jackson ImmunoResearch 006-000-001	1 ul/rxn	IP
Rabbit α-human RCOR2	Dr. Michael Rosenfeld laboratory	1 ul/rxn	IP
Normal rabbit serum	Jackson ImmunoResearch 011-000-120	1 ul/rxn	IP
Mouse α-human RCOR1	NeuroMab clone K72/8	1:1000	WB, 1˚
Rabbit α-human RCOR2	Dr. Michael Rosenfeld laboratory	1:10,000	WB, 1˚
Rabbit α-histone H3	Cell Signaling 9715	1:1000	WB, 1˚
Rabbit α-human N-terminal RCOR1	Dr. Gail Mandel laboratory	1:1000	WB, 1˚
Guinea pig α-INSM1	Gift from Dr. Carmen Birchmeier	1:10,000	WB, 1˚
Donkey α-guinea pig IgG (H + L) HRP	Jackson ImmunoResearch 706-035-148	1:10,000	WB, 2˚
Mouse α-rabbit IgG (L) HRP	Jackson ImmunoResearch 211-032-171	1:2000	WB, 2˚
DyLight 680 goat α-rabbit IgG (H+L)	Thermo Fisher Scientific 35569	1:5000	WB, 2˚
IRDye800 goat α-mouse IgG (H+L)	Rockland 610-132-121	1:5000	WB, 2˚

Table 2.3. Secondary antibodies for immunohistochemistry and antibodies for immunoprecipitation and Western blotting.

Gene symbol	Gene name	Transcript accession numbers (UCSC Genome Browser)	Forward	Reverse	Intron-spanning	Amplifies all transcripts?
Celsr3	cadherin EGF LAG seven-pass G-type receptor 3	uc009rrb.1, uc009rrc.2	TGCTGTGAGGACAGCTCCTA	CTTCAGGACCAGTCGGAAAC	no	yes
Chrnb2	neuronal acetylcholine receptor subunit beta-2	uc008qaa.2	GATGATGACCAGAGTGTGAGG	GGTCCCAAAGACACAGACAA	yes	yes
Fam65b	family with sequence similarity 65, member B	uc007pwa.2, uc007pwb.2, uc007pwc.1, uc007pwd.1, uc007pwe.1, uc011yxo.2, uc033glb.1	CCGCAGCTACAAGGAATACA	CCAGCCAGACCTTTCATCTT	yes	yes
Gad2	glutamate decarboxylase 2	uc008ini.1, uc008inj.1, uc008ink.1	CTGTGCGCTCTGCTCTATG	AGAAACGCGTAGTTGACATCC	yes	yes
Prox1	prospero homeobox protein 1	uc007ebc.2, uc033fol.1	AAAGAACAGAAGCGAGAGGAG	GCTGTCATAGACCTGGTAGAAC	no	yes
Scrt1	transcriptional repressor scratch 1	uc007wko.1	GGTCAAACTTGACACATTCTCTTC	CGTAGTCACTGAGGTATCCTTTATC	yes	yes
Trim67	tripartite motif-containing protein 67	uc012gmz.1	CCCATACCAACAGGACTGAAG	CTGTTGCCCATTGATGAAGAAG	yes	yes
Unc13a	unc-13 homolog A	uc009mej.2, uc033jgb.1, uc033jgc.1	GAAGGTGCAGAACGTGAAGA	GCGGTTGATCTCAAACATGAAG	yes	yes
Rest	restriction 1 element silencing transcription factor	uc008xvz.2, uc008xwa.2	GGCTGCTCTCAAGGAGTCTG	TTCTGCTCAGTGTCCACGTC	no	no (not uc029vis.1)
Aip	aryl-hydrocarbon receptor-interacting protein	uc008fyp.2, uc008fyq.2	ATGCGTGAGGGGGAGATT	TGGCCACTAGAGGATACAGGAC	yes	yes
Cxxc1	CXXC finger 1	uc008fpg.1	TCTGTGAGCGGAGATATGGA	TCCCCATTCTCAGACTTGCT	yes	yes
Rn45s	45S pre-ribosomal RNA	uc012ath.2	CGGACACGGACAGGATTGACA	ACCACCCACGGAATCGAGAAA	no	yes
Rps20	ribosomal protein S20	uc008rwn.2	GGCATTTAAAGATACCGGAAAG	GTCCGCACAAACCTTCT	yes	yes

Table 2.4. RT-qPCR primers.

CHAPTER 3: REST CO-REPRESSORS 1/2 IN THE DEVELOPING NERVOUS SYSTEM

This and the subsequent chapter constitute an expanded version of the following submitted manuscript:

Association of the REST co-repressors RCOR1 and RCOR2 with the transcriptional repressor INSM1 regulates the balance of proliferation and differentiation in developing brain

Caitlin E. Monaghan, Tamilla Nechiporuk, Sophia Jeng, Shannon McWeeney, Jianxun Wang, Michael G. Rosenfeld, and Gail Mandel

T.N., G.M., and I designed research. I performed research and analyzed data. J.W. and M.G.R. contributed the *Rcor2*$^{fl/fl}$ mouse and discussed results. S.J. and S.M. performed bioinformatics. G.M. and I wrote the paper.

3.1 Introduction

For my thesis work, I investigated the roles of RCOR1 and RCOR2 using knockout mice. To circumvent the potential for redundancy, I primarily used mice lacking both RCOR1 and RCOR2 in nestin+ neural progenitors (*Rcor1/2* KOs) to circumvent the potential for redundancy. The mice die perinatally and have smaller brains. The neural progenitor domains are greatly expanded in the embryonic brain, reflecting excessive self-renewal of the progenitors, and numbers of mature neurons and oligodendrocyte progenitors are reduced significantly compared to controls.

3.2 RCOR1 and RCOR2 are each expressed in nearly all telencephalic neurons at E13.5 and E18.5

At E13.5, RCOR1 is expressed nearly ubiquitously, and at uniform levels in neural progenitors (Fig. 3.1*A*). It appears to be expressed at approximately the same level, or a slightly lower level, in the mantle. Its expression is particularly high in cells identified as endothelial cells on the basis of their morphology (Fig. 3.1*B*-*D*), as well as meningeal cells and cells in the head mesenchyme. A small number of cells express no RCOR1. These have especially round nuclei and are found inside blood vessels (Fig. 3.1*E*-*G*). In most cells, RCOR1 is dispersed throughout the nucleus. However, its localization is more restricted in cells lining the lateral ventricle, likely apical neural progenitors (Fig. 3.1*H*-*J*).

RCOR2 is ubiquitously expressed in the brain at E13.5 (Fig. 3.1*K*), but its expression level varies between cells in the neural progenitor domain. Periventricular progenitors exhibited a wide range of RCOR2 expression levels,

with most having relatively low expression. In contrast, abventricular progenitors and neurons consistently expressed high levels of RCOR2. Like RCOR1, RCOR2 is distributed throughout the nucleus in most cells, but its localization is restricted within the nucleus in two distinct subsets of cells likely to be apical (Fig. 3.1*L-N)* and basal progenitors (Fig. 3.1*O-Q)*, respectively.

At E18.5, RCOR1 remains expressed in nearly all cells in the forebrain (Fig. 3.2). However, there appears to be increased variability in nuclear intensity between cells in different regions. For instance the deep layers of the cortex are markedly brighter than the upper layers. In contrast, RCOR2 expression is restricted to certain cells at E18.5 (Fig. 3.2). The most intense RCOR2 labeling appears in the deep layers of the neocortex, the subplate and intermediate zone of the neocortex, the pallial VZ/SVZ, many subpallial VZ/SVZ cells, a subset of cells near the midline at the anterior-posterior level of the ventral hippocampal commissure, and ventral hippocampal commissure cells. Weaker staining is visible in the upper layers of the neocortex, some subpallial VZ/SVZ cells, and the striatum.

3.3 Loss of *Rcor1* in the developing brain has little effect on brain development

Dr. Huilan Yao, a previous student in the Mandel lab, investigated the germline *Rcor1* knockout, and found that loss of *Rcor1* causes hematopoietic defects that kill 75% of knockouts by E16.5 (Yao et al., 2014). The Mandel laboratory therefore initiated a conditional approach to study loss of *Rcor1* in the brain. Dr. Tamilla Nechiporuk generated mice lacking RCOR1 in neural cells by

combining the floxed *Rcor1* line (*Rcor1*^{fl})(Yao et al., 2014), in which Cre-mediated recombination produces a null allele, with a Nes-Cre line (Tronche et al., 1999). Dr. Yao analyzed their phenotypes, examining brain morphology, and measuring body weight, activity levels, and memory formation in the context of a fear conditioning trial. She found no evidence that *Rcor1*$^{fl/fl}$; Nes-Cre mice (hereafter, *Rcor1* KOs) differed from heterozygotes or floxed controls.

Given that Fuentes et al. (2012) observed transient phenotypes in *in vivo* *Rcor1* knockdown experiments, I examined the morphology of the E18.5 *Rcor1* KO brain using hematoxylin and eosin (H&E) staining. Hematoxylin stains nucleic acids blue or purple, while eosin stains protein pink (Fischer et al., 2008). I found that that three of six *Rcor1* KOs had small clefts in the ventricular zone (VZ) of the lateral subpallium that were not present in Nes-Cre controls (Fig. 3.3). Clefts were defined as distinct indentations in the surface of the ventricular zone. Of the three affected mice, one had bilateral clefts, while the other two had unilateral clefts. These clefts were mildly reminiscent of interganglionic sulci (IGS), which separate the LGE and MGE until these structures coalesce between E15.5 and E16.5. This suggests that cell migration is perturbed in some *Rcor1* KOs. However, because the process by which the LGE and MGE fuse has not been previously described, I do not know the identity of the affected cells.

Surprisingly, despite examining coronal sections at several rostral-caudal positions, I was unable to identify any other features that differed between *Rcor1* KOs and Nes-Cre controls.

3.4 Loss of Rcor2 in the developing brain causes no abnormalities in brain morphology

Dr. Yao also made *Rcor2*$^{fl/fl}$; Nes-Cre mice (hereafter, *Rcor2* KOs), using a conditional *Rcor2* mouse line generated by Dr. Jianxun Wang in Dr. Michael Rosenfeld's laboratory at the University of California, San Diego (Fig. 2.1). She used a conditional allele because Dr. Wang had found that germline knockouts died at mid-embryonic stages (personal communication). Like the consequences of the *Rcor1* conditional KO, H&E staining of the *Rcor2* KO did not reveal any consistent differences between *Rcor2* KOs and Nes-Cre controls at E18.5 (Fig. 3.3). However, Dr. Yao believes that *Rcor2* KO mice are infertile and smaller than littermates in adulthood.

3.5 Generation of a brain-targeted *Rcor1/2* conditional knockout

Hypothesizing that the lack of clear phenotypes in the individual RCOR KOs was due to compensating for each other, the lab generated an *Rcor1*$^{fl/fl}$; *Rcor2*$^{fl/fl}$; Nes-Cre mouse (*Rcor1/2* KO). If *Rcor1* and *Rcor2* share functions, I would predict the *Rcor1/2* KO to show phenotypes absent in each single knockout. PCR analysis of brain genomic DNA confirmed the expected excision events in the *Rcor1/2* KO. Western blot analysis of nuclear extracts from E13.5 brain showed that RCOR1 and RCOR2 protein levels were reduced to 27.3 ± 13.9% and 16.6 ± 10.1% of control levels, respectively (Fig. 3.4*A* and 3.5; four mice/genotype). The reduced protein levels were reflected at the level of immunohistochemistry at E13.5 (Fig. 3.4*B*). Importantly, the ventricular and subventricular zones (VZ/SVZ) of the lateral subpallium (ganglionic eminences),

the focus of this study, as indicated in the introduction, were almost entirely devoid of both RCOR1 and RCOR2. RCOR1 and RCOR2 were still present in some cells of the ventral hippocampus/dorsal septum, cortex, and subpallial mantle (Fig. 3.4*B*). However, by E18.5, very few cells in the *Rcor1/2* KO expressed either RCOR1 or RCOR2 (Fig. 3.6). RCOR1 expression was limited to cells in the ventral hippocampus/dorsal septum and endothelial cells, while RCOR2 expression was limited to cells in the ventral hippocampus/dorsal septum and the neocortex (Fig. 3.6). It is likely that the presence of RCOR1 and RCOR2 in some cells in the KO represent mosaicism of the Cre expression and the cell-type specificity of the nestin promoter.

3.6 Deletion of both *Rcor1* and *Rcor2* genes results in embryonic lethality and diminished brain weight

Although *Rcor1/2* KO mice all died by P1, they were present at Mendelian ratios at E18.5 (22.7% of live pups), which indicates that they died between E18.5 and P1. *Rcor1/2* KO pups had normal body weights at E18.5 (wild-type, 1029 ± 99 mg, 13 pups; Nes-Cre, 1022 ± 105 mg, 17 pups; *Rcor1/2* fl, 1149 ± 59 mg, 8 pups; $Rcor1^{fl/fl}$; $Rcor2^{fl/wt}$; Nes-Cre, 1083 ± 95 mg, 6 pups; *Rcor1/2* KO, 1130 ± 59 mg, 6 pups). However, *Rcor1/2* KO brain weights were reduced to 82%-85% of those of controls (Fig. 3.7*A*; wild-type, 67.8 ± 4.6, 13 pups; Nes-Cre, 68.4 ± 3.8 mg, 17 pups; *Rcor1/2* fl, 70.7 ± 4.7 mg, 11 pups; $Rcor1^{fl/fl}$; $Rcor2^{fl/wt}$; Nes-Cre, 69.5 ± 3.1 mg, 9 pups; *Rcor1/2* KO, 57.8 ± 3.7 mg, 14 pups). Unfixed bodies and brains were used for this analysis.

To determine when *Rcor1/2* KO brain weights first differed from those of

controls, I weighed brains at E14.5, E15.5, E16.5, and E18.5 (Fig. 3.7*B*). *Rcor1/2* fl and *Rcor1*$^{fl/fl}$; *Rcor2*$^{fl/wt}$ embryos were combined to make the control group. For this analysis, I used brains that had been fixed overnight. As a result, the brain weights cannot be compared to those in Fig. 3.7*A*. At E14.5, *Rcor1/2* KO brains were already lighter than those of controls (controls, 37.5 ± 3.0 mg [11 mice]; KOs, 31.3 ± 4.1 mg [5 mice]; p = 0.0233). Surprisingly, while the KO brains trended toward being smaller at E15.5 and E16.5, this difference was not significant (E15.5; controls, 47.5 ± 5.0 mg [5 mice]; E15.5 KOs, 41.1 ± 4.6 mg [7 mice]; E15.5, p = 0.0541; E16.5 controls, 65.2 ± 5.1 mg [11 mice]; E16.5 KOs, 62.33 ± 4.8 mg [4 mice]; E16.5, p = 0.3589). At E18.5, in contrast, brain weights significantly lower than control brain weights (controls, 104.1 ± 6.1 mg [12 mice]; KOs, 79.2 ± 2.0 mg [3 mice]; p < 0.0001), consistent with the analyses of fresh brain weights.

3.7 The *Rcor1/2* knockout has abnormal brain morphology

Morphologically, the E18.5 *Rcor1/2* KO brains differed from those of Nes-cre and *Rcor1/2* fl controls in numerous ways (Fig. 3.8 and 3.9). Notably, the VZ/SVZ, especially in the subpallium, were disproportionately large. Further, the interganglionic sulcus (IGS), which is the cavity separating the LGE and MGE until these structures coalesce between E15.5 and E16.5, persisted in the *Rcor1/2* KO at E18.5. The circumference of the lateral ventricle appeared to be increased. In addition, the neocortices in the KO brains were abnormally thin, and the striatum was small. Multiple axonal tracts were also affected: the corpus callosum never fully developed, axons traversing the striatum were either

defasciculated or absent, and the anterior commissure was unusually narrow (Fig. 3.8 and 3.9). In the hippocampus, the dentate gyrus and CA3 failed to develop into distinct structures. The thalamus and hypothalamus were hypoplastic (Fig. 3.9). Taken together, these abnormalities demonstrate that telencephalic development in the *Rcor1/2* KO was severely compromised. Further, these phenotypes were very different from those of the *Rest* KO, as will be discussed in greater detail in the discussion.

3.8 *Rcor1/2* knockouts have more neural progenitors than *Rcor1/2* fl controls

We hypothesized that the dramatic expansion of the subpallial VZ/SVZ in the KO was due to excessive proliferation. To test this hypothesis, I labeled sections from E18.5 brain with an antibody directed against MKI67 (Ki67), a marker for proliferating cells (Fig. 3.10*A*). Because the MKI67+ cells were not distributed homogeneously in the KO, I first measured the width between the lateral ventricle and the basal edge of the MKI67+ region in the lateral subpallium. The width was ~2.7 times as large in the *Rcor1/2* KO as in the controls (Fig. 3.10*B*; Nes-Cre, 149 ± 36 μm; *Rcor1/2* fl, 159 ± 42 μm; *Rcor1/2* KO, 412 ± 18 μm; five mice/genotype). In contrast, single knockouts had MKI67+ zones roughly comparable to those of controls (*Rcor1* KO, 142 ± 15 μm; *Rcor2* KO, 183 ± 37 μm; five mice/genotype).

The increase in width in the KO reflected higher numbers of both proliferating cells (*Rcor1/2* fl, 686 ± 273 MKI67+ cells; *Rcor1/2* KO, 1470 ± 141 MKI67+ cells; $p = 0.0023$) and non-proliferating cells (*Rcor1/2* fl, 280 ± 67 MKI67-

cells; *Rcor1/2* KO, 1212 ± 166 MKI67- cells; $p < 0.0001$; five mice/genotype; these cell counts were graciously performed by Susan Kim). The presence of additional MKI67+ cells in the *Rcor1/2* KO at E18.5 could indicate a deficit in cell cycle arrest, while the retention of many MKI67- cells in the VZ/SVZ could indicate deficits in neuronal and/or oligodendroglial specification and/or migration.

To better assess the distribution of MKI67+ cells, I quantified the numbers of these cells as a function of distance from the lateral ventricle (Fig. 3.10*C*; three mice/group). *Rcor1/2* KOs had significantly more proliferating cells than controls in two regions: 60-120 μm and 220-360 μm from the ventricle, with the latter constituting a much larger difference. Further, these data verify that the expanded progenitor zone of the *Rcor1/2* KO is not homogeneously filled with proliferating cells. There is a region with a moderate density of proliferating cells (18 cells/bin) from 200-280 μm between two regions of higher density (20-200 μm, 36 cells/bin; 280-380, 25 cells/bin). The MKI67+ zone was also enlarged in the septum (medial subpallium), although to a lesser extent than in the lateral subpallium (Fig. 3.10*D*; three mice/group).

The increase in MKI67+ cells strongly suggested that large numbers of cells were retained in the cell cycle in the *Rcor1/2* KO. To confirm that these cells were actively proliferating, I also stained sections with antibodies recognizing PCNA (proliferating cell nuclear antigen), another proliferation marker, and phosphorylated histone H3 serine 10, a marker of mitotic cells (Fig. 3.11). This experiment confirmed that augmented numbers of cells were actively dividing in the *Rcor1/2* subpallium.

Next, I used *in situ* hybridization histochemistry and immunohistochemistry to confirm that the expanded population of proliferating cells consisted of neural progenitors, and to ascertain whether a specific subpopulation of subpallial neural progenitors was affected in the *Rcor1/2* KO. More cells in *Rcor1/2* KOs compared to *Rcor1/2* fl controls expressed *Dlx2* transcripts, and OLIG2, ASCL1 (MASH1), and NKX2-1 proteins, markers for progenitors in the lateral subpallium (Fig. 3.12*A*). This finding suggests that the mechanism preventing cessation of cell division in *Rcor1/2* KOs is common to all subpallial progenitors. Further, the region with lower MKI67+ cell numbers within the expanded MKI67+ zone (*i.e*. ~200-280 μm from the lateral ventricle) also had reduced numbers of *Dlx2*-, OLIG2-, and ASCL1-expressing cells. To test whether this region was filled with interneurons migrating from the MGE to the neocortex, I used *in situ* hybridization to look for the expression of *Lhx6*, which is expressed in such cells (Fig. 3.12*B*). While *Lhx6* expression was abundant in the expanded VZ/SVZ of the *Rcor1/2* KO, I did not observe any accumulation of *Lhx6*-expressing cells in the LGE of the KO.

3.9 *Rcor1/2* knockouts have fewer neurons than *Rcor1/2* fl controls

Given the increased number of progenitors and the smaller brain size in the *Rcor1/2* KO mice at E18.5, I expected *Rcor1/2* KOs to have smaller numbers of differentiated cells. To investigate how neuronal differentiation was affected, I analyzed early and late neuronal markers. The VZ/SVZ of the *Rcor1/2* KO expressed the same markers as that of the *Rcor1/2* fl. Early pan-neuronal markers such as TUBB3 (TUJ1/tubulin beta 3 class III) and DCX (doublecortin)

were expressed at low levels in many VZ/SVZ cells (Fig. 3.13*A*-*B*). The late pan-neuronal marker MAP2 was almost entirely absent from the VZ/SVZ (Fig. 3.13*C*). Measurements of the MAP2+ area in each hemisection show that *Rcor1/2* KOs had ~26% less neuronal territory than *Rcor1/2* fl controls (*Rcor1/2* fl, 5.38 ± 0.36 mm^2; *Rcor1/2* KO, 3.99 ± 0.19 mm^2; five mice/genotype). Reduced brain size presumably explains part of the decrease in MAP2+ territory. Further, normalizing the area of the MAP2+ domain to total area demonstrates that MAP2 occupies a smaller proportion of the total area in *Rcor1/2* KOs than in *Rcor1/2* fl controls (Fig. 3.13*D*; percentage of area occupied by MAP2: *Rcor1/2* fl, 84.9 ± 0.6%; *Rcor1/2* KO, 76.5 ± 1.3%; five mice/genotype).

Closer inspection of the TUBB3 expression pattern in the *Rcor1/2* KO suggested that the region within the VZ/SVZ with the highest density of TUBB3 approximately corresponded to the part of the VZ/SVZ with the lowest density of cells MKI67-, PCNA-, PH3-, *Dlx2*-, and ASCL1-positive cells (Fig. 3.10-3.13). We therefore suspected that many of the cells in this region might be neurons. For further confirmation, I performed immunohistochemistry with antibodies recognizing the early and late medium spiny neuron markers BCL11B/CTIP2 and FOXP1 (Fig. 3.14; Arlotta et al., 2008). Like TUBB3, BCL11B/CTIP2 was expressed at low levels in many VZ/SVZ cells. And within the KO VZ/SVZ, it was expressed at the highest density in a band of cells corresponding to the region with a reduced proportion of progenitors. In contrast, BCL11B/CTIP2 was distributed evenly across the VZ/SVZ of Rcor1/2 fl controls. Although FOXP1 was expressed in many fewer cells in both genotypes, the same pattern was

apparent. FOXP1 was evenly distributed in the *Rcor1/2* fl, but was more highly expressed in the middle of the VZ/SVZ than at its borders in the *Rcor1/2* KO. These results suggest that many of the MKI67-negative cells are medium spiny neurons.

Neuronal markers were also used to examine the axonal phenotype of the *Rcor1/2* KO (Fig. 3.15). L1CAM (L1 cell adhesion molecule) and CNTN2 (contactin 2, also known as TAG-1) are both immunoglobulin superfamily proteins specifically expressed in axons (Rathgen and Schachner, 1984; Moos et al., 1988; Furley et al., 1990). L1CAM expression reveals that the *Rcor1/2* KO has bundles of axons traversing the striatum, but fewer than the control has. Further, the bundles are much smaller than in the control. In the intermediate zone, the *Rcor1/2* KO also has fewer axons. While the bed of axons only narrows slightly to cross the corpus callosum in the control, it narrows dramatically in the *Rcor1/2* KO, and no axons actually cross the midline at this level. CNTN2 expression shows that this is in part because the CNTN2-expressing axons in *Rcor1/2* KOs are diverted or arrested as they approach the site where the corpus callosum would normally be. This suggests that in addition to having fewer neurons, *Rcor1/2* KOs probably also have problems with axon growth or pathfinding.

3.10 *Rcor1/2* knockouts have fewer oligodendrocyte precursor cells (OPCs) than *Rcor1/2* fl controls

To determine whether *Rcor1/2* KOs had fewer Oligodendrocyte Precursor Cells (OPCs), I examined OLIG2 immuno-labeling. Embryonic OLIG2+ cortical

cells are considered to be OPCs that have migrated from the ganglionic eminences (Kessaris et al., 2006). We determined the density of OLIG2+ cells in 3 x 10^4 μm^2 areas within the neocortical Intermediate Zone (IZ), which is the region between the cell-dense SVZ and the cortical subplate (Fig. 3.16). *Rcor1/2* KOs had 70% fewer OLIG2+ cells per unit area than *Rcor1/2* fl controls (Fig. 3.16; in 1.8 x 10^5 μm^2 of IZ representing the sum of six areas: *Rcor1/2* fl, 209 ± 15 cells; *Rcor1/2* KO, 62 ± 23 cells; five mice/genotype). This constitutes the first demonstration that RCOR1/2 are involved in oligodendrogenesis. However, this result is not completely surprising, as previous studies have shown that RCOR1 is bound to overlapping but discrete sets of targets at each sequential stage in oligodendrocyte differentiation (Abrajano et al., 2009a).

3.11 *Rcor1/2* knockouts do not have altered numbers of apoptotic cells

To rule out the possibility that cell death was responsible for a reduced number of differentiated neurons and OPCs in *Rcor1/2* KOs compared to controls, we performed immunohistochemistry for activated caspase 3. We found very few positive cells in either *Rcor1/2* KO or *Rcor1/2* fl brain at E13.5 and E18.5 (data not shown), and none in the striatum at E13.5.

3.12 *Rcor1/2* knockout brains can first be distinguished from control brains at ~E15.5-E16.5

Having established that the *Rcor1/2* KO had a severe brain phenotype at E18.5, I worked backward from that point to discover when the phenotype was first detectable. I did so, first, because this could have revealed distinctions between phenotypes arising at different times, and second, because it could

have unmasked phenotypes diminished by subsequent events. Although brain weights were not substantially different at E16.5 (Fig. 3.7*B*), H&E staining shows that the imbalance between progenitors and differentiated cells had already arisen by then (Fig. 3.17). In fact, these preliminary results indicate that the accumulation of progenitors in the E16.5 *Rcor1/2* KO ganglionic eminence may be even greater at E16.5 than at E18.5. However, at E15.5, preliminary results suggest there is little or no difference between *Rcor1/2* KOs and *Rcor1/2* fl controls (Fig. 3.18). Analysis of additional pups will be necessary to determine whether the genotypes can be distinguished on the basis of morphology at this stage. At E14.5, *Rcor1/2* KOs and *Rcor1/2* fl controls were indistinguishable (Fig. 3.18).

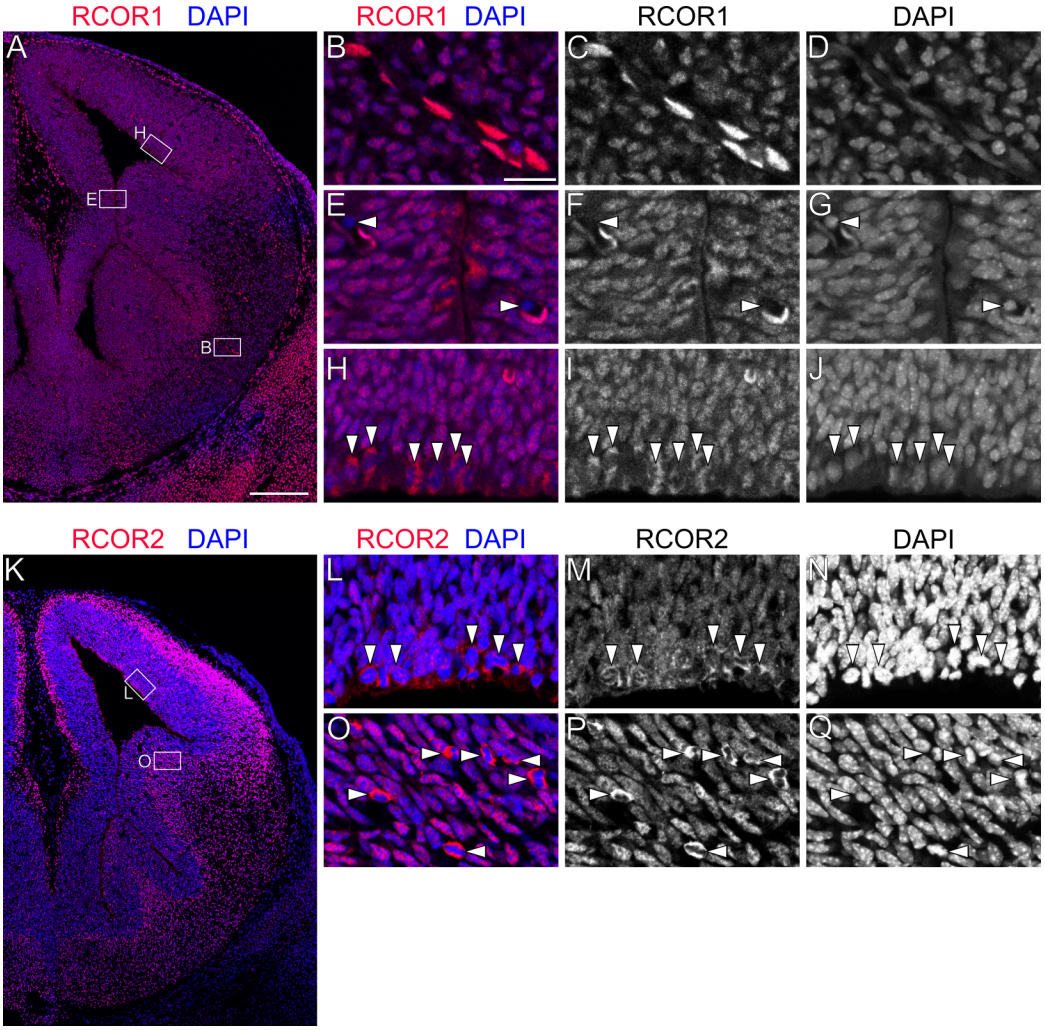

Figure 3.1. RCOR1 and RCOR2 expression in the E13.5 telencephalon. Representative immunohistochemistry on coronal hemisections of control (*Rcor1/2* fl) brains labeled with the indicated antibodies and DAPI to mark nuclei. Boxes indicate regions shown at higher magnification to the right. Scale bars are 200 μm and 20 μm. (*A*) RCOR1 is expressed in nearly every nucleus in the E13.5 brain. (*B-D*) RCOR1 is especially highly expressed in endothelial cells. (*E-G*) Very few nuclei entirely lack RCOR1 expression. Those that do (arrowheads) are inside blood vessels. (*H-J*) Many cortical cells lining the lateral ventricle have a distinctive RCOR1 distribution different from that in other cells. (*K*) RCOR2 is

expressed in nearly every nucleus in the E13.5 brain. (*L*-*N*) RCOR2 is distributed differently in cells lining the lateral ventricle than in most other cells. (*O*-*Q*) Some cells in the LGE (probably basal progenitors) also have an unusual RCOR2 distribution.

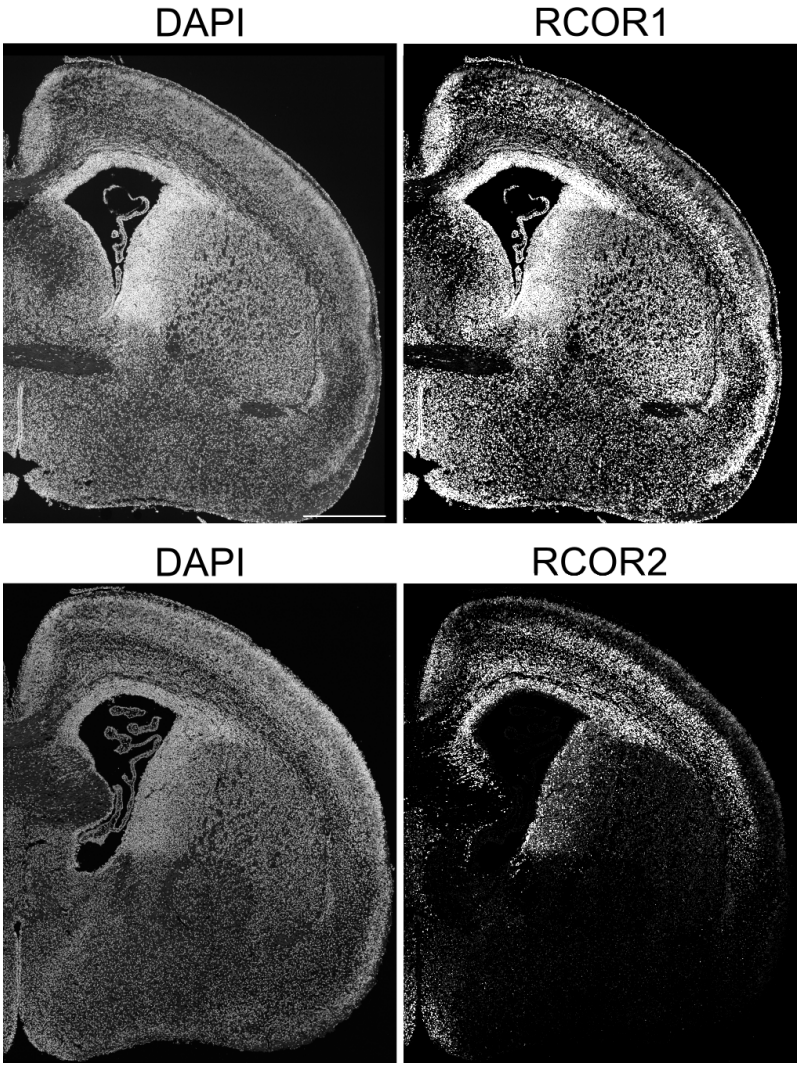

Figure 3.2. RCOR1 and RCOR2 expression in the E18.5 telencephalon.

Representative immunohistochemistry on coronal hemisections of E18.5 control (*Rcor1/2* fl) brains labeled with the indicated antibodies and DAPI to mark nuclei. Scale bar, 500 μm.

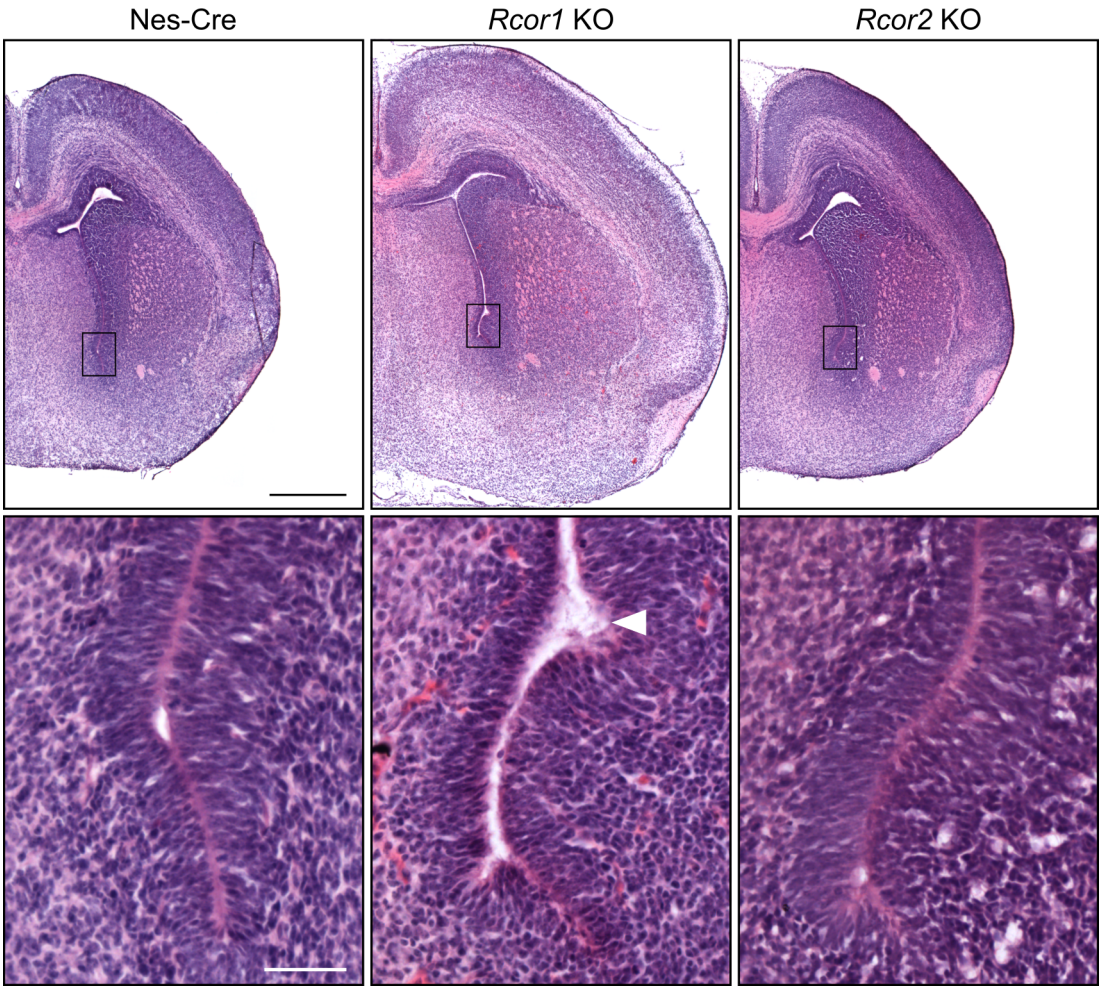

Figure 3.3. Brain phenotypes of *Rcor1* and *Rcor2* knockouts at E18.5.

Hematoxylin and eosin-stained coronal hemisections of telencephalon. Nes-Cre and *Rcor2* KO hemisections are representative. Three of six *Rcor1* KOs, including the one depicted here, had a cleft (arrowhead) at the surface of the ventral ventricular zone/subventricular zone (VZ/SVZ) of the lateral subpallium. In other respects, single *Rcor* KOs were indistinguishable from Nes-Cre controls. Boxes in top panel indicate insets shown below at higher magnification. Scale bars are 500 μm (*top*) and 50 μm (*bottom*).

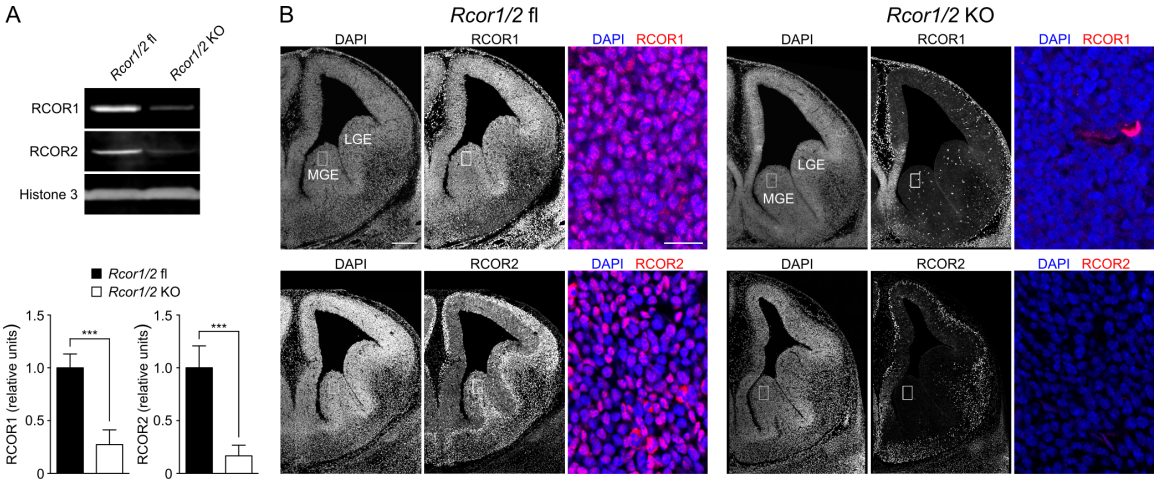

Figure 3.4. Analysis of RCOR1 and RCOR2 expression at E13.5 in the *Rcor1/2* fl and *Rcor1/2* knockout mice. (*A*) Western blot analysis. RCOR1 and RCOR2 levels were normalized to histone H3 levels. The means and standard deviations are indicated. Statistical significance was assessed by t test (n = 4 mice). ***, $p < 0.001$. (*B*) Representative immunohistochemistry on coronal hemisections of control (*Rcor1/2* fl) and *Rcor1/2* KO telencephalon labeled with the indicated antibodies and DAPI to mark nuclei. Boxes indicate regions shown at higher magnification to the right. Scale bars are 200 μm and 20 μm. LGE, Lateral Ganglionic Eminence; MGE, Medial Ganglionic Eminence.

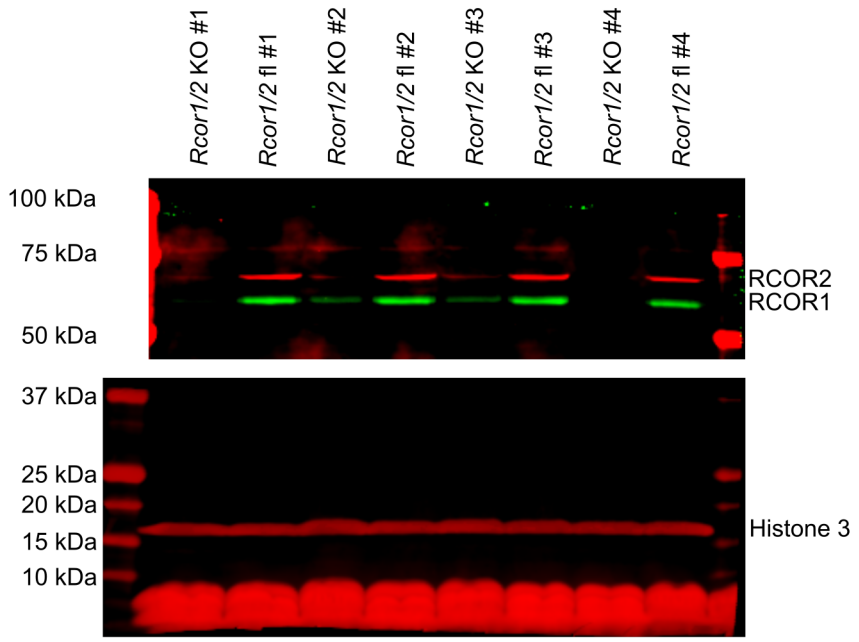

Figure 3.5. Western blot of E13.5 brain of *Rcor1/2* fl controls and *Rcor1/2* knockouts. Blots from which the bands from "*Rcor1/2* fl #2" and "*Rcor1/2* KO #3" were shown in Fig. 3.4.

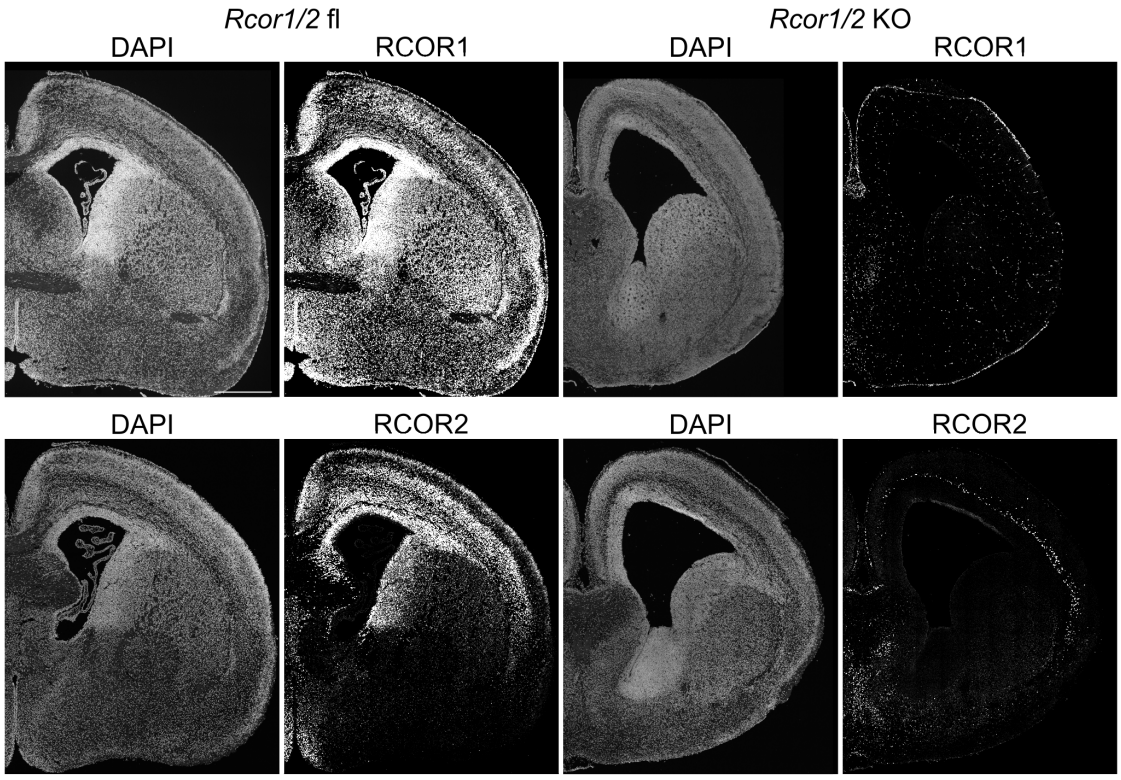

Figure 3.6. Analysis of RCOR1 and RCOR2 expression at E18.5 in the *Rcor1/2* fl and *Rcor1/2* knockout. Representative immunohistochemistry on coronal hemisections of E18.5 control (*Rcor1/2* fl) and *Rcor1/2* knockout brains labeled with the indicated antibodies and DAPI to mark nuclei. Scale bar, 500 μm.

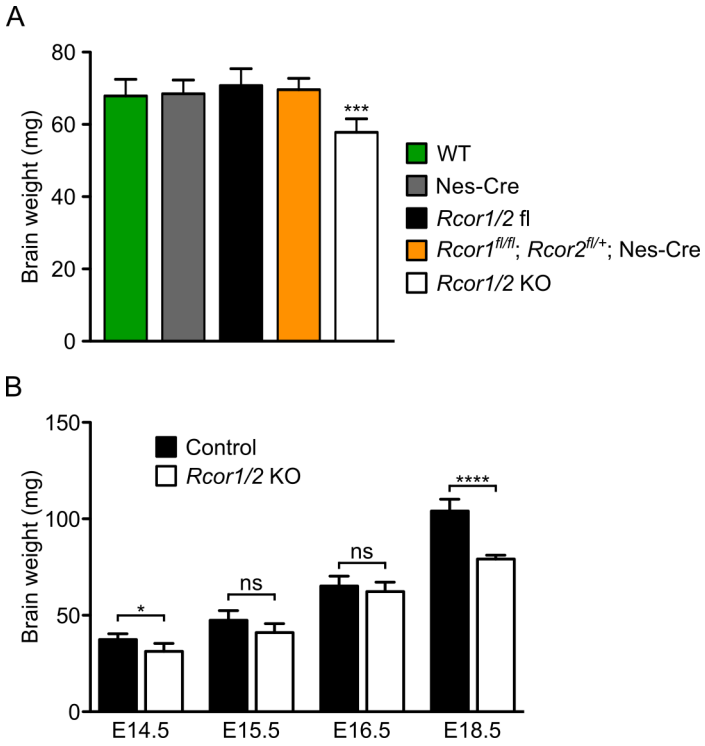

Figure 3.7. Brain weights of *Rcor1/2* knockouts and controls. (*A*) Brain weights of fresh E18.5 brains of the designated genotypes. Statistical significance was assessed using ANOVA followed by Tukey's multiple comparison test. The brain weights of each of the four other genotypes examined were significantly greater than those of *Rcor1/2* KOs ($p < 0.001$). Brain weights of the other four genotypes were not significantly different from one another. (*B*) Brain weights of fixed control (*Rcor1/2* fl and *Rcor1*$^{fl/fl}$; *Rcor2*$^{fl/+}$) and *Rcor1/2* KO brains at the specified timepoints. Statistical significance was assessed using t tests with Welch's correction. *, $p < 0.05$; ****, $p < 0.0001$.

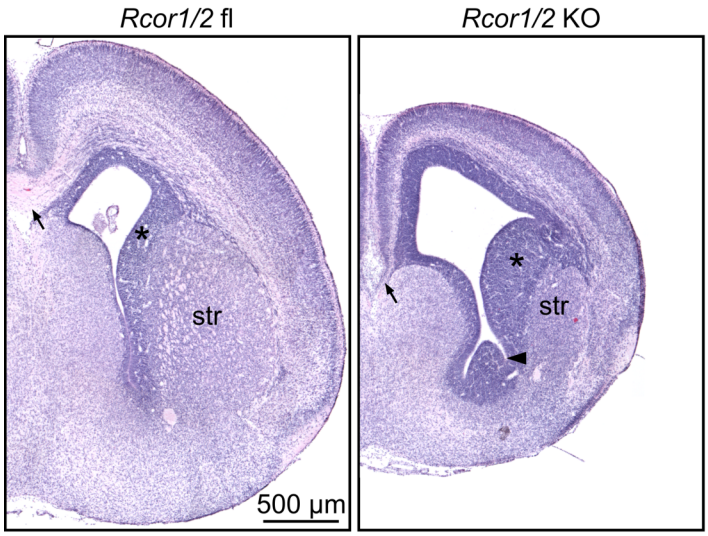

Figure 3.8. Brain phenotypes of *Rcor1/2* knockouts at E18.5. Representative H&E-stained coronal hemisections of *Rcor1/2* fl and *Rcor1/2* KO telencephalon. Note deep interganglionic sulcus (arrowhead), enlarged ventricular/subventricular zones (*), and diminished corpus callosum (arrow) and axonal fasciculation in the striatum (str) in the KO compared to the control.

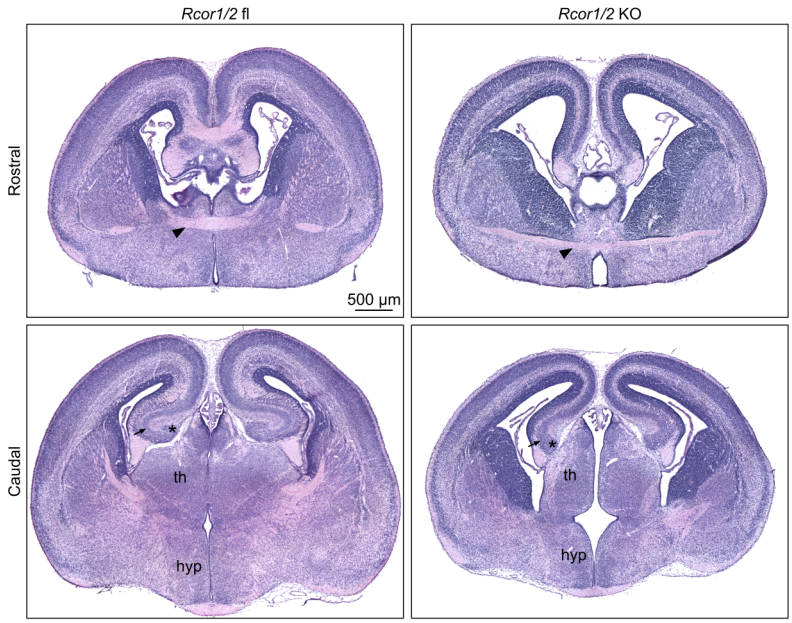

Figure 3.9. Representative H&E-stained coronal sections from the E18.5 *Rcor1/2* fl and *Rcor1/2* knockout. (*Top*) The anterior commissure (arrowhead) is abnormally thin in the *Rcor1/2* KO. (*Bottom*) In the *Rcor1/2* KO, CA3 (arrow) and the dentate gyrus (asterisk) of the hippocampus fail to resolve into distinct structures. The thalamus (th) and hypothalamus (hyp) of the *Rcor1/2* KO are also hypoplastic.

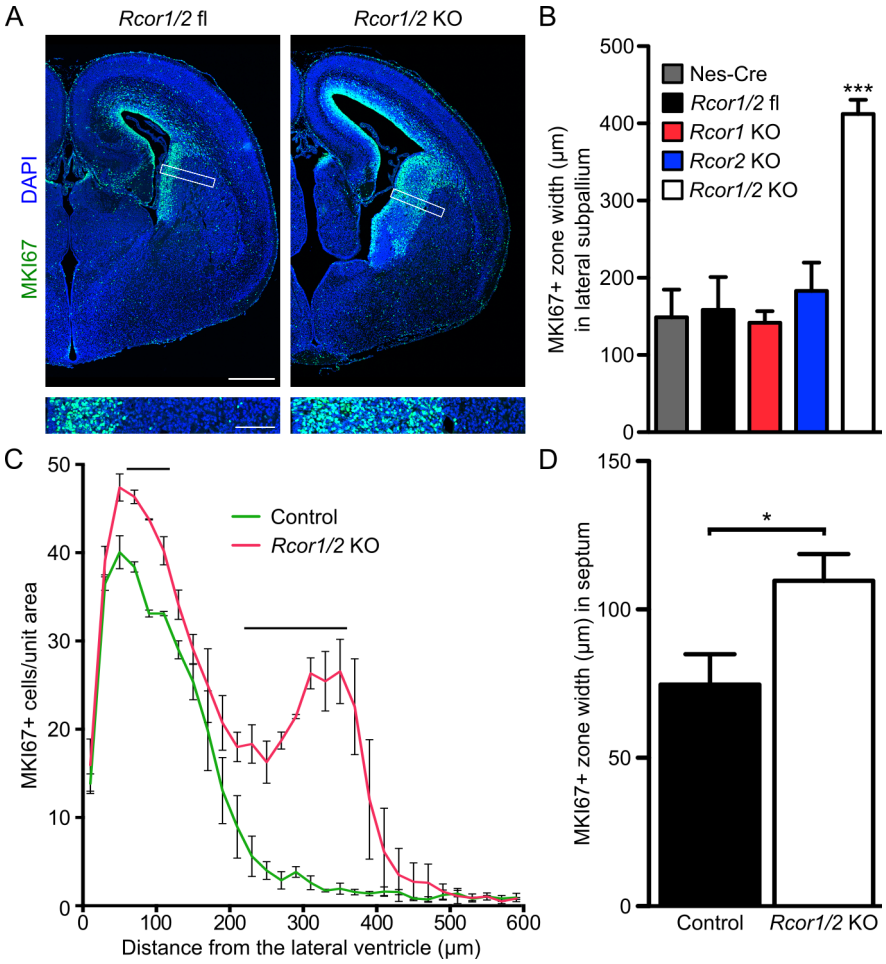

Figure 3.10. Increased numbers of proliferating progenitors in E18.5 brains of *Rcor1/2* knockouts compared to controls. (*A*) Immunohistochemical analysis of the subpallial progenitor region. Boxes indicate insets shown below at higher magnification. Scale bars are 500 μm (*top*) and 100 μm (*bottom*). (*B*) Quantification of the width of the lateral subpallial MKI67+ region in indicated controls and the *Rcor1/2* KO. Measurements were taken from images comparable to insets. The means and standard deviations are indicated. Statistical significance was assessed by ANOVA followed by Tukey's multiple comparison test (n = 5 mice). ***, $p < 0.001$. (*C*) Numbers of MKI67+ cells as a function of distance from the lateral ventricle in controls (*Rcor1*$^{fl/fl}$; *Rcor2*$^{fl/+}$ and

Rcor1/2 fl) and the *Rcor1/2* KO (n = 3 mice). Bars indicate significantly different values. Statistical significance was assessed using t tests with Welch's correction. The means and standard deviations are indicated. (*D*) Quantification of the width of the septal (medial subpallial) MKI67+ region in controls (the *Rcor1*$^{fl/fl}$; *Rcor2*$^{fl/+}$ and the *Rcor1/2* fl) and *Rcor1/2* KOs (n = 3 mice). *, $p < 0.05$.

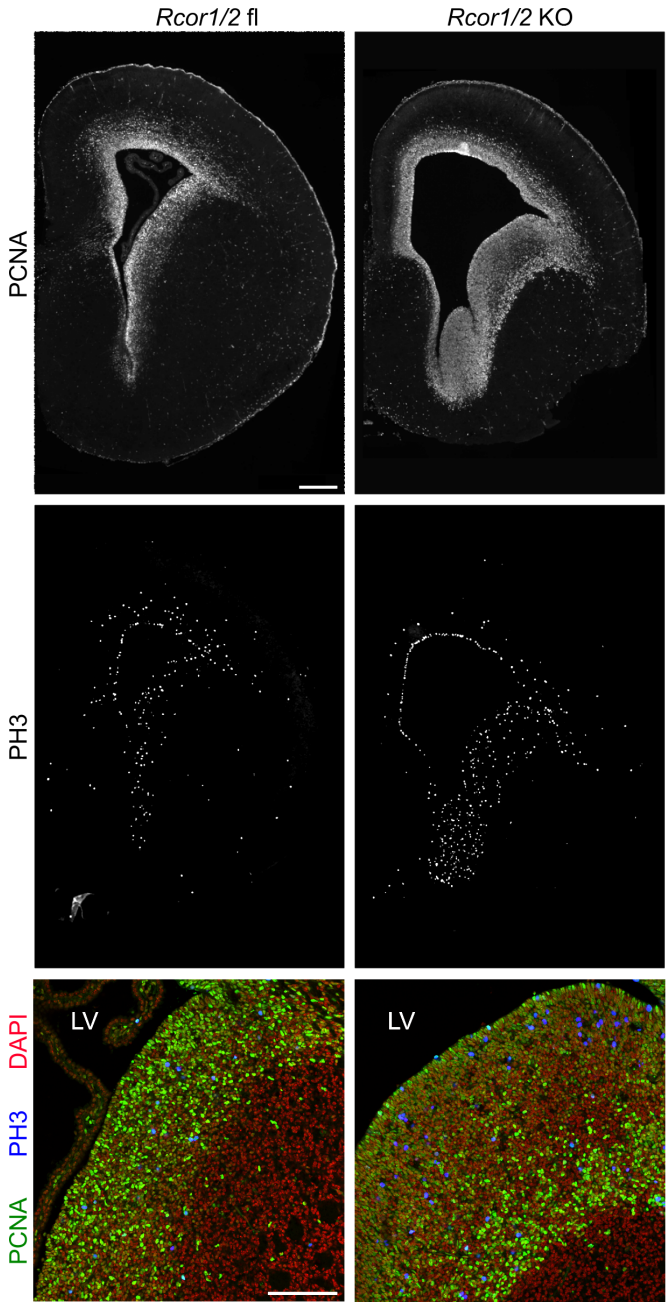

Figure 3.11. Analysis of proliferation and mitotic markers in E18.5 *Rcor1/2* fl and *Rcor1/2* knockout brains. Representative immunohistochemistry on coronal hemisections labeled with the indicated antibodies and DAPI. Scale bars are 200 μm (*top*) and 100 μm.

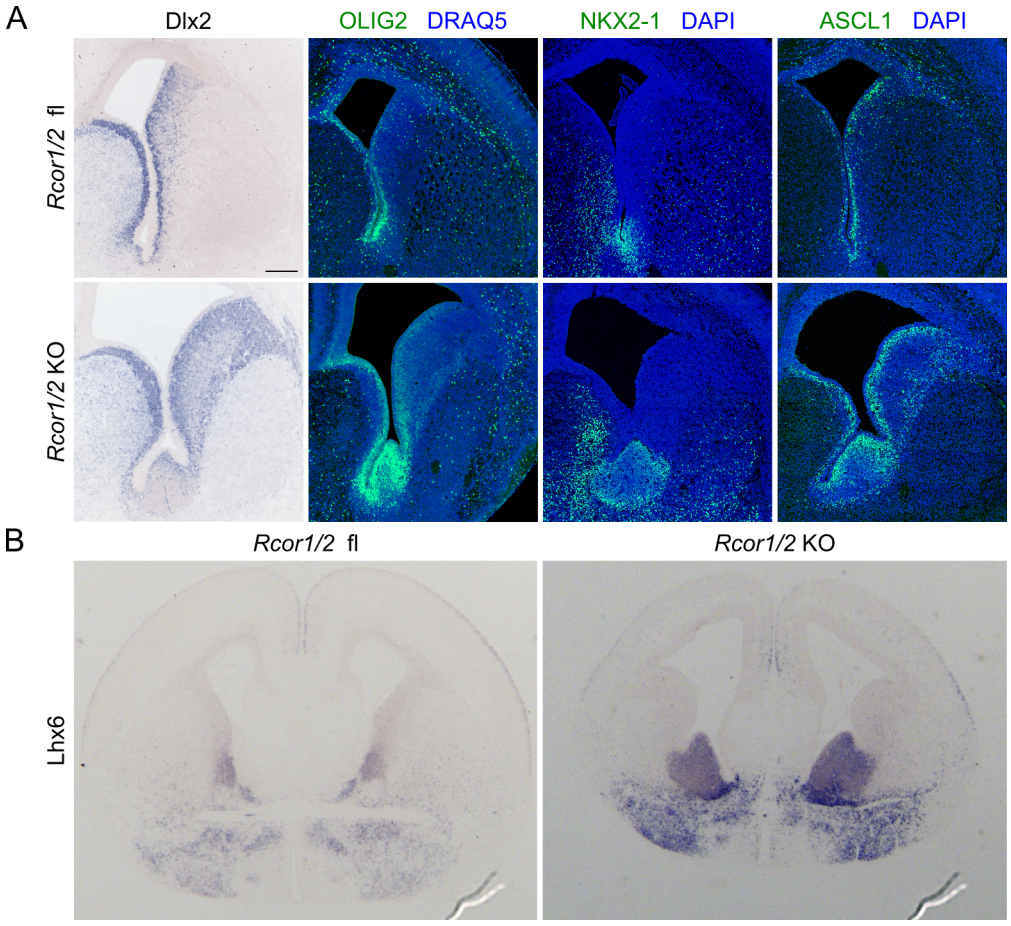

Figure 3.12 Markers expressed in the expanded VZ/SVZ of *Rcor1/2* KOs.

Scale bar, 200 μm. (*A*) Representative *in situ* hybridization for *Dlx2* and immunohistochemistry for OLIG2, NKX2-1, and ASCL1. (*B*) Representative *Lhx6* *in situ* hybridization.

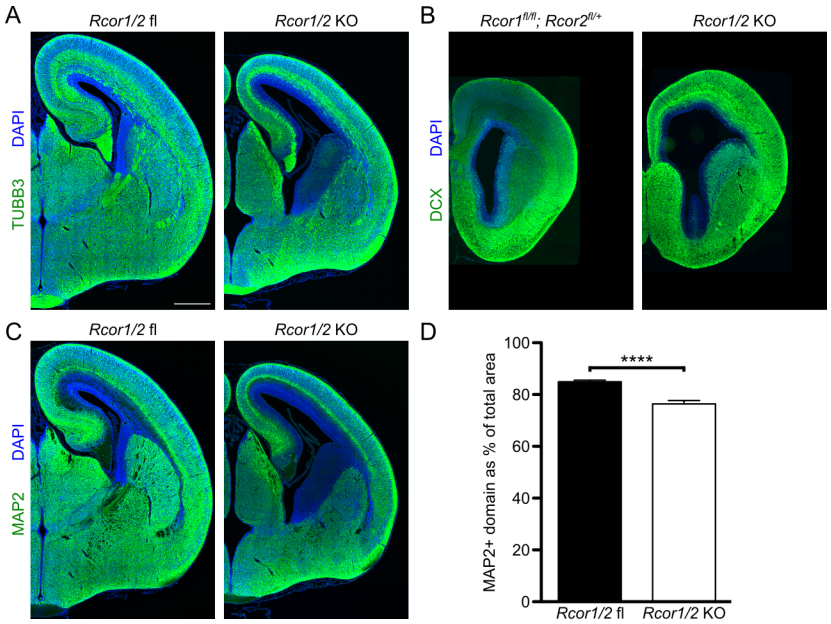

Figure 3.13. *Rcor1/2* knockouts have fewer neurons than controls. All analyses were performed on coronal sections from E18.5 brain. Scale bar, 500 μm. (*A*) Representative images of TUBB3 immunohistochemistry. (*B*) Representative images of DCX immunohistochemistry. The brains shown here were fixed for different durations. Scaling is approximate. (*C*) Representative images of MAP2 immunohistochemistry. (*D*) Quantification of MAP2 immuno-labeling, showing the percentage of each coronal hemisection occupied by the MAP2+ domain. The total area of the section was determined on the basis of DAPI labeling. The means and standard deviations are indicated. Statistical significance was assessed with a t test (n = 5 mice).

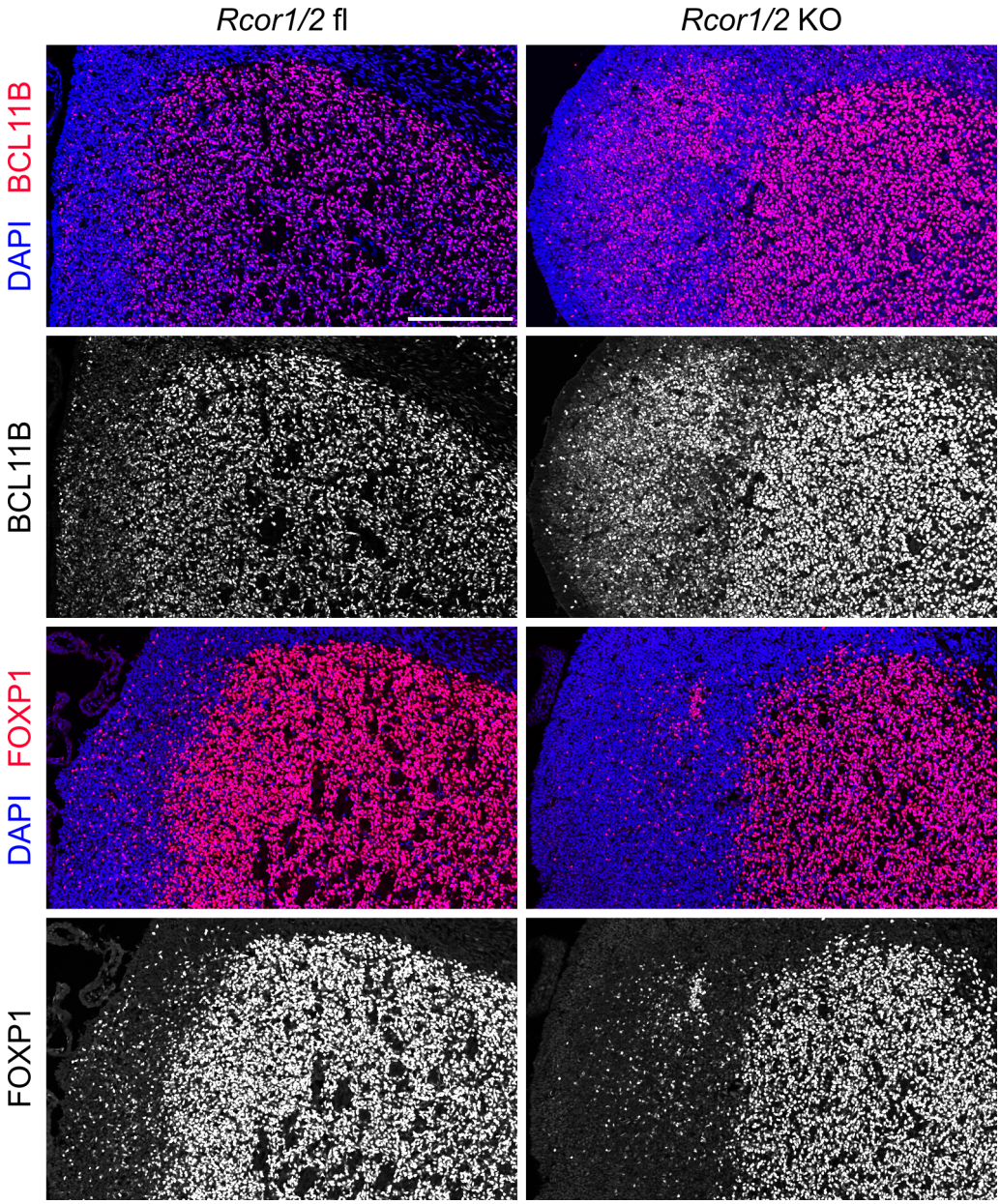

Figure 3.14. Immunohistochemical analysis of striatal markers in *Rcor1/2* fl and *Rcor1/2* knockout mice. Representative immunohistochemistry on coronal hemisections of E16.5 control (*Rcor1/2* fl) and *Rcor1/2* knockout brains labeled with the indicated antibodies and DAPI. Scale bar, 200 μm.

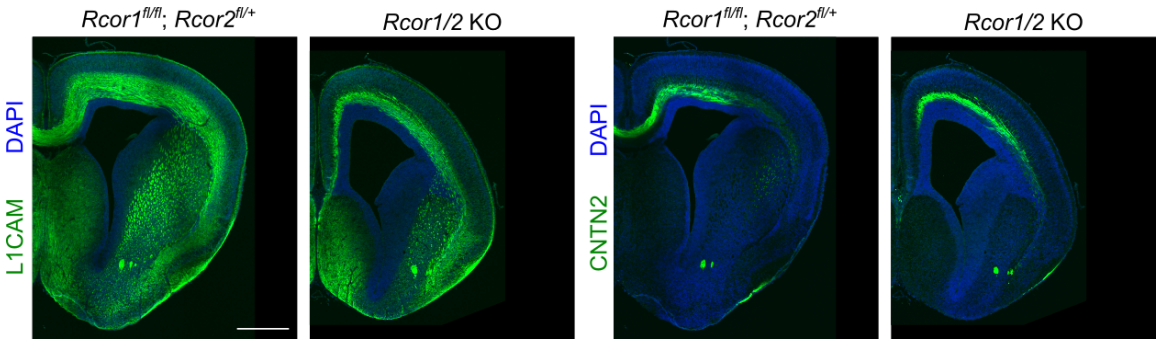

Figure 3.15. Immunohistochemical analysis of axonal markers in *Rcor1/2* fl and *Rcor1/2* knockout mice. (*A*-*B*) Preliminary images of immunohistochemistry with the indicated antibodies. Images may not be representative, as analyses were performed on only one mouse per genotype. Images were kindly acquired by Dr. Paul Barnes. Scale bar, 500 μm.

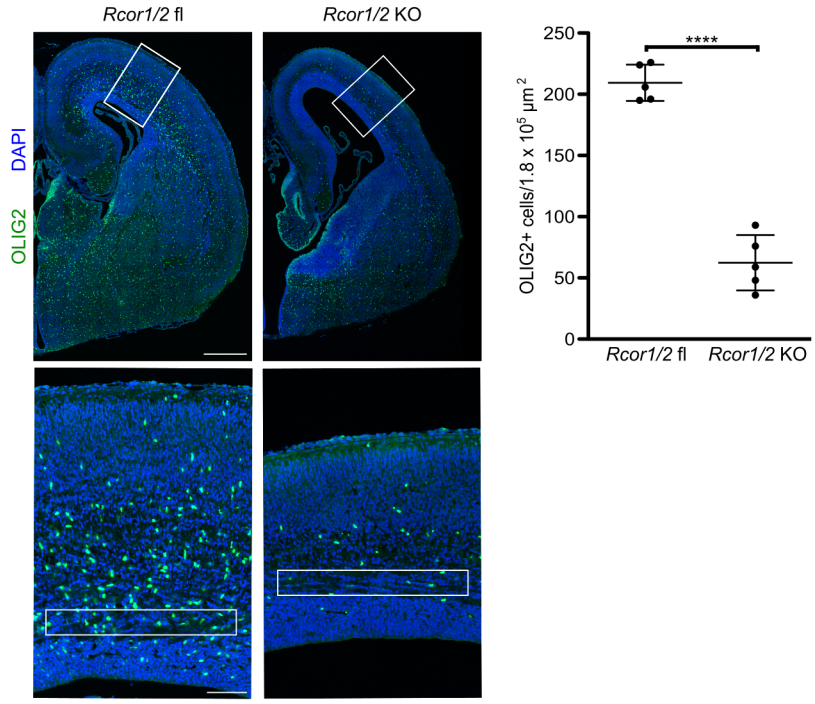

Figure 3.16. OLIG2 immunohistochemistry. (*Left*) Representative image of OLIG2 immunohistochemistry. Boxes in top panel indicate regions shown below at higher magnification. Boxes in bottom panel show the Intermediate Zone (IZ) of the neocortex. Scale bars are 500 μm (*top*) and 100 μm (*bottom*). (*Right*) Quantification of OLIG2+ immuno-labeling in the IZ of the neocortex. For each mouse, one region of 3 x 10^4 μm^2 was selected from each of six hemisections, and the numbers of OLIG2+ cells from all regions were added. Each mouse is represented by one dot. The means and standard deviations are indicated. Statistical significance was assessed by t test (n = 5 mice). ****, $p < 0.0001$.

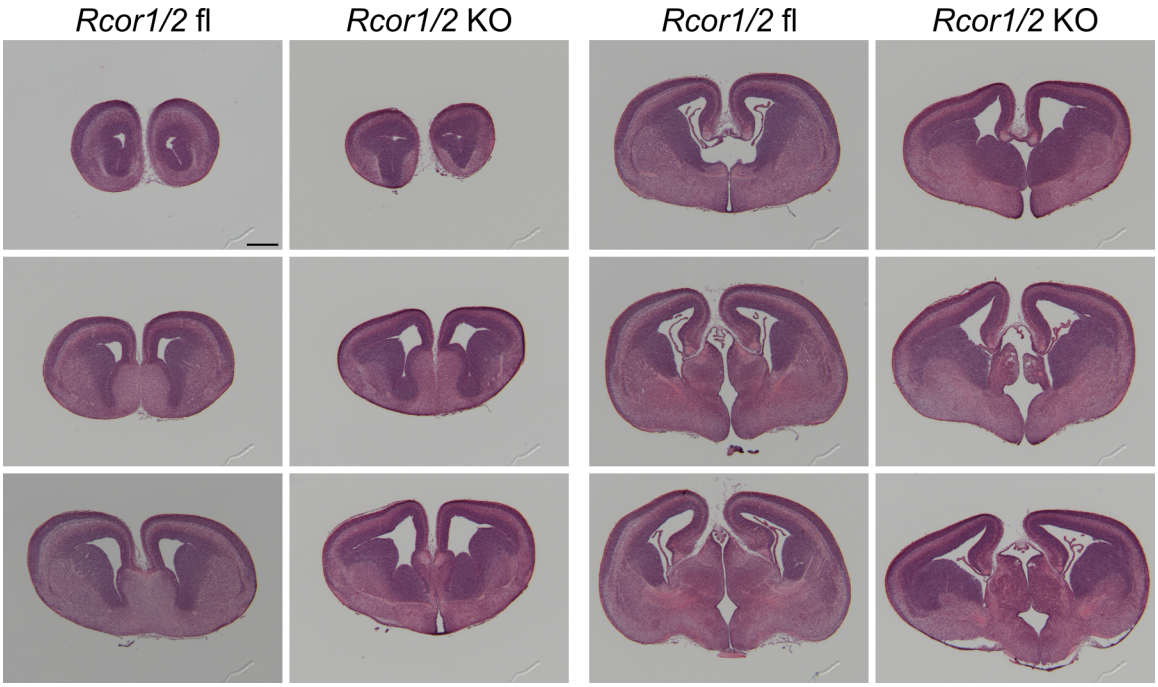

Figure 3.17. Hematoxylin and eosin-stained coronal hemisections of E16.5 *Rcor1/2* fl and *Rcor1/2* KO telencephalon. Six images from each of two mice are shown, arranged rostral-to-caudal in columns. Scale bar, 500 μm.

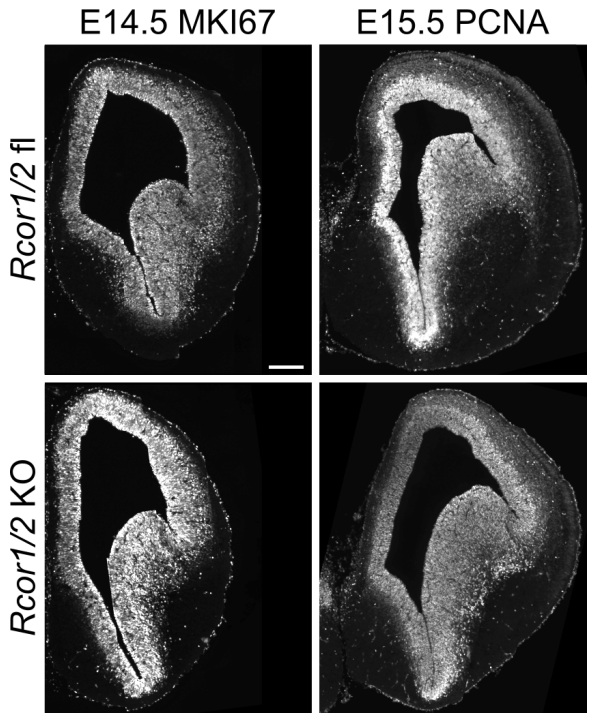

Figure 3.18. The neural progenitor accumulation phenotype is not robust at E14.5 and E15.5. Coronal hemisections of *Rcor1/2* fl and *Rcor1/2* KO telencephalon labeled with proliferation markers (MKI67 at E14.5 and PCNA at E15.5). Scale bar, 200 μm.

CHAPTER 4: INSM1 RECRUITS RCOR1/2 IN THE DEVELOPING SUBPALLIUM

This and the preceding chapter constitute an expanded version of the following submitted manuscript:

Association of the REST co-repressors RCOR1 and RCOR2 with the transcriptional repressor INSM1 regulates the balance of proliferation and differentiation in developing brain

Caitlin E. Monaghan, Tamilla Nechiporuk, Sophia Jeng, Shannon McWeeney, Jianxun Wang, Michael G. Rosenfeld, and Gail Mandel

T.N., G.M., and I designed research. I performed research and analyzed data. J.W. and M.G.R. contributed the *Rcor2*$^{fl/fl}$ mouse and discussed results. S.J. and S.M. performed bioinformatics. G.M. and I wrote the paper.

4.1 Introduction

Knowing that an RCOR complex regulates neuronal and oligodendrocytic differentiation, I wanted to identify the other proteins in this complex. An obvious candidate was KDM1A, a lysine-specific demethylase that co-immunoprecipitates RCOR1 (Shi et al., 2005; Yokoyama et al., 2014), and is co-immunoprecipitated by it (You et al., 2001; Mandel and Liu, unpublished). Further, both KDM1A and RCOR1 are co-immunoprecipitated by many of the same transcription factors, including REST (McGann et al., 2014) and INSM1 (Welcker et al., 2013). However, because RCOR1 functions independently of KDM1A to activate some of its targets (Boxer et al., 2014), we cannot assume that KDM1A is required for RCOR complex activity in the brain. I show here that KDM1A is coexpressed in RCOR1/2-expressing neural progenitors. Interestingly, preliminary data from Dr. Rosenfeld's lab suggests that many of the processes disrupted in the *Rcor1/2* KO are indeed KDM1A-dependent.

I sought to identify the transcription factor(s) that recruit RCOR1/2 in order to promote the transition of neural progenitors into neurons and OPCs. As noted previously, many transcription factors recruit RCOR1 or RCOR2 (Table 1.1 and 1.2). However, in the cases where these factors have been deleted from the developing brain in mice (Guy et al., 2001; Nechiporuk et al., 2016; Roy et al., 2004), the phenotypes did not resemble those of *Rcor1/2* KOs. One exception was the transcriptional repressor INSM1 (Breslin et al., 2002), which has been identified in complexes with RCOR1/2 in an endocrine cell line (Welcker et al., 2013), is expressed in late neural progenitors (Duggan et al., 2008), and has a

germline knockout phenotype that resembles that of the *Rcor1/2* KO (Farkas et al., 2008). However, no link has been established between RCOR1/RCOR2 and INSM1 in the developing nervous system.

In this work, I show that INSM1 is co-expressed with RCOR1 and RCOR2 in a subset of progenitors, and is present in RCOR1- and RCOR2-containing complexes. Furthermore, I characterize the *Insm1*$^{-/-}$ mouse, demonstrating that the predominant phenotypes of the *Rcor1/2* KO are recapitulated in the *Insm1*$^{-/-}$ mouse, and identifying *Rest* as a target of the RCOR-INSM1 complex.

4.2 KDM1A expression in RCOR1/2 expressing cells in the developing subpallium

At E13.5, KDM1A is ubiquitously expressed in the telencephalon (Fig. 4.1 *top left*). It therefore is present in RCOR1/2-expressing neural progenitors. Examination of subpallial progenitors at E18.5 confirms that it is also expressed in all of these cells (Fig. 4.1 *top right*). KDM1A levels were slightly higher in the mantle than in progenitor zones.

Because RCOR1 has been reported to increase the stability of KDM1A (Shi et al., 2005; Lin et al., 2010), I also assessed KDM1A expression in the knockout. As in the control, KDM1A was expressed in all cells examined in the *Rcor1/2* KO at E13.5 and E18.5 (Fig. 4.1 *bottom left* and *right*, respectively). However, the discrepancy between the lower levels in the progenitor zone and the higher levels in the mantle was more striking in the *Rcor1/2* KO, suggesting that RCOR1/2 might be more important for KDM1A stabilization in progenitors than they are in neurons. However, Western blotting would be needed to

determine whether KDM1A levels are lower in *Rcor1/2* KO than *Rcor1/2* fl progenitors.

4.3 The *Kdm1a* knockout exhibits several phenotypes present in the *Rcor1/2* knockout

If KDM1A is required for RCOR1/2 to promote neuronal and oligodendroglial differentiation, a mouse in which Nes-Cre activity drives loss of *Kdm1a* in neural progenitors (*Kdm1a*$^{fl/fl}$; Nes-Cre, henceforth referred to as the *Kdm1a* KO) should exhibit some of the abnormalities apparent in the *Rcor1/2* KO. Our collaborators, Dr. Rosenfeld and Dr. Wang, provided us with images of E18.5 H&E-stained coronal hemisections from *Kdm1a* control and KO brains (Fig. 4.2). These suggested that the *Kdm1a* KO might share several elements of the *Rcor1/2* KO phenotype. The subpallial progenitor zones were enlarged. The circumference of the lateral ventricle was lengthened. The neocortex was thin, and the striatum small. Axon bundles crossing the striatum perpendicular to the section were thinner, and the corpus callosum was thinner. Neither of the latter phenotypes, however, was as pronounced as in the *Rcor1/2* KO (Fig. 3.8), in which the axon bundles were too small to be distinguished from the surrounding tissue, and the corpus callosum was nonexistent. Together, these phenotypes strongly suggested that KDM1A is required for many of the same developmental processes as RCOR1/2. Unfortunately, these sections were too far rostral to indicate whether a vestigial IGS persists in the *Kdm1a* KO.

4.4 INSM1 is co-expressed with RCOR2 in subpallial neural progenitors

To explore the possibility that an RCOR/KDM1A/INSM1 complex

promotes neural differentiation, I first tested whether these proteins were co-expressed in neural progenitors. RCOR1 and KDM1A are expressed nearly ubiquitously, and at uniform levels in neural progenitors (Fig. 3.1, 3.2, 4.1) at both E13.5 and E18.5. Although RCOR2 is also expressed ubiquitously within the brain at E13.5 (Fig. 3.1), its expression level varies between cells in the neural progenitor domain: periventricular progenitors, in particular, exhibited a wide range of RCOR2 expression levels, while abventricular progenitors consistently expressed high levels. At E13.5, INSM1 is not expressed in all progenitors, but resembled RCOR2 in being expressed at a range of levels in periventricular progenitors and more uniformly in abventricular progenitors. Outside of the progenitor cell layer, INSM1 is expressed in a number of cells proximal to the progenitor zone, which I speculate might be newborn neurons. This protein expression pattern is consistent with the mRNA expression pattern described by Duggan et al. (2008). Many cells in the cortical plate express low levels of INSM1 at E13.5, which was not observed at the mRNA level (Duggan et al., 2008). One possible explanation for this discrepancy is that in neurons, INSM1 protein persists after *Insm1* transcription is turned off and its transcripts degraded. Importantly, co-staining for RCOR2 and INSM1 showed that many VZ/SVZ cells had moderate or high expression of both of these proteins (Fig. 4.3).

At E18.5, INSM1 is most highly expressed in a layer within the VZ/SVZ of the neocortex, and in scattered midline cells (at the rostral-caudal level of the hippocampal commissure; Fig. 4.4). It is also expressed in a majority of the VZ/SVZ cells on the basal side of the high-INSM1 layer, as well as most IZ cells.

It is expressed at lower levels in some cells in the cortex, subpallial progenitor region, and midline. Comparison of INSM1 and RCOR2 expression indicates that the layer of neocortical VZ/SVZ cells with the highest INSM1 staining is mostly RCOR2-negative, but a majority of the VZ/SVZ and IZ cells with lower INSM1 signal intensity also express RCOR2. In the subpallial progenitor zone, many INSM1-expressing progenitors co-express RCOR2.

4.5 The Rcor1/2 knockout has increased numbers of INSM1-expressing cells

I have hypothesized that in the *Rcor1/2* KO, the loss of RCOR/INSM1 complex activity prevents some progenitors from leaving the cell cycle and differentiating, and that this leads to the accumulation of progenitors. If the RCOR/INSM1 complex acts cell-autonomously to promote cell cycle exit, then the supernumerary progenitors in the *Rcor1/2* KO would all be predicted to be derived from INSM1+ cells, and would probably continue to express INSM1 themselves.

I therefore examined the expression of INSM1 in the *Rcor1/2* KO (Fig. 4.5). Like the other progenitor markers, INSM1 is not evenly distributed across the LGE VZ/SVZ, but rather is especially highly expressed in two parallel zones separated by a region of lower expression. Except for a border of cells approximately three nuclei thick lining the lateral ventricle, a majority of subpallial progenitors in the *Rcor1/2* KO expressed INSM1. This contrasts with the *Rcor1/2* fl, in which a minority of subpallial progenitors expressed INSM1. This comparison suggests that indeed, many of the additional progenitors present in

the *Rcor1/2* KO express INSM1. To verify that this is the case, I would need to co-label sections with MKI67 and INSM1. If the overabundance of progenitors in the *Rcor1/2* fl is due to excessive self-renewal within the INSM1+ population, I would expect the *Rcor1/2* fl and the *Rcor1/2* KO to have comparable numbers of MKI67+/INSM1- cells, but for the KO to have more MKI67+/INSM1+ cells.

4.6 RCOR1/2 and INSM1 form immunocomplexes in brain

Having established that all members of an RCOR1/RCOR2/INSM1 complex were expressed in a subset of VZ/SVZ cells, I performed co-immunoprecipitation analysis to test for complexes biochemically, using nuclear extracts from E13.5 brains. RCOR1 and RCOR2 immuno-complexes, but not immunoprecipitates of IgG or normal serum, each contained INSM1 (Fig. 4.6). In a reciprocal experiment, RCOR2 was also present in INSM1 immuno-complexes from *Insm1*$^{+/+}$, but not *Insm1*$^{-/-}$, brain extracts. However, I was not able to interpret the parallel test for the presence of RCOR1 in INSM1 immuno-complexes due to non-specific precipitation of RCOR1 from *Insm1*$^{-/-}$ brain by the INSM1 antibody (Fig. 4.6).

4.7 *Insm1*$^{-/-}$ mice phenocopy aspects of the *Rcor1/2* knockout phenotype

If INSM1 recruits RCOR1 and RCOR2 to facilitate neuronal and oligodendroglial differentiation, we would expect an *Insm1*$^{-/-}$ mouse (Osipovich et al., 2014) to exhibit a subset of phenotypes resembling those seen in the *Rcor1/2* KO mouse. Consistent with this idea, H&E stained sections of E18.5 brain showed that the *Insm1*$^{-/-}$ mouse phenocopied three prominent features of the *Rcor1/2* KO phenotype (Fig. 4.7). First, the *Insm1*$^{-/-}$ brain had an enlarged

subpallial VZ/SVZ compared to its control, as had been noted previously (Farkas et al., 2008). Second, *Insm1*$^{-/-}$ mice typically retained an interganglionic sulcus at E18.5 (Fig. 4.7), although it was less pronounced and more variable than in *Rcor1/2* KO mice. Third, the circumference of the lateral ventricle appeared to be increased in the *Insm1*$^{-/-}$ mouse. In contrast, anatomical abnormalities of the cortex, corpus callosum, striatal axons, anterior commissure, hippocampus, thalamus, and hypothalamus in the *Rcor1/2* KO were not phenocopied in *Insm1*$^{-/-}$ mice. This is not surprising, because RCOR1 and RCOR2 can be recruited by transcription factors other than INSM1.

4.8 *Insm1*$^{-/-}$ mice have more neural progenitor cells in the lateral subpallial progenitor zone than *Insm1*$^{+/+}$ controls

To better assess the concordance between the *Rcor1/2* KO and *Insm1*$^{-/-}$ mice, we analyzed the expression of MKI67 in *Insm1*$^{-/-}$ mice. As in the *Rcor1/2* KO, we found that the distance between the lateral ventricle and the basal edge of the MKI67+ zone was more than twice as wide in *Insm1*$^{-/-}$ as in *Insm1*$^{+/+}$ mice (Fig. 4.8*A*; *Insm1*$^{+/+}$, 103 ± 24 μm; *Insm1*$^{-/-}$, 256 ± 22 μm; five mice/genotype). And as in the *Rcor1/2* KO, this was due to increased numbers of both proliferating cells (*Insm1*$^{+/+}$, 531 ± 120 MKI67+ cells; *Insm1*$^{-/-}$, 789 ± 153 MKI67+ cells; p = 0.0206; five mice/genotype) and non-proliferating cells (*Insm1*$^{+/+}$, 312 ± 61 MKI67- cells; *Rcor1/2* KO, 660 ± 122 MKI67- cells; p = 0.0023 five mice/genotype). Cell counts were provided by Susan Kim.

While both KOs exhibit expansions of the MKI67+ zone, the expression pattern of MKI67 differs between them in two ways. First, the *Rcor1/2* KO, like

each control, has a margin approximately two nuclei wide of MKI67-negative cells between the lateral ventricle and the MKI67+ layer. In *Insm1*$^{-/-}$ mice, this margin is typically thicker (Fig. 4.8*B*). Second, the MKI67-expressing cells appeared to be evenly distributed within the VZ/SVZ of the *Insm1*$^{-/-}$ mice, in contrast to the bilayered distribution in *Rcor1/2* KO.

Immunohistochemistry for ASCL1 confirmed that many cells in the expanded progenitor zone were indeed neural progenitors (Fig. 4.8*C*). Interestingly, ASCL1 immuno-labeling was unevenly distributed within the LGE VZ/SVZ, with two bands of high expression similar to those seen in the *Rcor1/2* KO (compare to Fig. 3.12).

4.9 MAP2+ territories occupy a smaller proportion of total brain area in *Insm1*$^{-/-}$ than *Insm*$^{+/+}$ mice

I next examined the expression of neuronal markers in the *Insm1*$^{-/-}$. Based on the *Rcor1/2* KO, I expected the enlarged subpallial progenitor zone of the *Insm1*$^{-/-}$ to exhibit low expression of TUBB3 and no expression of MAP2; this proved to be the case (Figure 4.9*A* and *B*). As in the *Rcor1/2* KO, the proportion of the brain expressing MAP2 was significantly lower in *Insm1*$^{-/-}$ (83.2 ± 0.9%) than in *Insm1*$^{+/+}$ mice (86.7 ± 0.9%) (Fig. 4.9*C*; five mice/genotype). However, this difference (3.5%) was smaller than that observed between the *Rcor1/2* KO and the *Rcor1/2* fl (8.4%).

4.10 The *Insm1*$^{-/-}$ mouse has fewer OLIG+ cells

Similarly, there were fewer OLIG2+ cells in the IZ of the *Insm1*$^{-/-}$, but the difference was more modest than that seen in the *Rcor1/2* KO (Fig. 4.9*D*-*F*);

Insm1$^{+/+}$, 225 ± 27 cells; *Insm1*$^{-/-}$, 162 ± 15 cells; exploratory data analysis identified the sample indicated in red as an outlier, and it was removed from the analysis; five mice/genotype).

4.11 Many of the same genes are mis-regulated in *Rcor1/2* knockout and *Insm1*$^{-/-}$ mice

The above results suggested that INSM1 recruited RCOR1/RCOR2 to genes that must be repressed to promote neural differentiation. Therefore, we expected a shared subset of genes to be up-regulated in both the *Rcor1/2* and *Insm1* KOs. To test this expectation, we sequenced cDNA libraries made from the VZ/SVZ of the E13.5 MGE of each KO genotype, as well as their respective controls. I used ventral telencephalic progenitor cells because, in *Rcor1/2* KOs, this population showed the most complete loss of RCOR1 and RCOR2 at E13.5, as well as the most pronounced morphological abnormalities at E16.5 and thereafter. The VZ/SVZ, where neural progenitors were located, was isolated using laser capture microdissection.

Sophia Jeng and Dr. Shannon McWeeney analyzed the RNA-seq data. For all analyses, they defined putative differential gene expression based on False Discovery Rate (FDR) adjusted p-value < 0.05. Candidates that were also differentially expressed between the two controls (*Rcor1/2* fl and *Insm1*$^{+/+}$), as genes for which differential expression may have been independent of the loss of either INSM1 or RCOR1/2, were flagged and removed from downstream analyses. They examined both up- and down-regulated genes for each KO. Because RCOR1/2 and INSM1 are repressors, we expected many of the up-

regulated genes to be direct targets of these proteins. In *Rcor1/2* KO and *Insm1*$^{-/-}$ mice, we identified 451 and 100 genes that were up-regulated, respectively (Table 4.1 and 4.2). Twenty-one of the up-regulated genes were shared between the KOs (Fig. 4.10*A, p<<0.01*). This suggests that a common pathway is disrupted in both knockouts. We also identified 300 and 197 genes that were down-regulated, relative to the controls, in the *Rcor1/2* and *Insm1* KOs, respectively (Table 4.3 and 4.4). These genes could be direct targets of RCOR1/RCOR2- or INSM1-mediated gene activation, or could represent secondary effects of RCOR1/RCOR2- or INSM1-mediated repression. The overlap between the two genotypes was 105 (Fig. 4.10*A p<<0.01*).

In contrast, very few genes (only 6) were regulated oppositely in the two KOs, reinforcing our conclusion that the significance of the concordantly regulated genes was not spurious.

4.12 A majority of the genotype-specific and shared down-regulated genes are targets of REST

Upon assessment of the candidates, it was noted that the majority of the down-regulated genes, 55% (166 of 300) in the *Rcor1/2* KO and 60% in the *Insm1*$^{-/-}$ mouse (118 of 197), had a functional REST binding site within two kilobases upstream of the TSS or within the DNA encoding the primary transcript (Tables 4.1-4.4; McGann et al., 2014). Of the 105 down-regulated genes shared by the *Rcor1/2* and *Insm1* KOs, 64% (67) were REST targets (Fig. 4.10*B*). The proportion of REST targets is even higher among genes down-regulated by at least two-fold (Table 4.5; shared, 31 of 45 [69%]; just *Rcor1/2* KO, 47 of 81

[58%]; just *Insm1*$^{-/-}$, 21 of 35 [60%]). In contrast, only a minority of up-regulated genes were REST targets (Fig. 4.10*B*; shared, 6 of 21 [29%]; *Rcor1/2* KO alone, 148 of 430 [34%]; *Insm1*$^{-/-}$ alone, 33 of 79 [42%]), which suggests that the large proportion of REST targets among the down-regulated genes is not simply a reflection of large numbers of differentially-expressed REST targets.

4.13 The *Rest* gene is up-regulated in *Rcor1/2* and *Insm1* knockouts

We sought to validate the mRNA profiling results using E13.5 MGE. To this end, we analyzed RNA from *Rcor1/2* and *Insm1* KOs by RT-qPCR. We selected 8 (of 105) down-regulated genes that were shared between the genotypes based on the following criteria: genes were down-regulated by at least two-fold and detected at log CPM > 5 (CPM, counts per million). For seven of the eight genes, we observed statistically significant down-regulation in the *Rcor1/2* KO relative to the *Rcor1/2* fl control and the Nes-Cre control (Fig. 4.11*A*; six mice/genotype). In a separate experiment, we performed RT-qPCR to validate the *Insm1*$^{-/-}$ mRNA profiling results. Six of eight genes were significantly down-regulated compared to the *Insm1*$^{+/+}$ control, and one of the other two barely missed significance with a p-value of 0.051 (Fig. 4.11*B*; six mice/genotype). Because a majority of the down-regulated genes contained REST binding sites (Fig. 4.10*B*), we asked whether REST expression was up-regulated in the KOs relative to controls. While an increase in *Rest* expression was not detected from the mRNA profiling results, the RT-qPCR did show that REST expression was increased by more than two-fold in the *Rcor1/2* KO (2.3-fold relative to Nes-Cre; 2.1-fold relative to *Rcor1/2* fl) and in the *Insm1*$^{-/-}$ (2.2-fold relative *Insm1*$^{+/+}$) (Fig.

4.11*A* and *B*; six mice/genotype).

4.14 Normalizing Rest expression in the *Rcor1/2* knockout increases transcript levels of repressed REST targets

We therefore hypothesized that the down-regulation of REST targets in the two knockouts might be due to increased REST-mediated gene repression, rather than to loss of INSM1/RCOR-mediated gene activation. Several studies suggested that *Rest* overexpression could explain some phenotypes seen in the *Rcor1/2* KO. *In vitro* loss-of-function experiments suggested that in neural progenitors, REST reinforces progenitor identity and inhibits the acquisition of neuronal and oligodendroglial traits (Covey et al., 2012). Consistent with these experiments, forced expression of REST prevented neuronal migration and delayed acquisition of mature neuronal markers in *in utero* electroporation experiments (Mandel et al., 2011). Therefore, we thought overexpression of Rest in the two knockouts might contribute to their reduced neuronal and oligodendroglial differentiation.

To test whether diminishing *Rest* expression would rescue the major phenotypes in the *Rcor1/2* KO brains, we utilized mice with a *Rest* allele containing a conditional gene trap cassette. Cre-mediated recombination of this allele results in the loss of mature *Rest* transcripts (Nechiporuk et al., 2016). We generated an $Rcor1^{fl/fl}$; $Rcor2^{fl/fl}$; $Rest^{GTi/+}$; Nes-Cre mouse (hereafter, *Rest* rescue), in which *Rest* transcript levels are equivalent to control levels (Fig. 4.11*A*; six mice/genotype). By RT-qPCR analysis, we found that of seven REST target transcripts down-regulated in the *Rcor1/2 KO,* one of them*, Celsr3,* was

restored fully to control levels in the *Rest* rescue (Fig. 4.11*A*; six mice/genotype). Three other transcripts were partially restored (*Chrnb2, Trim67, and Unc13a*), and three were not rescued (*Fam65b, Gad2, and Scrt1*).

4.15 Reduction of Rest transcript to control levels in the *Rcor1/2* knockout ameliorates the interganglionic sulcus (IGS) phenotype

Hematoxylin and eosin staining showed that E18.5 *Rest* rescue mice exhibited less pronounced IGS than *Rcor1/2* KOs, as assessed by an investigator blinded to genotype. The difference between the KO and rescue phenotypes was most apparent at levels caudal to the peak depth of the IGS. In such sections, the IGS of the *Rcor1/2* KO is still quite large, while that of the *Rest* rescue is subtle or nonexistent (Fig. 4.12). However, in all other regards, the *Rest* rescues could not be distinguished visually from the *Rcor1/2* KOs. We therefore did not analyze MKI67 and MAP2 to evaluate the progenitor accumulation and neuronal differentiation phenotypes. Quantification of the number of OLIG2+ cells in the IZ of the neocortex indicated that OPC production was not rescued (in 1.8 x 10^5 μm^2 of IZ representing the sum of six areas: *Rest* rescue, 60 ± 12 cells; compare to Fig. 3.16; five mice/genotype).

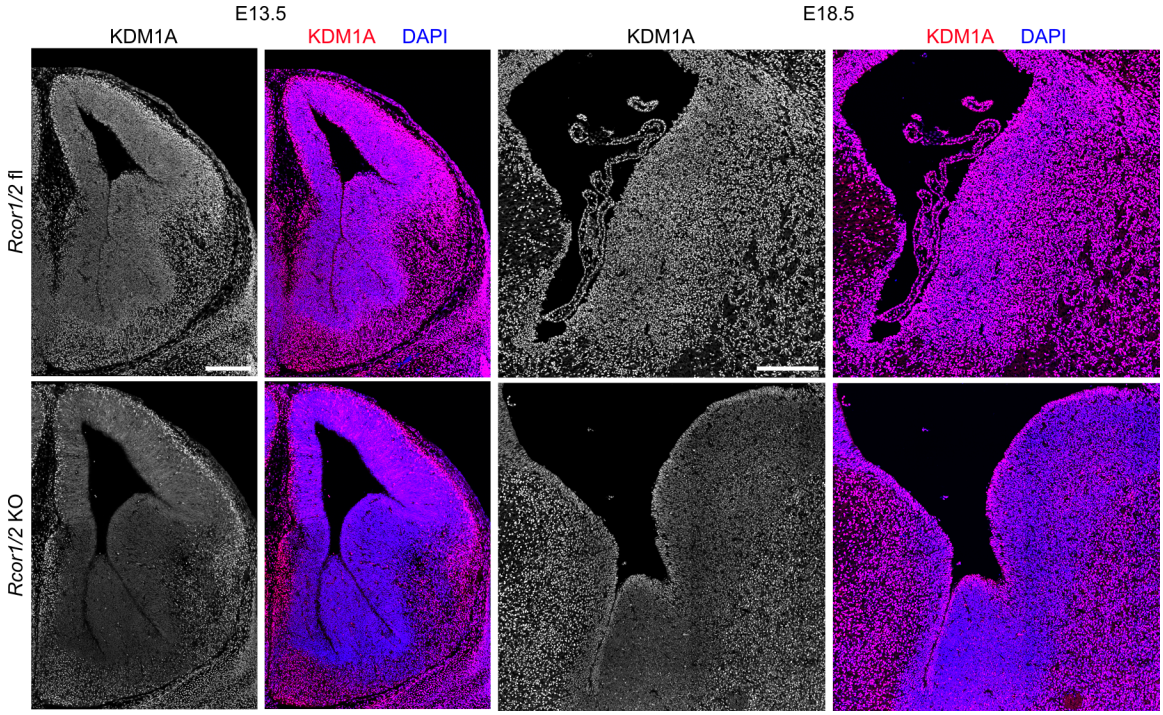

Figure 4.1. KDM1A expression at E13.5 and E18.5. Scale bar, 200 μm.

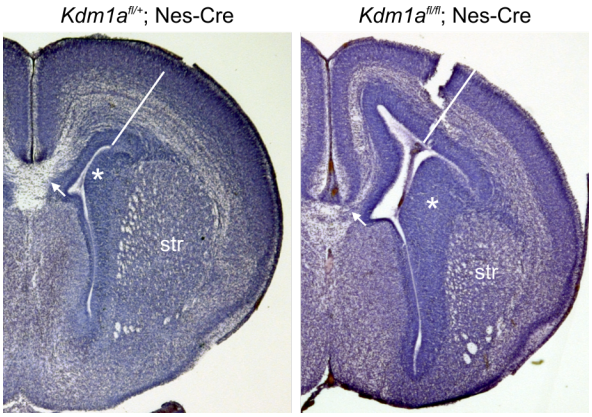

Figure 4.2. The *Kdm1a* knockout may recapitulate some phenotypes present in the *Rcor1/2* knockout. Preliminary images of H&E-stained coronal sections of E18.5 *Kdm1a* control and KO telencephalon were provided by Dr. Jianxun Wang. The lateral subpallial progenitor zone is enlarged in the knockout relative to the control (asterisks). The neocortex is thinner in the KO; to facilitate comparison, one of a pair of lines of equal length is superimposed on each cortex. The striatum (str) in the knockout is smaller, and the axon bundles traversing it are thinner. The corpus callosum (arrow) is thinner.

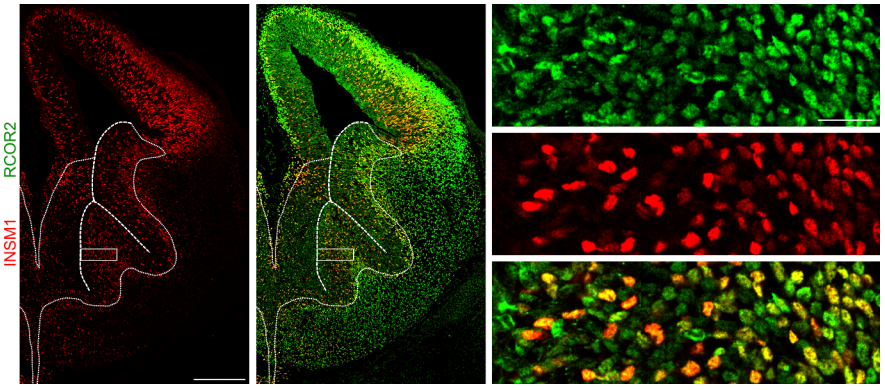

Figure 4.3. Immunohistochemical analysis of RCOR2 and INSM1 in E13.5 coronal telencephalic hemisections. Representative immunohistochemistry on a coronal hemisection of E13.5 telencephalon shows a subset of cells expressing both RCOR2 and INSM1. Dashed and dotted lines indicate the boundaries of the subpallial progenitor zone, determined by alignment of the section to an adjacent section immuno-labeled with the subpallial progenitor marker ASCL1. Dashed lines indicate the borders between the subpallial progenitor zone and the lateral ventricle. Dotted lines indicate the boundaries between the subpallial progenitor zone and other brain regions. The box indicates the region shown to the right at higher magnification. Scale bars are 200 μm (*left*) and 20 μm (*right*).

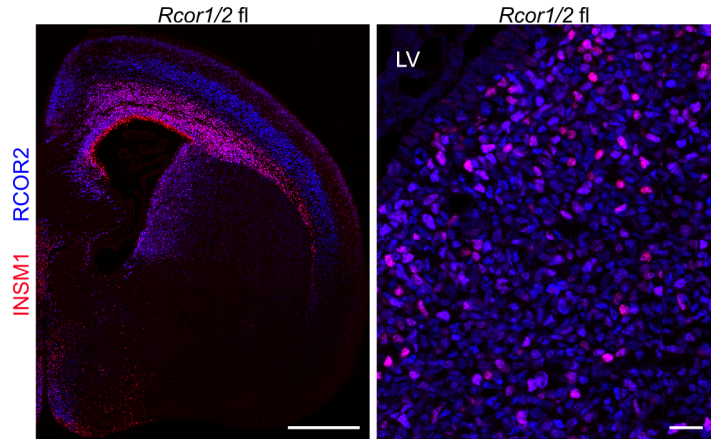

Figure 4.4. Immunohistochemical analysis of RCOR2 and INSM1 in E18.5 coronal telencephalic hemisections. Representative immunohistochemistry on coronal hemisections of E13.5 telencephalon shows a subset of cells expressing both RCOR2 and INSM1. Scale bars are 200 μm (*left*) and 20 μm (*right*).

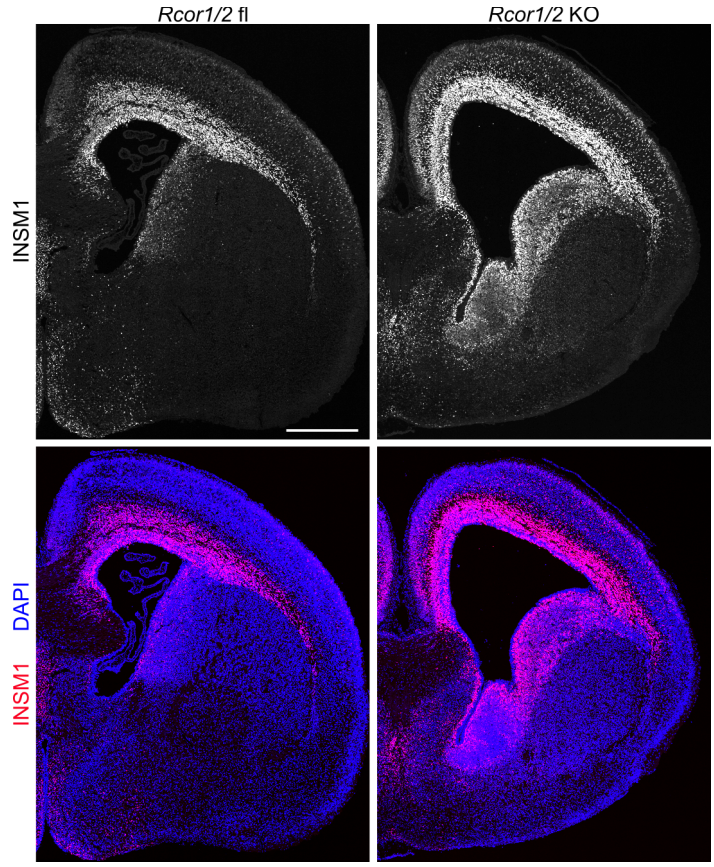

Figure 4.5. Immunohistochemical analysis of INSM1 in E18.5 *Rcor1/2* fl and *Rcor1/2* knockout coronal telencephalic hemisections. Representative immunohistochemistry on coronal hemisections of E13.5 telencephalon shows a subset of cells expressing both RCOR2 and INSM1. Scale bars are 200 μm (*left*) and 20 μm (*right*).

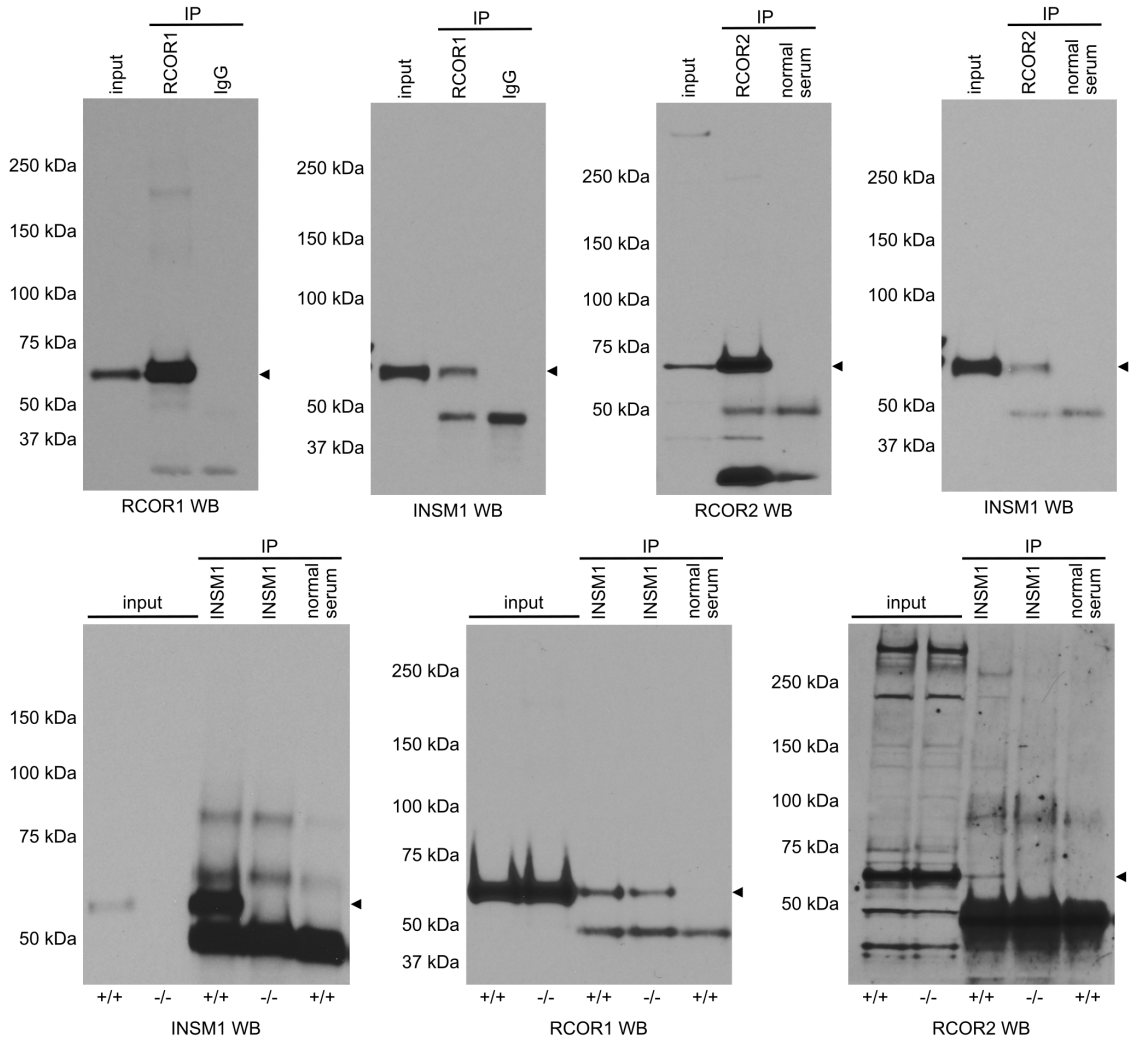

Figure 4.6 Co-immunoprecipitation analysis for INSM1/RCOR1/2 complexes. Immunoprecipitations (IPs) were performed on nuclear extracts prepared from E13.5 brain. Labels underneath each blot indicate the antibodies used for Western blotting. IgG is rabbit IgG. The normal serum controls are rabbit serum for the RCOR2 IP and guinea pig serum for the INSM1 IP. +/+, *Insm1*$^{+/+}$ nuclear extracts; -/-, *Insm1*$^{-/-}$ nuclear extracts. Arrowheads indicate Western blot proteins of interest.

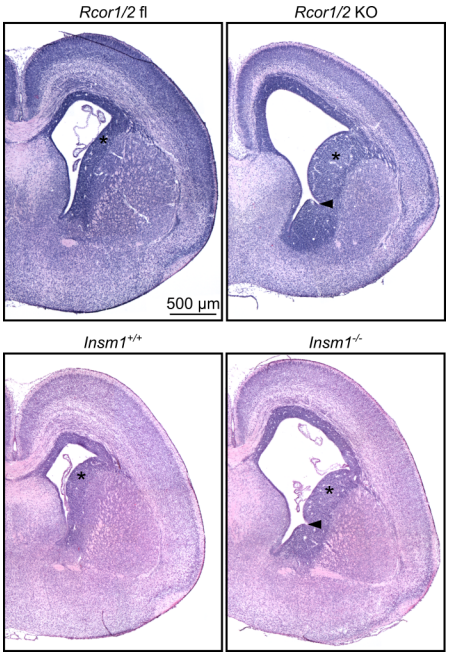

Figure 4.7. *Insm1*$^{-/-}$ mice phenocopy several *Rcor1/2* knockout phenotypes in E18.5 brain. Hematoxylin and eosin-stained E18.5 coronal sections. Asterisks indicate the VZ/SVZ, arrowheads indicate interganglionic sulci.

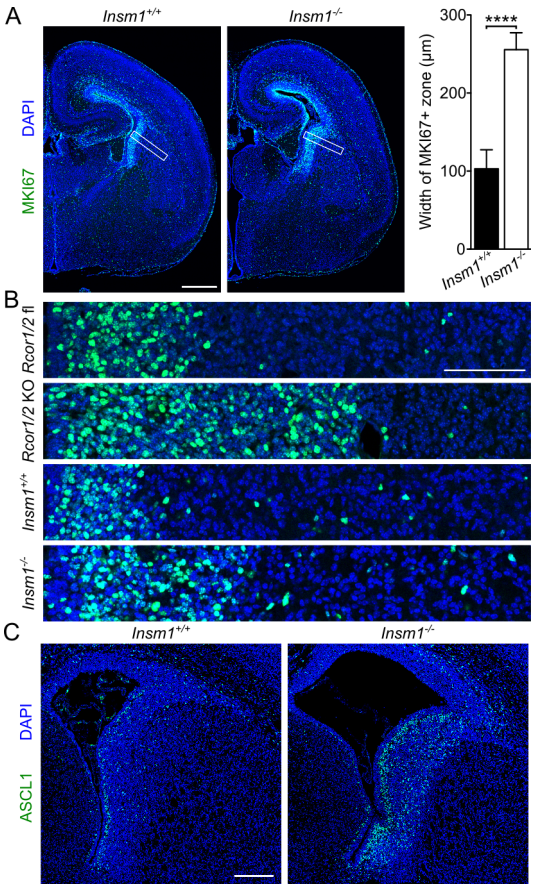

Figure 4.8. *Insm1*$^{-/-}$ mice have more neural progenitors at E18.5 than *Insm1*$^{+/+}$ mice. (*A, Left*) Representative sections immuno-labeled for the proliferation marker MKI67 and counterstained with DAPI. Boxes indicate insets shown in *B* at higher magnification. Scale bar, 500 μm. (*Right*) Quantification of the width of the MKI67+ zone. Measurements were made from areas comparable to those depicted in the insets. Statistical significance was assessed by t tests. The means and standard deviations are indicated. (*B*) Insets from *A*. Images from Fig. 3.10*A* are reprinted for purposes of comparison. MKI67 and DAPI post-processing were identical within each pair, but differed between pairs. Scale bar, 100 μm. (*C*) Representative sections immuno-labeled for the progenitor marker ASCL1 and counterstained with DAPI. Scale bar, 200 μm.

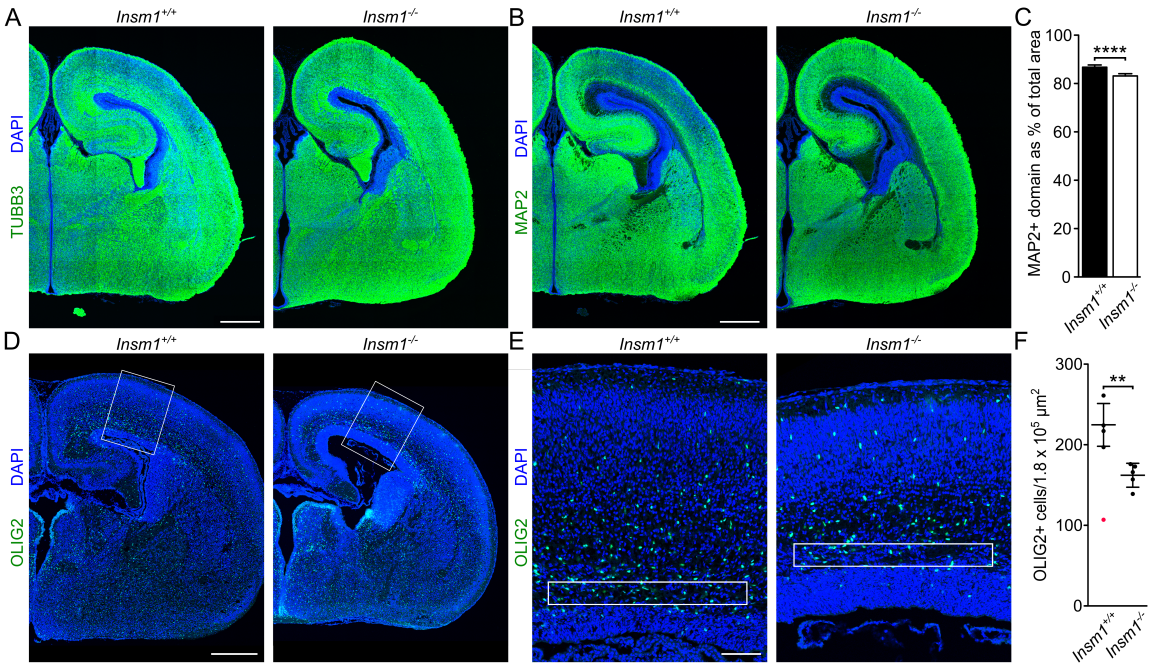

Figure 4.9. *Insm1*$^{-/-}$ mice have less neuronal territory and fewer oligodendrocyte precursor cells at E18.5 than *Insm1*$^{+/+}$ mice. (*A*) Representative immunohistochemistry for TUBB3, an early neuronal marker. (*B*) Representative immunohistochemistry for MAP2, a late neuronal marker. (*C*) Quantification of MAP2 immuno-labeling, showing the percentage of each E18.5 coronal hemisection occupied by the MAP2+ domain. (*D*) Representative immunohistochemistry for OLIG2. Boxes indicate the insets depicted in *E*. (*E*) OLIG2 expression in the neocortex. Boxes indicate the regions quantified in *F*. (*F*) Quantification of the number of OLIG2+ cells in the IZ of the neocortex. For each mouse, one region of 3 x 10^4 μm^2 was selected from each of six hemisections, and the numbers of OLIG2+ cells from all regions were added. Each mouse is represented by one dot. Exploratory data analysis identified one wild-type count (107, indicated in red) as an outlier, so it was omitted from the

statistical analysis. ns, $p > 0.05$; **, $p < 0.01$; ****, $p < 0.0001$. Scale bars in A, B, and D are 500 μm, and the scale bar in E is 100 μm.

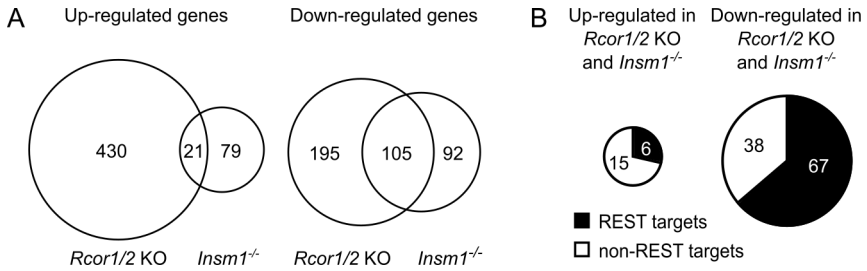

Figure 4.10. *Rcor1/2* knockout and *Insm1*$^{-/-}$ mice share many common mis-regulated genes at E13.5. (*A*) Venn diagrams comparing the genes mis-regulated in *Rcor1/2* KO and *Insm1*$^{-/-}$ mice (relative to *Rcor1/2* fl and *Insm1*$^{+/+}$ mice, respectively). (*B*) Proportions of up- and down-regulated genes that are REST targets.

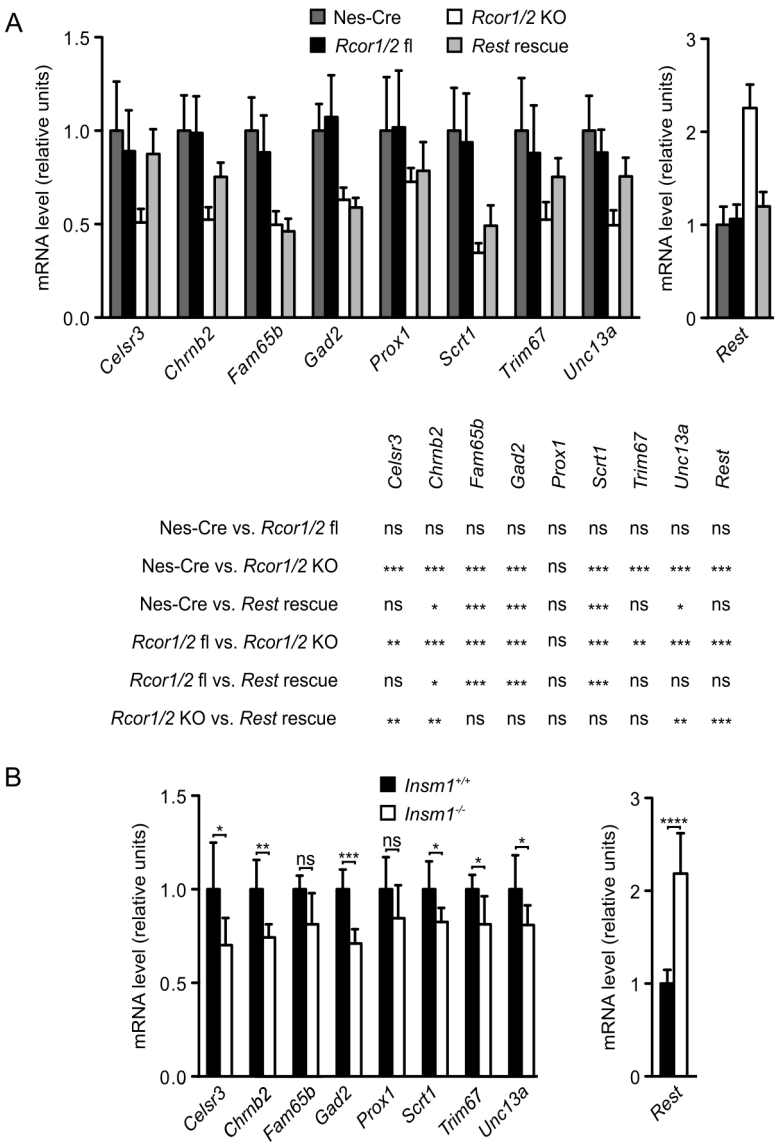

	Celsr3	*Chrnb2*	*Fam65b*	*Gad2*	*Prox1*	*Scrt1*	*Trim67*	*Unc13a*	*Rest*
Nes-Cre vs. *Rcor1/2* fl	ns	ns	ns	ns	ns	ns	ns	ns	ns
Nes-Cre vs. *Rcor1/2* KO	***	***	***	***	ns	***	***	***	***
Nes-Cre vs. *Rest* rescue	ns	*	***	***	ns	***	ns	*	ns
Rcor1/2 fl vs. *Rcor1/2* KO	**	***	***	***	ns	***	**	***	***
Rcor1/2 fl vs. *Rest* rescue	ns	*	***	***	ns	***	ns	ns	ns
Rcor1/2 KO vs. *Rest* rescue	**	**	ns	ns	ns	ns	ns	**	***

Figure 4.11. Differential gene expression in the *Rcor1/2* knockout and the *Insm1*$^{-/-}$ mouse at E13.5. (*A*, *Top*) RT-qPCR analysis of cDNA prepared from E13.5 medial ganglionic eminence. Each transcript quantity was normalized to the geometric mean of the quantities of four reference genes: Aip, Cxxc1, Rn45s, and Rps20. The means and standard deviations are indicated (n = 6 mice). (*Bottom*) Significance was determined by ANOVA with Tukey's multiple

comparison tests on log-transformed data. (*B*) RT-qPCR analysis as described in *A*. Statistical significance was assessed using t tests with Welch's correction on log-transformed data. ns, $p > 0.05$; *, $p < 0.05$; **, $p < 0.01$; ***, $p < 0.001$, ****, $p \leq 0.0001$.

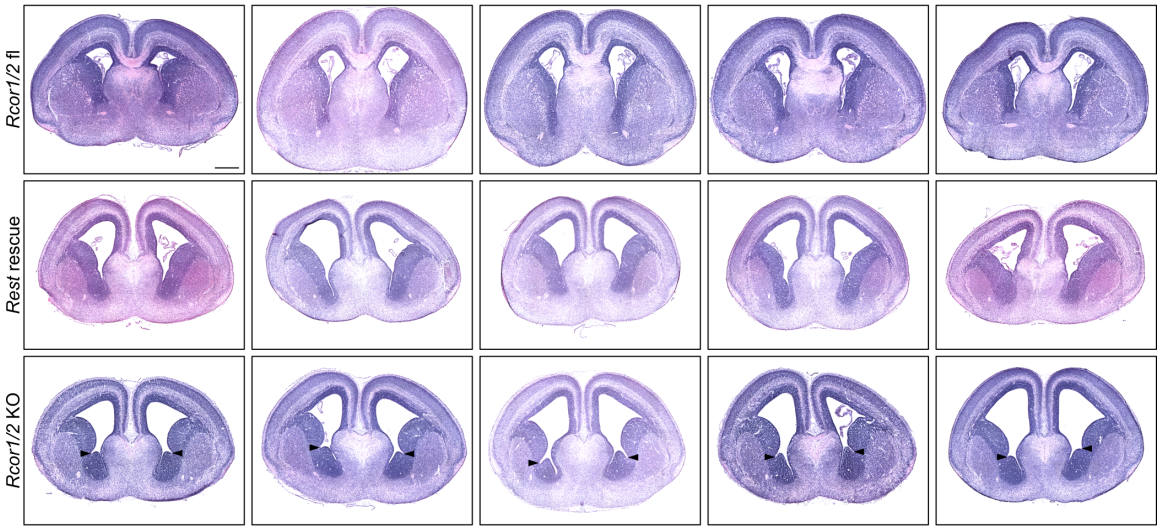

Figure 4.12. Reducing *Rest* transcript levels to control levels in the *Rcor1/2* knockout partly rescues the interganglionic sulcus phenotype at E18.5. Hematoxylin and eosin-stained coronal sections of telencephalon from five mice of each genotype. Images were correctly sorted into groups by morphology by a person blind to the genotypes. Scale bar, 500 μm. Arrowheads, intermediate ganglionic sulcus.

Geneid	FDR	FC	REST
ELF4	0.001033	30.72	no
CHRNA2	0.01166	21.3	no
POU6F2	0.011703	12.33	no
KLHL14	0.049478	10.88	no
LPAR1	0.028787	10.67	no
NXPH3	3.51E-27	9.444	no
RTN4RL2	7.42E-10	7.35	yes
ALDH1A2	0.007867	7.28	no
MFAP5	0.037931	6.804	no
2810433D01RIK	0.012782	6.434	yes
DOC2B	5.95E-69	6.167	no
TGIF1	8.95E-20	6.058	yes
EGR3	3.94E-20	5.763	no
AK163103	0.016326	5.516	no
SCN9A	2.38E-16	5.448	no
1700012D01RIK	0.000145	5.428	yes
SLC5A7	2.11E-08	5.351	no
GM266	3.74E-07	5.134	no
FAM83F	0.026456	5.127	no
AK040865	0.000554	5.122	no
AK037070	1.93E-06	5.04	no
RBM46	5.30E-14	5.03	yes
LOXL1	8.01E-20	5.003	no
CNTN4	1.42E-09	4.975	yes
GPR139	5.96E-06	4.965	no
HES7	0.006657	4.893	no
CLVS2	6.90E-07	4.776	no
DNAJC22	3.48E-08	4.675	no
HEPH	0.040704	4.656	no
TRANK1	1.08E-09	4.619	yes
PDGFRA	0.001477	4.547	no
DNAHC5	0.037246	4.431	yes
PLA2R1	8.96E-07	4.395	yes
AK052878	0.024735	4.343	no
PERP	4.00E-08	4.255	no
CRABP1	2.96E-14	4.145	no
XLR3C	0.007518	4.14	no
THBS4	8.01E-20	4.138	no
LRRC7	0.005801	4.097	yes
BC035947	6.82E-07	4.07	no
NUP62CL	0.002027	4.066	no
HMCN1	2.32E-21	3.927	yes
COL1A2	8.83E-35	3.902	yes
WDR86	2.09E-15	3.832	no
BC044745	0.014499	3.798	no
IFLTD1	0.014499	3.759	no
PRSS50	0.033762	3.711	no

Geneid	FDR	FC	REST
4933403O08RIK	2.26E-12	3.662	no
AK137397	0.009932	3.661	no
ASCL4	0.005359	3.648	no
TEX16	1.76E-16	3.638	no
DAB2	2.05E-08	3.567	no
MARVELD3	1.19E-06	3.559	yes
PRSS41	0.028309	3.541	no
MMU-MIR-155*	0.002188	3.506	no
8030423F21RIK	0.040729	3.494	no
9030625A04RIK	1.81E-23	3.458	no
VIPR1	1.03E-05	3.445	no
ALCAM	2.05E-18	3.39	no
DDX43	1.63E-07	3.323	no
TCHH	6.13E-08	3.31	no
SLC6A4	0.00214	3.291	no
PAPPA2	6.44E-06	3.277	yes
AK087024	0.01022	3.23	no
FBLN5	0.026823	3.151	no
PTPN3	1.93E-09	3.09	yes
ELFN1	2.02E-21	3.077	no
EDN3	1.64E-05	3.076	yes
DENND1C	1.38E-18	3.042	no
GM11837	6.75E-11	3.039	no
TPM2	6.49E-12	3.031	no
TRIM6	6.21E-06	3.026	no
TCEAL7	0.046554	3.019	no
SUSD5	0.000842	2.98	no
LIN28A	0.000241	2.978	yes
AK086087	0.010515	2.965	no
EPCAM	3.27E-10	2.963	yes
AK080063	0.040089	2.948	no
GRIN2D	1.23E-08	2.945	no
TRIM71	3.48E-08	2.912	yes
IL28RA	0.00789	2.9	no
AK147021	0.004456	2.888	no
RNF151	0.021453	2.885	yes
AB347559	2.44E-05	2.881	no
GM1564	0.009685	2.868	no
FZD10	4.07E-05	2.866	yes
SLC39A8	2.91E-05	2.839	no
HNMT	1.43E-06	2.83	no
GABRA3	2.39E-21	2.815	no
CAR13	9.73E-16	2.804	no
AK076318	0.010225	2.801	no
DUSP9	1.36E-11	2.78	no
1700001L19RIK	0.034373	2.756	no
A330009N23RIK	0.003998	2.752	no

Table 4.1. Genes up-regulated more than two fold in the *Rcor1/2* fl relative to the *Rcor1/2* knockout. Page 1 of 2. FDR, tagwise false discovery rate. FC, tagwise fold change. Fold change is expressed as (*Rcor1/2* KO level)/(*Rcor1/2* fl level). The "REST" column indicates whether a gene is a REST target. Genes concordantly regulated between the two KOs are shown in blue (genes that are up-regulated in the *Insm1*$^{-/-}$, but by less than two fold, are included).

Geneid	FDR	FC	REST
LRRC55	0.00022	2.751	no
RPH3AL	0.005513	2.748	yes
GM684	0.01786	2.743	no
FLRT1	5.93E-11	2.735	no
NRK	2.28E-12	2.731	no
CAPN6	1.08E-23	2.73	no
IGSF1	0.00962	2.728	no
RUNX3	0.019141	2.721	no
BHLHE22	0.044805	2.718	no
TGM2	1.53E-08	2.713	no
SEMA3D	8.56E-05	2.692	no
INHBB	1.47E-09	2.684	yes
TEX15	1.29E-07	2.682	yes
RBM20	0.004441	2.648	yes
SPEG	0.026719	2.647	yes
CCDC114	2.97E-12	2.646	no
TRPC3	0.012574	2.646	yes
SHISA3	4.74E-08	2.636	no
GRIK1	0.026162	2.621	no
LEPREL1	0.008554	2.62	yes
SNX7	0.00357	2.611	no
MCOLN3	3.60E-06	2.609	no
ACSS3	0.003182	2.607	no
GSDMD	5.89E-09	2.602	no
BAG3	7.66E-13	2.573	no
MAP3K15	9.28E-12	2.565	yes
SOX10	3.29E-05	2.521	no
NPTX1	0.003653	2.519	yes
DCDC2A	6.61E-06	2.519	no
PGM5	6.71E-05	2.517	no
ABCA4	4.97E-07	2.509	no
PALM2	9.12E-07	2.502	no
BC064078	0.011058	2.481	no
FAM176A	2.20E-05	2.481	yes
PRKCD	0.044937	2.477	yes
LAPTM4B	4.35E-05	2.476	yes
AK202427	0.049478	2.458	no
LIN28B	2.41E-06	2.456	no
A530098C11RIK	0.001403	2.451	no
LRFN2	6.98E-11	2.448	yes
AK021280	0.000508	2.446	no
4930447C04RIK	0.037167	2.442	no
CRABP2	4.10E-24	2.438	no
PCDH7	0.000722	2.421	yes
AB347592	0.005664	2.414	no
AK039624	5.20E-09	2.402	yes
DNAIC2	4.72E-08	2.395	yes
GPR156	3.68E-15	2.389	yes
PRRT4	0.000131	2.383	no
MMP2	1.07E-05	2.368	no
CACNA1E	6.69E-08	2.363	yes
USP44	1.05E-13	2.358	no
FBLN7	2.91E-05	2.343	yes
SLC16A2	1.00E-14	2.338	no
EMILIN3	4.62E-10	2.329	no
QPRT	2.91E-05	2.32	yes
STX3	0.007545	2.315	no
LANCL3	8.61E-11	2.314	no
SNAI1	0.000329	2.313	no

Geneid	FDR	FC	REST
P2RX7	4.53E-08	2.302	yes
COLEC12	8.74E-07	2.294	yes
DDIT4L	3.38E-15	2.281	no
GM12824	0.000206	2.277	no
GM8773	0.000109	2.277	no
PLA2G4A	0.000673	2.261	no
SFRP4	1.52E-06	2.259	no
UCP2	3.02E-15	2.257	no
EDARADD	0.005681	2.257	no
KANK1	0.04698	2.248	no
GLI2	1.65E-08	2.232	yes
GNG8	0.008297	2.232	no
HBS1L	0.009644	2.226	no
D630003M21RIK	0.000156	2.223	yes
8030462N17RIK	0.03003	2.221	yes
TMEM45A	0.000532	2.219	yes
ADAMTS12	0.015639	2.214	no
GAP43	4.97E-15	2.213	no
PHLDB2	0.036324	2.21	no
B2M	8.88E-16	2.202	no
4933407L21RIK	0.011703	2.175	yes
SPRY3	0.001612	2.175	no
CPNE5	0.001184	2.174	yes
STOX1	2.47E-07	2.173	yes
PDE5A	1.44E-16	2.173	no
CYBRD1	0.000117	2.166	no
COL9A2	5.98E-10	2.161	yes
FUCA2	0.003396	2.159	no
6030405A18RIK	5.19E-06	2.158	no
PRRX1	7.87E-09	2.156	no
AK145614	0.004695	2.155	yes
MAOB	0.00014	2.14	no
ARSI	3.95E-08	2.133	no
MAPK13	0.018786	2.12	yes
LGALS1	3.56E-12	2.119	no
LPL	4.92E-09	2.108	no
AB347501	6.37E-10	2.105	no
NAB2	0.010762	2.098	yes
RGS9	1.54E-11	2.094	no
A430107O13RIK	0.003789	2.092	yes
CCDC158	0.004123	2.092	yes
BVES	5.31E-05	2.083	no
CTSO	3.91E-08	2.079	no
NSUN7	0.034937	2.075	no
SMARCA1	0.000376	2.074	no
RASL11B	9.12E-11	2.058	no
TMEM159	3.58E-06	2.056	no
GSTT1	4.33E-08	2.048	yes
RIMBP2	0.006378	2.041	yes
PTCHD1	6.93E-08	2.039	no
GPC3	2.48E-05	2.037	yes
COL4A6	5.73E-12	2.036	no
2810055F11RIK	0.00207	2.035	no
KDELR3	0.000943	2.035	no
CRTAC1	4.55E-07	2.03	yes
SLC2A12	0.002288	2.027	no
SH3BGRL2	3.62E-11	2.014	no
S100A11	2.75E-09	2.003	no
1700001L05RIK	0.030275	2.003	no

Table 4.1. Genes up-regulated more than two fold in the *Rcor1/2* fl relative to the *Rcor1/2* knockout. Page 2 of 2.

Geneid	FDR	FC	REST
POU6F2	0.000352	19.655	no
CCL9	0.015558	16.724	no
GPR183	0.012547	6.0528	yes
MGAM	0.000402	5.3114	no
SOX10	8.55E-16	5.0808	no
PPNR	0.027512	5.0223	no
GM4980	0.015133	4.1338	no
MRC1	0.026236	3.5732	no
TGIF1	1.05E-06	3.1612	yes
EFCAB9	0.048423	3.0032	no
HIST1H4H	0.00232	2.953	yes
AK164218	0.009225	2.8973	no
DDIT4L	2.05E-27	2.8121	no
HIST1H1A	3.15E-07	2.7679	yes
SNAI1	0.028991	2.6285	no
RMRP	2.12E-07	2.6237	no
CD180	0.005326	2.6028	no
HIST1H1B	2.32E-11	2.5366	yes
AK132189	0.009747	2.527	no
C3AR1	0.002303	2.4116	no
HIST1H1D	2.69E-08	2.3931	yes
BCAN	2.61E-05	2.3928	yes
HIST1H3E	0.001039	2.3621	yes
HIST1H2BM	0.013395	2.3395	yes
FCRLS	2.13E-05	2.3062	no
HIST2H2BB	1.95E-07	2.3046	yes
GPR17	8.50E-11	2.2101	no
AK083706	0.022444	2.1258	yes
NFIB	0.009847	2.112	yes
RTN3	0.00241	2.0684	yes
AK082948	0.046049	2.0475	no
RN45S	1.39E-11	2.0124	yes

Table 4.2. Genes up-regulated more than two fold in the *Insm1*$^{-/-}$ relative to the *Insm1*$^{+/+}$. FDR, tagwise false discovery rate. FC, tagwise fold change. Fold change is expressed as (*Insm1*$^{-/-}$ level)/(*Insm1*$^{+/+}$ level). The "REST" column indicates whether a gene is a REST target. Genes concordantly regulated between the two KOs are shown in blue (genes that are up-regulated in the *Rcor1/2* KO, but by less than two fold, are included).

Geneid	FDR	FC	REST
COL6A5	0.00245115	-97.3774895	yes
MLPH	0.03951127	-66.1984094	yes
AKR1C13	0.03951127	-66.1983661	no
EMCN	0.03735817	-65.369332	no
KRT73	1.41E-11	-16.3304194	no
PTPRN	0.01311083	-12.1104963	yes
SST	2.08E-06	-11.1132002	yes
GALNT9	0.00507848	-9.88581631	yes
DIRAS2	0.00251708	-8.94998206	yes
AK047238	2.32E-06	-8.51020594	no
AVPR1A	0.00275879	-8.18328534	no
PTF1A	0.00340233	-7.32464056	no
CACNG3	2.31E-06	-6.81321073	yes
CACNG2	6.01E-06	-6.01760255	yes
PCDHAC1	4.85E-06	-5.6224508	yes
WNK1	0.02827734	-5.35700947	yes
SCRT1	8.59E-47	-5.25594405	yes
TBC1D30	0.00011699	-5.18169617	yes
TMEM179	8.68E-09	-5.10581942	yes
UNC13A	1.87E-33	-4.96329461	yes
CPS1	1.31E-06	-4.93427538	no
COL4A3	0.00190427	-4.91875974	yes
GBX1	2.67E-08	-4.70028315	yes
FN3K	0.00043547	-4.6349981	no
2700090O03RIK	7.15E-06	-4.60862961	no
SCGN	0.02337732	-4.53611141	yes
SVOP	1.29E-29	-4.3337322	yes
FAM65B	1.35E-20	-4.22298394	yes
AK009785	0.0122418	-4.14659138	no
GP1BB	0.00292573	-4.13186686	no
CELF6	0.00074657	-4.11402386	yes
AMPD2	0.00571453	-4.02385337	no
CHRNB2	1.14E-27	-3.863244	yes
HRH3	2.32E-09	-3.83648576	yes
ACTL6B	2.02E-21	-3.75808892	yes
SLC2A8	0.00195127	-3.7325926	yes
CELSR3	3.87E-26	-3.65254931	yes
GALNT14	0.00162863	-3.64628281	no
TSHR	3.81E-06	-3.57308184	no
NEB	8.20E-13	-3.51973881	yes
AK138505	0.00339608	-3.44731882	yes
SRRM3	0.04621299	-3.44358539	yes
XKR7	6.56E-07	-3.3896026	yes
MMP24	1.53E-20	-3.38432648	yes
EEF1A2	4.34E-05	-3.37452968	no
GM11346	3.39E-07	-3.26980534	yes
UNC79	0.00228436	-3.24121646	yes
AK042845	0.00223504	-3.22638419	no
SPIRE2	0.000135	-3.21272764	yes
CHGB	3.23E-12	-3.18779796	yes
HIST2H3C2	0.03772369	-3.14906945	no
RAB3C	0.02431119	-3.12401176	yes
CCDC163	0.03399526	-3.06056652	no
TH	4.78E-21	-3.02027238	no
NAV2	0.00721694	-3.00691224	yes
PTGDS	0.03690509	-2.99161938	no
DIRAS1	2.11E-11	-2.969373	yes
VGF	0.00301565	-2.96910408	yes
FAM123C	4.55E-07	-2.94106688	yes
PCDHGC4	5.47E-13	-2.83156427	yes
TRIM67	1.04E-15	-2.81917862	yes
SLC37A1	0.0010929	-2.77641245	yes
SLC43A2	0.03761629	-2.77331169	no

Geneid	FDR	FC	REST
SHH	1.19E-08	-2.746476	no
FGF11	2.76E-07	-2.7427989	yes
ZFP608	1.10E-09	-2.7353346	no
PSD	0.004213924	-2.7312069	yes
SLC10A4	1.67E-14	-2.7275341	no
FBLL1	0.000124971	-2.6314593	yes
GAD1	7.40E-11	-2.600874	no
LASS3	0.003226759	-2.5858674	no
DOC2G	1.22E-07	-2.5711823	no
CNPY1	0.017438715	-2.5603014	yes
TMEM130	0.001410124	-2.5508511	yes
E130309D14RIK	6.61E-10	-2.5349076	yes
RUNX1T1	0.000145974	-2.530404	no
MAGEL2	1.10E-09	-2.5046264	no
MYH7B	0.033741496	-2.4436165	no
HR	0.00315662	-2.4429382	no
SIX2	0.012780734	-2.4148266	no
NACAD	6.90E-09	-2.3782082	yes
DCX	0.001403477	-2.3780476	yes
HAGHL	0.029780598	-2.3339819	yes
AK080597	2.05E-08	-2.3335977	no
BSN	2.81E-12	-2.3321973	yes
HEATR5B	0.006156158	-2.328194	no
APC2	1.42E-15	-2.3268836	no
CPLX1	2.44E-12	-2.3088557	yes
NRXN3	6.75E-09	-2.3073004	yes
CYTH1	0.035103096	-2.3053431	yes
CELF3	2.04E-07	-2.305102	yes
USF1	0.039348368	-2.279302	no
DLX6AS2	0.003198444	-2.2450598	yes
AK142161	0.022888192	-2.2423603	no
RAI2	0.026943083	-2.2370853	no
PCDHGC5	0.001216078	-2.2287731	no
SEL1L3	4.75E-11	-2.2226714	yes
HCN4	1.67E-05	-2.2216878	yes
AP3B2	1.94E-12	-2.2199235	yes
PROX1	6.10E-09	-2.2137649	yes
ANKRD37	0.005714526	-2.2031867	no
ZFP503	3.58E-05	-2.203071	no
AK083547	6.52E-15	-2.1980742	no
AJAP1	0.007018473	-2.1898819	yes
RLTPR	0.000985996	-2.1602122	yes
GAD2	1.21E-13	-2.1506389	yes
SH3GL2	0.004812119	-2.148598	yes
PHF21B	0.00315487	-2.1312404	yes
ZDHHC14	0.018811278	-2.1158616	yes
DPF3	0.026075029	-2.102202	yes
GM13889	5.31E-05	-2.1007483	no
PRRT2	1.67E-05	-2.1005853	no
RASSF10	0.000329044	-2.0963051	yes
SORBS1	0.000275676	-2.0931944	yes
SLC7A14	0.00209924	-2.0922182	yes
RPP25	0.000149463	-2.0899594	yes
SNAP25	1.31E-10	-2.0733205	yes
XKR4	0.009427104	-2.0640661	yes
PGBD5	7.37E-07	-2.0595754	yes
INA	2.78E-06	-2.0576127	yes
AI606473	4.98E-06	-2.041616	no
PNPLA3	0.015882272	-2.0353522	yes
OLFML2B	1.52E-06	-2.0320153	yes
TRP53INP2	2.00E-12	-2.0171806	no
SHC2	3.13E-09	-2.0127961	no
LHX8	9.75E-10	-2.0031949	no

Table 4.3. Genes down-regulated more than two fold in the *Rcor1/2* fl relative to the *Rcor1/2* KO. FDR, tagwise false discovery rate. FC, tagwise fold change. Fold change is expressed as (*Rcor1/2* fl level)/(*Rcor1/2* KO level), with a minus sign to emphasize that this differs from how up-regulated genes are expressed. The "REST" column indicates whether a gene is a REST target. Genes concordantly regulated between the two KOs are shown in blue (genes that are down-regulated in the *Insm1*$^{-/-}$, but by less than two fold, are included).

Geneid	FDR	FC	REST
TTR	4.50E-07	-142.9	yes
9530036O11RIK	0.009657	-61.001	yes
AK131776	0.04917	-17.917	no
FOXD2	0.009017	-13.406	no
TET1	0.03365	-11.508	yes
DISP2	0.000646	-8.1777	yes
BC039771	0.01064	-6.9637	yes
SRRM3	0.023879	-6.0325	yes
AVPR1A	0.004651	-5.9017	no
XKR7	7.10E-15	-5.5821	yes
PCDHA12	0.036749	-4.7303	yes
CHGB	2.39E-17	-4.5507	yes
TBC1D30	0.000624	-4.5311	yes
CACNA1B	0.003178	-3.9185	yes
PCDHA3	0.037881	-3.6686	yes
SLC7A14	9.05E-07	-3.5244	yes
CACNG3	0.010668	-3.4805	yes
SEL1L3	7.80E-18	-3.3168	yes
GM2694	3.83E-07	-3.1545	no
VGF	0.017608	-3.0815	yes
SIX2	0.005499	-3.0583	no
TNR	0.019404	-2.98	yes
HRH3	4.85E-05	-2.9737	yes
ST8SIA3	1.97E-23	-2.9179	yes
CALB1	8.77E-07	-2.8557	yes
CHRNB2	1.40E-25	-2.7833	yes
FAM123C	1.01E-06	-2.7517	yes
SERTAD4	0.02511	-2.7443	no
GAD1	2.08E-16	-2.7412	no
CELSR3	1.16E-22	-2.7184	yes
MMP24	2.93E-12	-2.6982	yes
OLFM2	0.005335	-2.6681	yes
ST6GAL1	0.005171	-2.6657	no
KRT73	0.002366	-2.6533	no
KCNH4	2.19E-13	-2.6445	yes
ACTL6B	7.13E-13	-2.6432	yes
SNAP25	2.39E-17	-2.5809	yes
NAV2	0.005915	-2.5493	yes
NEB	0.026335	-2.5431	yes
GBX1	2.29E-06	-2.5416	yes

Geneid	FDR	FC	REST
CPS1	0.015106	-2.5189	no
SCRT1	2.39E-21	-2.4981	yes
NAV3	0.001004	-2.492	yes
SHH	5.03E-14	-2.4599	no
SVOP	6.00E-12	-2.4579	yes
SPIRE2	0.024922	-2.453	yes
GRIN2D	0.000739	-2.4497	no
ZFP503	0.012233	-2.4494	no
INSM1	1.13E-33	-2.445	no
CDK5R2	6.13E-09	-2.397	yes
TRIM67	4.39E-12	-2.3903	yes
GM16702	0.026203	-2.385	no
AK142949	0.001174	-2.3531	no
E130309D14RIK	8.18E-06	-2.3424	yes
TH	2.60E-10	-2.3206	no
ARL4D	1.14E-35	-2.3172	no
XKR4	0.012392	-2.3083	yes
DCX	0.000289	-2.2862	yes
OOEP	0.000938	-2.2646	no
WSCD2	1.01E-06	-2.2061	yes
PLCXD3	0.00305	-2.2053	no
GM11346	0.010472	-2.2052	yes
NPTX2	8.19E-05	-2.1737	yes
TSHR	0.029427	-2.1484	no
GRIP2	8.27E-05	-2.1401	yes
LHX8	8.10E-19	-2.1386	no
GM13889	4.39E-12	-2.1273	no
GAD2	1.39E-11	-2.1262	yes
FAM65B	2.00E-06	-2.1222	yes
SCN3A	1.08E-10	-2.1098	no
UNC13A	8.05E-11	-2.0933	yes
AP3B2	7.53E-10	-2.0791	yes
NRSN1	3.30E-10	-2.0652	yes
AI606473	4.08E-17	-2.0568	no
MAGEL2	6.01E-14	-2.0531	no
ALDH1B1	0.000145	-2.0434	no
FAM110A	0.01006	-2.0239	yes
CHGA	3.47E-09	-2.0224	yes
SLC10A4	7.07E-09	-2.0207	no
PROX1	1.99E-07	-2.0174	yes

Table 4.4. Genes differentially down-regulated more than two fold in the *Insm1*$^{-/-}$ relative to the *Insm1*$^{+/+}$. FDR, tagwise false discovery rate. FC, tagwise fold change. Fold change is expressed as (*Insm1*$^{+/+}$ level)/(*Insm1*$^{-/-}$ level), with a minus sign to emphasize that this differs from how up-regulated genes are expressed. The "REST" column indicates whether a gene is a REST target. Genes concordantly regulated between the two KOs are shown in blue (genes that are down-regulated in the *Rcor1/2* KO, but by less than two fold, are included).

No fold change cutoff

	Down-regulated in *Rcor1/2* KO	Unchanged in *Rcor1/2* KO	Up-regulated in *Rcor1/2* KO	Total
Up-regulated in *Insm1*$^{-/-}$	1 (0)	78 (33)	21 (6)	100 (39)
Unchanged in *Insm1*$^{-/-}$	194 (99)		425 (147)	
Down-regulated in *Insm1*$^{-/-}$	105 (67)	87 (50)	5 (1)	197 (118)
Total	300 (166)		451 (154)	

1.5x fold change cutoff

	Down-regulated in *Rcor1/2* KO	Unchanged in *Rcor1/2* KO	Up-regulated in *Rcor1/2* KO	Total
Up-regulated in *Insm1*$^{-/-}$	1 (0)	55 (22)	15 (5)	71 (27)
Unchanged in *Insm1*$^{-/-}$	172 (87)		369 (124)	
Down-regulated in *Insm1*$^{-/-}$	82 (56)	63 (40)	5 (1)	150 (97)
Total	255 (143)		389 (130)	

2x fold change cutoff

	Down-regulated in *Rcor1/2* KO	Unchanged in *Rcor1/2* KO	Up-regulated in *Rcor1/2* KO	Total
Up-regulated in *Insm1*$^{-/-}$	0	27 (13)	5 (1)	32 (14)
Unchanged in *Insm1*$^{-/-}$	81 (47)		206 (59)	
Down-regulated in *Insm1*$^{-/-}$	45 (31)	34 (21)	1 (0)	80 (52)
Total	126 (78)		212 (60)	

Table 4.5. Numbers of differentially expressed genes by fold change.

Numbers of genes that are REST targets are provided parenthetically. Unchanged genes are not listed, because our stringent method for calling differentially expressed genes means that we cannot be confident that a gene we fail to detect as differentially expressed is truly expressed at the same levels.

CHAPTER 5: DISCUSSION AND FUTURE DIRECTIONS

5.1 Introduction

Nervous system development involves a delicate balance between neural progenitor proliferation and neuronal differentiation. Achieving this balance involves regulation of expression of genes that encode proteins and RNA mediating self-renewal versus cessation of proliferation and terminal differentiation. As discussed earlier, transcriptional activators, repressors, and chromatin modifiers are key players in this balance, but in this thesis I have focused on repression and on histone modifications associated with repression. In most cases, the existence of repressor complexes *in vivo* has not been shown. Here, I have identified a repressor/co-repressor complex in embryonic brain consisting of the repressor INSM1 and the co-repressors RCOR1 and RCOR2. Elimination of RCOR1 and RCOR2, or INSM1, robustly promotes neural proliferation over neuronal and oligodendrocyte differentiation. Further, their elimination results in over-expression of REST, a direct target gene of INSM1. Normalizing REST levels in the RCOR1/2-deficient brain partially restores aberrant brain morphology. Our results identify a new repressor/co-repressor complex required for critical events during normal brain development.

5.2 Discussion

5.2.1 RCOR1/2 expression

My work is the first to illustrate the protein expression patterns of RCOR1 and RCOR2. To investigate the role of RCOR1/2 in brain development, I first characterized their expression patterns. An early *in situ* hybridization study mistakenly identified *Rcor3* as *Rcor1*, because it was performed before the

mouse genome was completely annotated (Grimes et al., 2000). My analysis of control mice indicates that RCOR1 is expressed nearly ubiquitously in the telencephalon at E13.5 and E18.5. I show that RCOR2 protein is also expressed almost ubiquitously in E13.5 telencephalon, but that it is expressed at higher levels in the abventricular progenitor zone and mantle layer than in the progenitors directly adjacent to the lateral ventricle. This is consistent with previous *in situ* hybridization histochemistry studies showing *Rcor2* mRNA throughout the cortex at ~E13.5, with the highest expression in the cortical plate (Wang et al., 2016; Tontsch et al., 2001). By E18.5, RCOR2 is no longer expressed ubiquitously, consistent with previous studies that suggested that *Rcor2* mRNA and protein levels diminish during late embryonic stages (Wang et al., 2016; Tontsch et al., 2001). Further, in revealing that these proteins are co-expressed in nearly all neural cells at E13.5, it suggested that RCOR1 and RCOR2 might compensate for one another.

5.2.2 The *Rcor1* KO phenotype

A prediction from the compensation idea is that single KOs for RCOR1 and RCOR2 should not yield strong brain phenotypes. To test this prediction, I analyzed *Rcor1* KO mice, in which Cre-recombination was driven by the nestin promoter, at E18.5. Of seven *Rcor1* KOs, four were indistinguishable from controls. The other three, however, had only one obvious difference from controls and that was very subtle, specifically, abnormal clefts in the lateral ventral subpallial progenitor zone (Fig. 3.4). Further, these clefts were not consistent in appearance from mouse to mouse, or even from hemisphere to hemisphere

within an individual. In the case depicted in Fig. 3.4, the cleft resembled an IGS, the cavity between the LGE and MGE that disappears when these structures fuse between E15.5 and E16.5. The overall mild phenotype that I observed in the *Rcor1* KO is in contrast to previous *Rcor1* RNAi studies. For example, in cultured neural stem/progenitor cells, loss of RCOR1 increased the number of neurons after three days of differentiation (Covey et al., 2012). This discrepancy may reflect differences between *in vitro* and *in vivo* conditions or the fact that we are not comparing the same types of progenitors. Supporting the idea of *in vitro* versus *in vivo* differences, a previous study showed that REST-deficient progenitors in culture show up-regulation of REST target genes that does not occur in REST-deficient neural progenitors *in vivo* (Covey et al., 2012), (Nechiporuk et al., 2016). The role of culture conditions in the context of our knockout model could be tested with cultures from the *Rcor1* KOs. I predict that *in vitro*, *Rcor1/2* KO cells would have a premature neuronal differentiation phenotype, despite not exhibiting this phenotype *in vivo*.

More difficult to explain is the finding that mouse brain electroporated *in utero* with shRNAs targeting *Rcor1* at E14.5 showed decreased neuronal migration and aberrant neuronal morphology at E17.5 (Fuentes et al., 2012). Had the *Rcor1* KO mice exhibited neuronal migration defects comparable to those described by Fuentes et al., I expect that I would have seen an accumulation of cells in the intermediate zone when I performed H&E staining at E18.5. Further investigation is needed to ascertain whether *Rcor1* KO mice have defects in neuronal morphology similar to those reported in the electroporation study.

5.2.3 The *Rcor2* KO phenotype

I found that the *Rcor2* KO brain lacked any morphological abnormalities at E18.5. (Fig. 3.3 and 3.10). In contrast, a previous study published recently that brain deletion of *Rcor2* alone resulted in abnormal cortical development (Wang et al., 2016). This group reported that their *Rcor2* knockout had a smaller brain, fewer cortical progenitors at E13.5, apoptosis, fewer neurons, and deficits in interkinetic nuclear migration, similar to the *Rest* KO phenotype (Nechiporuk et al., 2016) and unlike my *Rcor2* KO phenotype. Further, they identified genes mis-regulated in their *Rcor2* KO cortex that were not concordantly mis-regulated in the *Rcor1/2* KO. In fact, two genes that Wang et al. show to be directly repressed by RCOR2 in cortex, sonic hedgehog (Shh) and distal-less homeobox 2 (Dlx2) were down-regulated in the *Rcor1/2* KO.

One possible explanation for the difference between the Wang laboratory's results and mine is that their knockout could be more complete at early stages due to more efficient Cre-mediated recombination. At E13.5, they detected absolutely no *Rcor2*/RCOR2 in the KO by *in situ*, immunohistochemistry, western blotting, and RNA-seq. This is a highly unusual result for Cre-mediated excision that is established to be mosaic. Indeed, in my *Rcor1/2* KO, RCOR2 is still expressed in some telencephalic mantle cells at E13.5. If we assume that their Cre-mediated excision is for some reason more efficient than most other situations that have been described, there are several possible explanations for the differential recombination. While they report using a Nes-Cre mouse line, they don’t describe the transgenic mouse in any detail. Therefore, their mouse

may regulate Cre expression using a different promoter fragment than ours, and/or be integrated at a different genomic position, which could lead to different recombination efficiencies. Because they used a different floxed allele, another possibility is that their LoxP sites were much more readily accessible to Cre than ours, or that the secondary structure of their allele allowed more efficient recombination. Given that Cre expression sometimes varies dependent upon the parent of origin (Heffner et al., 2012), differences in this regard are another possible source of variability. Cre was transmitted paternally in my work, but Wang et al. did not report their breeding scheme.

At least two factors independent of recombination efficiency could also contribute to the difference between the two *Rcor2* KOs. First, recombination of the Wang *Rcor2* floxed allele is predicted to produce a transcript encoding only the first 42 aa of RCOR2, while recombination of our floxed allele produces an additional 46 correctly-encoded amino acids. I therefore cannot rule out the possibility that this fragment is translated and serves some function. However, what function might be preserved is not clear, given that the truncated RCOR2 lacks domains required for the recruitment of HDAC1/2 and KDM1A. A final possibility is that the difference is attributable to background differences. Wang et al. state that they used CD-1 mice for *in utero* electroporation experiments, but do not report the background of the *Rcor2* KO mice. As will be discussed in greater detail below, control CD-1 mice differ from their C57BL/6 counterparts in several ways that might have relevance to these experiments.

The reason that my RNA profiling results differ from those of Wang et al. (2016) is probably that I focused on the ventral subpallium, while Wang et al. (2016) studied the neocortex. *Dlx2* and *Shh*, two genes up-regulated in the *Rcor2* KO studied by the Wang laboratory, are both expressed specifically in ventral domains, so the mechanisms by which these genes are repressed in the cortex would not be predicted to occur in the MGE. Given that RCOR2 itself is more highly expressed in dorsal than ventral regions at E18.5 (Fig. 3.2), it is possible that RCOR2 titrates repression of subpallium-specific genes. Alternatively, it may function differently in the cortex than in the subpallium because it interacts with region-specific transcription factors. An interesting candidate for being a region-specific RCOR-interacting protein is GSX2, a subpallial transcription factor important for dorsal-ventral specification (Toresson et al., 2000; Yun et al., 2001; Yun et al., 2003). GSX2 has a SNAG domain like INSM1, GFI1, and GFI1B, making it a candidate to recruit RCOR1/2 (Welcker et al., 2013).

5.2.4 RCOR1/2 have redundant functions in the brain

Several lines of evidence support the hypothesis that the mild phenotypes of the *Rcor1* and *Rcor2* single KOs could be explained by redundancy between the two RCOR proteins. They are co-expressed throughout the E13.5 brain (Fig. 3.1). Further, they are highly homologous. In addition, they are recruited by some of the same transcription factors, including REST, GFI1, and INSM1 (Zeng et al., 2010; Saleque et al., 2007; Welcker et al., 2013; see also Tables 1.1 and 1.2). Importantly, both RCOR1 and RCOR2 stimulate the demethylase activity of KDM1A (Upadhyay et al., 2014; Yang et al., 2011). Together, these findings

suggest that the mild *Rcor1* and *Rcor2* single KO phenotypes might be the result of functional compensation between these two proteins. Because RCOR3 protein was not detected in E13.5 mouse brain (Yao, 2014), I did not investigate whether RCOR3 could also compensate in the absence of RCOR1 or RCOR2.

5.2.5 Phenotype of the *Rcor1/2* KO

The brain-targeted *Rcor1/2* KO has a profound phenotype. Several observations suggest that the fundamental problem in the *Rcor1/2* KO is that many neural progenitors are unable to produce properly-positioned neurons and OPCs. The subpallial progenitor zone is expanded by excessive numbers of neural progenitors (Fig. 3.10-3.12). The proportion of each brain occupied by neurons is diminished (Fig 3.13). Axonal tracts are also thinner, which likely reflects reduced numbers of neurons (Fig. 3.8, 3.9, and 3.15). In addition, OPCs are reduced by 70% (Fig. 3.16). The lower number of neurons and their processes could contribute to the smaller brain sizes of the *Rcor1/2* KOs compared to control brains at E18.5 (Fig. 3.7), although I do not have any data to support a direct relationship between the number of neurons and brain size.

In addition to the above phenotypes, *Rcor1/2* KOs also exhibited a perturbation in the morphology of the subpallial progenitor zone. These mice retained a vestigial IGS days after this structure had disappeared from the control (Fig. 3.8). Experimental manipulations that reversed this phenotype (described below; Fig. 4.11) without reversing the progenitor accumulation phenotype indicate that this is not a side effect of reduced migration out of the progenitor

zone. Unfortunately, because the mice die neonatally, I was not able to determine whether the closure of the IGS was delayed or arrested.

I believe two distinct mechanisms contribute to the reduction of mature neurons and OPCs in *Rcor1/2* KO. One mechanism, which I infer from the overabundance of MKI67+ cells in the subpallial progenitor zone, is the propensity of neural progenitors to continue dividing instead of differentiating into either neurons or OPCs. Because increased numbers of progenitors were observed at multiple rostral-caudal levels, and because each progenitor marker examined was expressed in larger numbers of cells in the knockouts (Fig. 3.12), I hypothesize that this propensity of neural progenitors to remain in the cell cycle could be a general mechanism, and therefore likely contributes to reduced numbers of multiple neuronal and oligodendroglial subpopulations. The second mechanism, implicated by increased numbers of non-proliferating cells in the subpallial progenitor zones of the knockouts, is that the specification and/or migration of neurons and/or OPCs is perturbed. Supporting the possibility that neuronal migration might be inhibited, several genes required for neuronal migration, including *Celsr3* (cadherin EGF LAG seven-pass G-type receptor 3), *Dcx* (doublecortin), and *Dclk2* (doublecortin like kinase 2), were down-regulated in both knockouts. Large numbers of immature neurons are present in the subpallial progenitor zone of the *Rcor1/2* KO. The number of these cells will need to be compared to the number in controls in order to determine whether the additional MKI67-negative cells are immature neurons, which would indicate that there is a deficit in neuronal migration, or not, in which case those cells could be

either OPCs that are unable to migrate, or cells that have failed to become specified as either neurons or OPCs.

The *Rcor1/2* KO phenotype was surprising in that it did not strongly resemble that of the brain-targeted conditional *Rest* KO (Nechiporuk et al., 2016; Stenman et al., 2003; Roy et al., 2004). In contrast to the *Rcor1/2* KO, the *Rest* KO had reduced numbers of apical and basal progenitors in the cortex (Nechiporuk et al., 2016). Further, it had many apoptotic neurons at the border of the VZ/SVZ with the cortical plate (the corticostriatal boundary) as a result of increased levels of DNA damage. While the *Rest* KO did resemble the *Rcor1/2* KO in having thin cortices, this phenotype was likely a secondary effect of excessive apoptosis and depletion of the progenitor pool in the *Rest* KO, although direct effects cannot be ruled out (Nechiporuk et al., 2016). Phenotypes present in *Rest* KOs but not *Rcor1/2* KOs could be explained by the fact that REST can recruit the co-repressors SIN3A/B and CDYL in the absence of RCOR1/2 (Huang et al., 1999; Ballas et al., 2001; Greenway et al., 2007; Mulligan et al., 2008). Perhaps the loss of these complexes from REST binding sites contributes to the *Rest* KO-specific phenotypes. Conversely, phenotypes present in *Rcor1/2* KOs but absent in transcription factor KOs reflect the many transcription factors capable of recruiting RCOR1/2 (Tables 1.1 and 1.2).

5.2.6 INSM1 is a candidate to recruit RCOR1/2 in the developing subpallium

While in most cases where RCOR-associated transcription factors have been deleted from the developing brain in mice the phenotypes did not resemble those of *Rcor1/2* KOs, there was one exception. That was the deletion of the

repressor INSM1 (Welcker et al., 2013). INSM1 causes cell cycle arrest (Zhang et al., 2009), and is required for terminal differentiation of a variety of cell types (Gierl et al., 2006; Wildner et al., 2008; Ramachandran et al., 2012; Forbes-Osborne et al., 2013; Osipovich et al., 2014; Jia et al., 2015). Further, previous *Insm1* KO studies indicated that, similar to the *Rcor1/2* KO, the *Insm1* KO had a thin cortex and a thick PCNA+ proliferative region in E16.5 ventral telencephalon (27). However, the previous studies did not indicate whether the *Insm1* KO retained the IGS at E18.5 or had fewer OLIG2+ cells, two striking phenotypes in the *Rcor1/2* KO.

Because of the above findings, we performed co-immunoprecipitation analysis in embryonic brain and identified complexes containing both INSM1 and RCOR1 or RCOR2, as well as immunohistochemistry. My biochemical findings were consistent with previous studies showing RCOR1/2 in complexes with INSM1 in an endocrine cell line (Welcker et al., 2013). My immunohistochemistry was consistent with a previous study that detected *Insm1* transcripts in abventricular neural progenitors and nascent neurons (Duggan et al., 2008). Further, I found the highest levels of INSM1 staining in cells surrounding the border between the SVZ and the mantle area, where both RCOR1 and RCOR2 are also highly expressed.

5.2.7 Phenotype of the *Insm1*$^{-/-}$ mouse

I compared my *Insm1*$^{-/-}$ mouse (Osipovich et al., 2014) phenotypes to those in the *Rcor1/2* KO. Importantly, this mouse exhibited progenitor accumulation, incomplete IGS closure, and deficient neurogenesis and

oligodendrogenesis. In fact, all of the striking CNS phenotypes in the *Insm1*$^{-/-}$ were the same phenotypes observed in the *Rcor1/2* KO. However, the shared phenotypes were milder than in the *Rcor1/2* KO, and a few phenotypes were not reproduced at all. For example, brain size, cortical width, and axon tracts all appeared normal in the *Insm1*$^{-/-}$. It is likely that the distinct phenotypes are due to the fact that RCOR1/2, as major co-repressors in brain, are recruited by many transcription factors other than INSM1 (Tables 1.1 and 1.2; Ballas et al., 2005; Zeng et al., 2010; Saijo et al., 2009).

A possible explanation for distinct or milder phenotypes is differences in background. *Insm1*$^{-/-}$ mice were necessarily maintained on a different genetic background than the *Rcor1/2* KOs to mitigate the embryonic lethality of the *Insm1*$^{-/-}$ pups, which was more pronounced on the C57BL/6 than the CD-1 mice background. Indeed, comparison of the width of the progenitor zone in the *Rcor1/2* fl relative to the *Insm1*$^{+/+}$ mouse demonstrates that this parameter is background-dependent (Fig. 4.7). The subpallial progenitor zone was significantly wider ($p = 0.0341$) in the *Rcor1/2* fl (159 ± 42 μm) than in the *Insm1*$^{+/+}$ mouse (103 ± 24 μm).

5.2.8 The *Rcor1/2* and *Insm1* KOs regulate a shared set of gene targets

Given that INSM1 can regulate many different target genes, is it possible to identify a molecular basis for the phenotypes that are shared in the *Rcor1/2* KO and *Insm1*$^{-/-}$ mice? Because INSM1 and RCOR1/2 both mediate transcriptional repression (Breslin et al., 2002; Andrés et al., 1999; Barrios et al., 2014), we anticipated that we would identify a set of shared up-regulated genes

in the KOs. While we did identify such genes, we were surprised to find even more shared genes that were down regulated. Intriguingly, 64% of these genes in the *Rcor1/2* and *Insm1* KOs were REST target genes. INSM1 binds to the REST promoter *in vivo* (Osipovich et al., 2014), suggesting that loss of INSM1 could cause de-repression of *Rest*. Further, INSM1 is up-regulated at the transition from apical to basal progenitor, which corresponds precisely to the timing of REST down-regulation during embryogenesis (Nechiporuk et al., 2016). We used RT-qPCR to confirm that *Rest* transcript levels were indeed elevated in the *Rcor1/2* KO and *Insm1*$^{-/-}$ mice compared to controls.

5.2.9 The role of *Rest* overexpression in the *Rcor1/2* KO

An important question is whether increased REST protein could repress target genes in the absence of RCOR1 and RCOR2. As mentioned above, REST can repress at least some targets without recruiting RCOR proteins (Ballas et al., 2001; Greenway et al., 2007; Huang et al., 1999; Mulligan et al., 2008) by instead recruiting the SIN3/HDAC1/2 or CDYL/EHMT2 co-repressors. For this reason, we hypothesized that overexpression of REST was causing repression of REST targets in the *Rcor1/2* KO. Based on previous studies, we further hypothesized that this repression might contribute to the *Rcor1/2* KO and *Insm1*$^{-/-}$ phenotypes.

To analyze the role of REST in the *Rcor1/2* KO, we normalized REST levels through heterozygous loss of *Rest*. This restored or partially restored transcript levels of some selected REST target genes, which demonstrated that REST was one of the factors contributing to their repression in the *Rcor1/2* KO, and likely also in the *Insm1*$^{-/-}$ mouse. Consistent with this finding, the four genes

that were restored or partially restored–*Celsr3*, *Chrnb2*, *Trim67*, and *Unc13a*– were also among the genes that had been up-regulated in neural stem cells in a REST loss-of-function experiment (Johnson et al., 2008).

Why did heterozygous loss of *Rest* fail to restore all of the repressed REST targets to normal levels? The simplest explanation is that REST is not repressing these genes in the *Rcor1/2* KO. While I defined REST targets on the basis of REST binding in ESCs, only ~55% of REST binding sites in ESCs are also occupied by REST in neural stem cells (Johnson et al., 2008). Further, the genes bound by REST in neural stem cells are not all regulated in the same way. In a hippocampal neural stem cell line, different RE1 sites have been associated with different complements of co-repressors (Greenway et al., 2007). Because REST does not recruit the same co-repressors under all circumstances, it does not repress all of its targets equally. Surprisingly, REST binding fails to repress some targets at all. Overexpression of the DNA-binding domain of REST, which functions as a dominant-negative by outcompeting endogenous REST for binding sites, causes up-regulation of some, but not all, REST-bound genes (Chen et al., 1998; Otto et al., 2007). RNAi and knockout studies confirm that REST does not repress all the targets it binds (Nechiporuk et al., 2016; Aoki et al., 2012; Chen et al., 1998; Covey et al., 2012).

Therefore, we conclude that the most likely reason some Rest targets were not restored to normal levels in the *Rest* rescue is that other targets of the INSM1/RCOR complex were responsible for these phenotypes. Likely targets include *Tgif1* and *Hey1*, which were up-regulated in both *Rcor1/2* KO and *Insm1*$^{-}$

$^{-/-}$ mice. These genes encode transcriptional repressors involved in neural development (Kuang et al., 2006; Sakamoto et al., 2003) and are expressed widely in neural progenitors but down-regulated in neurons (Sakamoto et al., 2003; Shen and Walsh, 2005).

Normalization of *Rest* levels in the *Rcor1/2* KO did ameliorate the phenotype, but not in the way we expected: it partially repaired closure of the IGS. This suggests that the retention of the IGS in the *Rcor1/2* KO was due to repression mediated by the REST/SIN3 or REST/CDYL complexes. Future studies manipulating REST target genes with potential functions in migration, such as *Celsr3* (Ying et al., 2009), may shed new light on IGS closure.

While we had anticipated that normalizing REST levels might also restore or partially restore the generation of neurons and OPCs, this was not the case. In retrospect, this is not terribly surprising, because while diminishing *Rest* levels increases the production of neurons and OPCs *in vitro* (Covey et al., 2012), it does not do so *in vivo* (Nechiporuk et al., 2016). While the *in utero* electroporation experiments of Mandel et al. (2011) demonstrate that REST overexpression can cause deficits in neuronal differentiation, these experiments likely induce much greater increases in *Rest* levels than the modest 2.1-2.3-fold up-regulation observed in the *Rcor1/2* KO and *Insm1*$^{-/-}$ mouse.

5.2.10 The role of the INSM1/RCOR complex in brain development

My study, and others, of INSM1 in the mammalian nervous system demonstrate that it performs a great variety of functions. In mouse brain, INSM1 promotes the transition of apical progenitors into basal progenitors and the

acquisition of neuronal traits (Table 1.4; Farkas et al., 2008; Rosenbaum et al., 2011; Jacob et al., 2009). However, functions such as cell cycle regulation, which have been proposed outside of the brain (Zhang et al., 2009; Rosenbaum et al., 2011) or in lower organisms (Candal et al., 2007; Wu et al., 2001) have not been thoroughly investigated in the mammalian brain.

My work suggests that the INSM1-RCOR complex performs essentially the same role in mammalian subpallium as it does in invertebrates. Both *Insm1* and *Rcor1/2* have homologs in *C. elegans* (Wu et al., 2001; Jarriault and Greenwald, 2002). Interestingly, *C. elegans* that are mutant for the *Insm1* homolog *egl-46* have a phenotype similar to what we observe in the *Insm1*$^{-/-}$ and *Rcor1/2* KO mice. In these worms, certain neural progenitors also undergo aberrant additional rounds of cell division (Desai and Horvitz, 1989). However, in the mammalian subpallium, which produces a greater variety of neural cell types than the worm nervous system, INSM1 and RCOR1/2 regulate the production of OPCs as well as of neurons. While many studies indicate that INSM1 contributes to the production of neurons, this work is the first to demonstrate a link between INSM1 and oligodendrogliogenesis. Altogether, our studies suggest that an INSM1/RCOR complex facilitates neuronal and oligodendroglial differentiation.

5.3 Future directions

5.3.1 Identifying direct targets of the INSM1/RCOR complex

To be confident that the INSM1/RCOR complex that I identified biochemically mediates transcriptional repression, I would need to demonstrate that INSM1 and RCOR1/RCOR2 are bound to the same genomic locus

concurrently, and that the genes associated with these loci are de-repressed in both the *Rcor1/2* KO and the *Insm1*$^{-/-}$ mouse. Ideally, I would perform ChIP-seq with antibodies recognizing INSM1, RCOR1, RCOR2, and KDM1A to determine whether the binding peaks associated with each of these proteins align with one another. I predict that several of the genes up-regulated in both the *Rcor1/2* KO and the *Insm1*$^{-/-}$ mouse, including *Rest*, would be bound by INSM1/RCOR1/RCOR2/KDM1A. ChIP-seq would provide strong evidence that specific loci were bound by multiple INSM1/RCOR complex members. However, it would not allow us to rule out the possibility that, for example, RCOR1 is associated with a site on the *Rest* gene in some cells, but INSM1 is bound there in other cells. To address this possibility, I would use ChIP-reChIP. That is, I would perform ChIP with an antibody (e.g. against INSM1), and then perform a second ChIP with a different antibody (e.g. against RCOR1) on the eluate of the first ChIP. This would verify that two members of the complex were present together on the chromatin.

Although I sought to perform ChIPs with RCOR1, RCOR2, and INSM1 antibodies, I was unable to convincingly show a valid ChIP compared to control sequences, despite previous successful results by others. I could circumvent this problem by using mice expressing a tagged version of the protein of interest. For instance, Wang et al. (2016) successfully performed ChIP in mouse cortex using a transgenic mouse in which a FLAG tag was knocked in at the amino terminus of RCOR2. Using the CRISPR/Cas9 system (Cong et al., 2013), it would be possible to also generate mice with tagged RCOR1 and INSM1.

One barrier to identifying the INSM1/RCOR complex by ChIP is that this complex is absent in a majority of neural cells (Fig. 4.3). This creates the potential for high background, and also makes it difficult to judge the amount of chromatin needed for the experiment, given that a majority of that chromatin is from INSM1-negative cells. I would therefore use INTACT (*i*solation of *n*uclei *ta*gged in specific *c*ell *t*ypes), a method for isolating nuclei of specific cell types for downstream use in chromatin, RNA, or protein profiling (Deal and Henikoff, 2010). To do so, I would obtain the mouse generated by Mo et al. (2015), which has a Myc-tagged nuclear envelope protein that is only expressed when a transcriptional roadblock is removed by Cre-mediated recombination. I could then use Insm1-Cre mice to specifically tag INSM1-expressing cells, and would affinity-purify INSM1-expressing nuclei using Myc antibodies to generate starting material for the ChIP.

5.3.2 Confirming the role of KDM1A

Based on crystal structures showing that RCOR1 and INSM1 are held together in a complex by KDM1A, I predict that KDM1A targets the same genes as RCOR1/2 and INSM1. A ChIP analysis of KDM1A would be valuable. In the case of KDM1A, a tagged protein would probably not be necessary, as ChIP-seq has been successfully performed with antibodies to the endogenous protein (Whyte et al., 2012; Zhang et al., 2013).

Further, I predict that phenotypes shared between the *Rcor1/2* and *Insm1* KOs are also shared with the *Kdm1a* KO. While I was unable to pursue this avenue of research, preliminary evidence from the Rosenfeld laboratory

suggests that the *Kdm1a* KO shares with the *Rcor1/2* and *Insm1* KOs the subpallial progenitor accumulation phenotype. Further studies would be required to determine whether the *Kdm1a* KO has a vestigial IGS, smaller neuronal domains, and fewer OPCs. I predict that RNA profiling experiments on the MGE of the *Kdm1a* KO would show that a majority of the genes concordantly regulated in the *Rcor1/2* KO and the *Insm1*$^{-/-}$ mouse are similarly mis-regulated in this mouse.

5.3.3 Further characterization of *Rcor1/2* KO and *Insm1*$^{-/-}$ mice

In the cortex, loss of INSM1 leads to insufficient production of neurons, in part because fewer apical progenitors produce basal progenitors. However, I question whether a similar mechanism occurs in the ventral telencephalon, based on the expression of Dlx2, which encodes a transcription factor that promotes the generation of GABAergic neurons. *Dlx2*, which is more highly expressed in the SVZ than the VZ (Petryniak et al., 2007), is expressed in large numbers of cells in the VZ/SVZ of the *Rcor1/2* KO, which implies that these overrepresented cells likely have an SVZ, rather than a VZ, identity. To test whether apical or basal progenitors are expanded in the *Rcor1/2* KO and the *Insm1*$^{-/-}$ mouse, I could perform *in situ* hybridization histochemistry for markers, such as *Hey1 and Hes5*, that are most highly expressed in the VZ (Sakamoto et al., 2003). HEY1 and HES5 are Notch targets, transcriptional repressors that promote the maintenance of the progenitor state (Sakamoto et al., 2003; Ohtsuka et al., 1999). *Hey1* would be a particularly interesting target because it is up-regulated in the E13.5 *Rcor1/2* KO. Based on the *Dlx2* expression pattern, I

predict that expansion of the *Hey1* and *Hes5* populations cannot account for the increased number of MKI67+ cells in the subpallial progenitor zone.

5.3.4 Confirming the role of REST in *Rcor1/2* KO and *Insm1*$^{-/-}$ mice

Because the *Rest* rescue exhibits restoration of some *Rest* targets and amelioration of the IGS phenotype, we conclude that overexpression of REST leads to inappropriate repression of some of its targets in the *Rcor1/2* KO and *Insm1*$^{-/-}$ mice. However, our findings suggest a set of hypotheses that we have not tested. First, while it has been published that *Rest* is bound by INSM1 in embryonic pancreas (Osipovich et al., 2014), we have not established whether this is the case in the brain. As discussed above, performing ChIP on INSM1-positive nuclei from the MGE would be an attractive way to address this question. The antibody used by Osipovich et al. (2014) is publicly available, so this might be feasible. As discussed above, mice expressing the INTACT nuclear envelope tag in INSM1+ cells could be used to improve the signal-to-noise ratio.

Second, if *Rest* is repressed by INSM1, we should expect the increased levels of Rest observed by RT-qPCR to be due to increased expression in INSM1+, and not INSM1-, cells. Immunohistochemistry experiments co-labeling cells with antibodies recognizing INSM1 and REST could test whether, as I would predict, INSM1-positive cells typically have lower REST levels than INSM1-negative cells. Because the *Insm1*$^{-/-}$ mouse expresses GFP from the *Insm1* promoter, I could also assess whether GFP-positive cells have lower REST levels than GFP-negative cells as a negative control. I have performed preliminary experiments that suggest that indeed, nuclei with high INSM1 have

lower REST signal than low-INSM1 nuclei. Importantly, there was no relationship between GFP expression and REST, suggesting that the presence of INSM1 is responsible for the reduction in REST in wild-type INSM1+ cells. Unfortunately, the REST antibody I used produced a high level of background. While it is statistically improbable that I would see a strong negative correlation between INSM1 and REST signals by chance, I cannot be wholly confident in these results until they have been repeated with a cleaner antibody. If this yielded results comparable to those I have described, I would then analyze the relationship between INSM1 expression and REST expression in the *Rcor1/2* KO. My prediction would be that high INSM1 would not correlate with reduced REST in this knockout.

Third, performing ChIP for REST in the *Rcor1/2* fl, *Rcor1/2* KO, and *Rest* rescue would allow us to test whether, in the Rcor1/2 KO, there was elevated binding of REST to genes down-regulated in the *Rcor1/2 KO* but restored to control levels in the *Rest* rescue, such as *Celsr3*.

REFERENCES

Abrajano, J.J., Qureshi, I.A., Gokhan, S., Molero, A.E., Zheng, D., Bergman, A., and Mehler, M.F. (2010). Corepressor for element-1-silencing transcription factor preferentially mediates gene networks underlying neural stem cell fate decisions. Proc Natl Acad Sci U S A *107*, 16685-16690.

Abrajano, J.J., Qureshi, I.A., Gokhan, S., Zheng, D., Bergman, A., and Mehler, M.F. (2009a). Differential deployment of REST and CoREST promotes glial subtype specification and oligodendrocyte lineage maturation. PLoS One *4*, e7665.

Abrajano, J.J., Qureshi, I.A., Gokhan, S., Zheng, D., Bergman, A., and Mehler, M.F. (2009b). REST and CoREST modulate neuronal subtype specification, maturation and maintenance. PLoS One *4*, e7936.

Achim, K., Peltopuro, P., Lahti, L., Tsai, H.H., Zachariah, A., Astrand, M., Salminen, M., Rowitch, D., and Partanen, J. (2013). The role of Tal2 and Tal1 in the differentiation of midbrain GABAergic neuron precursors. Biol Open *2*, 990-997.

Achim, K., Salminen, M., and Partanen, J. (2014). Mechanisms regulating GABAergic neuron development. Cell Mol Life Sci *71*, 1395-1415.

Alberts, B., Johnson, A., Lewis, J., Raff, M., Roberts, K., Walter, P., Wilson, J.H., and Hunt, T. (2008). Molecular biology of the cell, 5th edn (New York: Garland Science).

Allis, C.D., and Jenuwein, T. (2016). The molecular hallmarks of epigenetic control. Nat Rev Genet *17*, 487-500.

Andres, M.E., Burger, C., Peral-Rubio, M.J., Battaglioli, E., Anderson, M.E., Grimes, J., Dallman, J., Ballas, N., and Mandel, G. (1999). CoREST: a functional corepressor required for regulation of neural-specific gene expression. Proc Natl Acad Sci U S A *96*, 9873-9878.

Aoki, H., Hara, A., Era, T., Kunisada, T., and Yamada, Y. (2012). Genetic ablation of Rest leads to in vitro-specific derepression of neuronal genes during neurogenesis. Development *139*, 667-677.

Ballas, N., Battaglioli, E., Atouf, F., Andres, M.E., Chenoweth, J., Anderson, M.E., Burger, C., Moniwa, M., Davie, J.R., Bowers, W.J.*, et al.* (2001). Regulation of neuronal traits by a novel transcriptional complex. Neuron *31*, 353-365.

Ballas, N., Grunseich, C., Lu, D.D., Speh, J.C., and Mandel, G. (2005). REST and its corepressors mediate plasticity of neuronal gene chromatin throughout neurogenesis. Cell *121*, 645-657.

Barrios, A.P., Gomez, A.V., Saez, J.E., Ciossani, G., Toffolo, E., Battaglioli, E., Mattevi, A., and Andres, M.E. (2014). Differential properties of transcriptional complexes formed by the CoREST family. Mol Cell Biol *34*, 2760-2770.

Benjamini, Y., and Hochberg, Y. (1995). Controlling the false discovery rate: a practical and powerful approach to multiple testing. J R Stat Soc Series B Stat Methodol *57*, 289-300.

Bhide, P.G. (1996). Cell cycle kinetics in the embryonic mouse corpus striatum. J Comp Neurol *374*, 506-522.

Breslin, M.B., Zhu, M., Notkins, A.L., and Lan, M.S. (2002). Neuroendocrine differentiation factor, IA-1, is a transcriptional repressor and contains a specific DNA-binding domain: identification of consensus IA-1 binding sequence. Nucleic Acids Res *30*, 1038-1045.

Brinton, R.D., Thompson, R.F., Foy, M.R., Baudry, M., Wang, J., Finch, C.E., Morgan, T.E., Pike, C.J., Mack, W.J., Stanczyk, F.Z.*, et al.* (2008). Progesterone receptors: form and function in brain. Front Neuroendocrinol *29*, 313-339.

Buck, A., Kispert, A., and Kohlhase, J. (2001). Embryonic expression of the murine homologue of SALL1, the gene mutated in Townes--Brocks syndrome. Mech Dev *104*, 143-146.

Cahoy, J.D., Emery, B., Kaushal, A., Foo, L.C., Zamanian, J.L., Christopherson, K.S., Xing, Y., Lubischer, J.L., Krieg, P.A., Krupenko, S.A.*, et al.* (2008). A transcriptome database for astrocytes, neurons, and oligodendrocytes: a new resource for understanding brain development and function. J Neurosci *28*, 264-278.

Candal, E., Alunni, A., Thermes, V., Jamen, F., Joly, J.S., and Bourrat, F. (2007). Ol-insm1b, a SNAG family transcription factor involved in cell cycle arrest during medaka development. Dev Biol *309*, 1-17.

Castro, D.S., Skowronska-Krawczyk, D., Armant, O., Donaldson, I.J., Parras, C., Hunt, C., Critchley, J.A., Nguyen, L., Gossler, A., Gottgens, B.*, et al.* (2006). Proneural bHLH and Brn proteins coregulate a neurogenic program through cooperative binding to a conserved DNA motif. Dev Cell *11*, 831-844.

Chen, Z.F., Paquette, A.J., and Anderson, D.J. (1998). NRSF/REST is required in vivo for repression of multiple neuronal target genes during embryogenesis. Nat Genet *20*, 136-142.

Chong, J.A., Tapia-Ramirez, J., Kim, S., Toledo-Aral, J.J., Zheng, Y., Boutros, M.C., Altshuller, Y.M., Frohman, M.A., Kraner, S.D., and Mandel, G. (1995). REST: a mammalian silencer protein that restricts sodium channel gene expression to neurons. Cell *80*, 949-957.

Cong, L., Ran, F.A., Cox, D., Lin, S., Barretto, R., Habib, N., Hsu, P.D., Wu, X., Jiang, W., Marraffini, L.A.*, et al.* (2013). Multiplex genome engineering using CRISPR/Cas systems. Science *339*, 819-823.

Coqueret, O. (2002). Linking cyclins to transcriptional control. Gene *299*, 35-55.

Corbin, J.G., and Butt, S.J. (2011). Developmental mechanisms for the generation of telencephalic interneurons. Dev Neurobiol *71*, 710-732.

Covey, M.V., Streb, J.W., Spektor, R., and Ballas, N. (2012). REST regulates the pool size of the different neural lineages by restricting the generation of neurons and oligodendrocytes from neural stem/progenitor cells. Development *139*, 2878-2890.

Cutter, A.R., and Hayes, J.J. (2015). A brief review of nucleosome structure. FEBS Lett *589*, 2914-2922.

Deal, R.B., and Henikoff, S. (2010). A simple method for gene expression and chromatin profiling of individual cell types within a tissue. Dev Cell *18*, 1030-1040.

Desai, C., and Horvitz, H.R. (1989). Caenorhabditis elegans mutants defective in the functioning of the motor neurons responsible for egg laying. Genetics *121*, 703-721.

Dessaud, E., McMahon, A.P., and Briscoe, J. (2008). Pattern formation in the vertebrate neural tube: a sonic hedgehog morphogen-regulated transcriptional network. Development *135*, 2489-2503.

Duggan, A., Madathany, T., de Castro, S.C., Gerrelli, D., Guddati, K., and Garcia-Anoveros, J. (2008). Transient expression of the conserved zinc finger gene INSM1 in progenitors and nascent neurons throughout embryonic and adult neurogenesis. J Comp Neurol *507*, 1497-1520.

Farkas, L.M., Haffner, C., Giger, T., Khaitovich, P., Nowick, K., Birchmeier, C., Paabo, S., and Huttner, W.B. (2008). Insulinoma-associated 1 has a panneurogenic role and promotes the generation and expansion of basal progenitors in the developing mouse neocortex. Neuron *60*, 40-55.

Farkas, L.M., and Huttner, W.B. (2008). The cell biology of neural stem and progenitor cells and its significance for their proliferation versus differentiation during mammalian brain development. Curr Opin Cell Biol *20*, 707-715.

Fischer, A.H., Jacobson, K.A., Rose, J., and Zeller, R. (2008). Hematoxylin and eosin staining of tissue and cell sections. CSH Protoc *2008*, pdb prot4986.

Flames, N., Pla, R., Gelman, D.M., Rubenstein, J.L., Puelles, L., and Marin, O. (2007). Delineation of multiple subpallial progenitor domains by the combinatorial expression of transcriptional codes. J Neurosci *27*, 9682-9695.

Forbes-Osborne, M.A., Wilson, S.G., and Morris, A.C. (2013). Insulinoma-associated 1a (Insm1a) is required for photoreceptor differentiation in the zebrafish retina. Dev Biol *380*, 157-171.

Fuentes, P., Canovas, J., Berndt, F.A., Noctor, S.C., and Kukuljan, M. (2012). CoREST/LSD1 control the development of pyramidal cortical neurons. Cereb Cortex *22*, 1431-1441.

Gierl, M.S., Karoulias, N., Wende, H., Strehle, M., and Birchmeier, C. (2006). The zinc-finger factor Insm1 (IA-1) is essential for the development of pancreatic beta cells and intestinal endocrine cells. Genes Dev *20*, 2465-2478.

Gocke, C.B., and Yu, H. (2008). ZNF198 stabilizes the LSD1-CoREST-HDAC1 complex on chromatin through its MYM-type zinc fingers. PLoS One *3*, e3255.

Gofflot, F., Chartoire, N., Vasseur, L., Heikkinen, S., Dembele, D., Le Merrer, J., and Auwerx, J. (2007). Systematic gene expression mapping clusters nuclear receptors according to their function in the brain. Cell *131*, 405-418.

Greenway, D.J., Street, M., Jeffries, A., and Buckley, N.J. (2007). RE1 Silencing transcription factor maintains a repressive chromatin environment in embryonic hippocampal neural stem cells. Stem Cells *25*, 354-363.

Grimes, J.A., Nielsen, S.J., Battaglioli, E., Miska, E.A., Speh, J.C., Berry, D.L., Atouf, F., Holdener, B.C., Mandel, G., and Kouzarides, T. (2000). The co-repressor mSin3A is a functional component of the REST-CoREST repressor complex. J Biol Chem *275*, 9461-9467.

Guy, J., Hendrich, B., Holmes, M., Martin, J.E., and Bird, A. (2001). A mouse Mecp2-null mutation causes neurological symptoms that mimic Rett syndrome. Nat Genet *27*, 322-326.

Hakimi, M.A., Bochar, D.A., Chenoweth, J., Lane, W.S., Mandel, G., and Shiekhattar, R. (2002). A core-BRAF35 complex containing histone deacetylase mediates repression of neuronal-specific genes. Proc Natl Acad Sci U S A *99*, 7420-7425.

Hakimi, M.A., Dong, Y., Lane, W.S., Speicher, D.W., and Shiekhattar, R. (2003). A candidate X-linked mental retardation gene is a component of a new family of histone deacetylase-containing complexes. J Biol Chem *278*, 7234-7239.

Hargreaves, D.C., and Crabtree, G.R. (2011). ATP-dependent chromatin remodeling: genetics, genomics and mechanisms. Cell Res *21*, 396-420.

Heffner, C.S., Herbert Pratt, C., Babiuk, R.P., Sharma, Y., Rockwood, S.F., Donahue, L.R., Eppig, J.T., and Murray, S.A. (2012). Supporting conditional mouse mutagenesis with a comprehensive cre characterization resource. Nat Commun *3*, 1218.

Hegeman, D.J., Hong, E.S., Hernandez, V.M., and Chan, C.S. (2016). The external globus pallidus: progress and perspectives. Eur J Neurosci *43*, 1239-1265.

Hirano, K., and Namihira, M. (2016). LSD1 Mediates Neuronal Differentiation of Human Fetal Neural Stem Cells by Controlling the Expression of a Novel Target Gene, HEYL. Stem Cells *34*, 1872-1882.

Hirayama, T., Tarusawa, E., Yoshimura, Y., Galjart, N., and Yagi, T. (2012). CTCF is required for neural development and stochastic expression of clustered Pcdh genes in neurons. Cell Rep *2*, 345-357.

Huang, Y., Myers, S.J., and Dingledine, R. (1999). Transcriptional repression by REST: recruitment of Sin3A and histone deacetylase to neuronal genes. Nat Neurosci *2*, 867-872.

Hunt, R.F., and Baraban, S.C. (2015). Interneuron Transplantation as a Treatment for Epilepsy. Cold Spring Harb Perspect Med *5*.

Jacob, J., Storm, R., Castro, D.S., Milton, C., Pla, P., Guillemot, F., Birchmeier, C., and Briscoe, J. (2009). Insm1 (IA-1) is an essential component of the regulatory network that specifies monoaminergic neuronal phenotypes in the vertebrate hindbrain. Development *136*, 2477-2485.

Jarriault, S., and Greenwald, I. (2002). Suppressors of the egg-laying defective phenotype of sel-12 presenilin mutants implicate the CoREST corepressor complex in LIN-12/Notch signaling in C. elegans. Genes Dev *16*, 2713-2728.

Jenuwein, T., and Allis, C.D. (2001). Translating the histone code. Science *293*, 1074-1080.

Jia, S., Wildner, H., and Birchmeier, C. (2015). Insm1 controls the differentiation of pulmonary neuroendocrine cells by repressing Hes1. Dev Biol *408*, 90-98.

Johnson, R., Teh, C.H., Kunarso, G., Wong, K.Y., Srinivasan, G., Cooper, M.L., Volta, M., Chan, S.S., Lipovich, L., Pollard, S.M.*, et al.* (2008). REST regulates distinct transcriptional networks in embryonic and neural stem cells. PLoS Biol *6*, e256.

Josling, G.A., Selvarajah, S.A., Petter, M., and Duffy, M.F. (2012). The role of bromodomain proteins in regulating gene expression. Genes (Basel) *3*, 320-343.

Kemp, K., Mallam, E., Scolding, N., and Wilkins, A. (2010). Stem cells in genetic myelin disorders. Regen Med *5*, 425-439.

Kessaris, N., Fogarty, M., Iannarelli, P., Grist, M., Wegner, M., and Richardson, W.D. (2006). Competing waves of oligodendrocytes in the forebrain and postnatal elimination of an embryonic lineage. Nat Neurosci *9*, 173-179.

Kouzarides, T. (2007). Chromatin modifications and their function. Cell *128*, 693-705.

Kuang, C., Xiao, Y., Yang, L., Chen, Q., Wang, Z., Conway, S.J., and Chen, Y. (2006). Intragenic deletion of Tgif causes defectsin brain development. Hum Mol Genet *15*, 3508-3519.

Kuwabara, T., Hsieh, J., Nakashima, K., Taira, K., and Gage, F.H. (2004). A small modulatory dsRNA specifies the fate of adult neural stem cells. Cell *116*, 779-793.

Laurent, B., Ruitu, L., Murn, J., Hempel, K., Ferrao, R., Xiang, Y., Liu, S., Garcia, B.A., Wu, H., Wu, F.*, et al.* (2015). A specific LSD1/KDM1A isoform regulates neuronal differentiation through H3K9 demethylation. Mol Cell *57*, 957-970.

Li, Q., Burgess, R., and Zhang, Z. (2012). All roads lead to chromatin: Multiple pathways for histone deposition. Biochim Biophys Acta *1819*, 238-246.

Liao, Y., Smyth, G.K., and Shi, W. (2013). The Subread aligner: fast, accurate and scalable read mapping by seed-and-vote. Nucleic Acids Res *41*, e108.

Liao, Y., Smyth, G.K., and Shi, W. (2014). featureCounts: an efficient general purpose program for assigning sequence reads to genomic features. Bioinformatics *30*, 923-930.

Lin, H.M., Zhao, L., and Cheng, S.Y. (2002). Cyclin D1 Is a Ligand-independent Co-repressor for Thyroid Hormone Receptors. J Biol Chem *277*, 28733-28741.

Liu, W.D., Wang, H.W., Muguira, M., Breslin, M.B., and Lan, M.S. (2006). INSM1 functions as a transcriptional repressor of the neuroD/beta2 gene through the recruitment of cyclin D1 and histone deacetylases. Biochem J *397*, 169-177.

Lorenzen, S.M., Duggan, A., Osipovich, A.B., Magnuson, M.A., and Garcia-Anoveros, J. (2015). Insm1 promotes neurogenic proliferation in delaminated otic progenitors. Mech Dev *138 Pt 3*, 233-245.

Luger, K., Mader, A.W., Richmond, R.K., Sargent, D.F., and Richmond, T.J. (1997). Crystal structure of the nucleosome core particle at 2.8 A resolution. Nature *389*, 251-260.

Lukaszewicz, A.I., and Anderson, D.J. (2011). Cyclin D1 promotes neurogenesis in the developing spinal cord in a cell cycle-independent manner. Proc Natl Acad Sci U S A *108*, 11632-11637.

Mandel, G., Fiondella, C.G., Covey, M.V., Lu, D.D., Loturco, J.J., and Ballas, N. (2011). Repressor element 1 silencing transcription factor (REST) controls radial migration and temporal neuronal specification during neocortical development. Proc Natl Acad Sci U S A *108*, 16789-16794.

Martynoga, B., Drechsel, D., and Guillemot, F. (2012). Molecular control of neurogenesis: a view from the mammalian cerebral cortex. Cold Spring Harb Perspect Biol *4*.

McGann, J.C., Oyer, J.A., Garg, S., Yao, H., Liu, J., Feng, X., Liao, L., Yates, J.R., 3rd, and Mandel, G. (2014). Polycomb- and REST-associated histone deacetylases are independent pathways toward a mature neuronal phenotype. Elife *3*, e04235.

Mo, A., Mukamel, E.A., Davis, F.P., Luo, C., Henry, G.L., Picard, S., Urich, M.A., Nery, J.R., Sejnowski, T.J., Lister, R.*, et al.* (2015). Epigenomic Signatures of Neuronal Diversity in the Mammalian Brain. Neuron *86*, 1369-1384.

Monchi, O., Petrides, M., Strafella, A.P., Worsley, K.J., and Doyon, J. (2006). Functional role of the basal ganglia in the planning and execution of actions. Ann Neurol *59*, 257-264.

Mulligan, P., Westbrook, T.F., Ottinger, M., Pavlova, N., Chang, B., Macia, E., Shi, Y.J., Barretina, J., Liu, J., Howley, P.M.*, et al.* (2008). CDYL bridges REST and histone methyltransferases for gene repression and suppression of cellular transformation. Mol Cell *32*, 718-726.

Nan, X., Campoy, F.J., and Bird, A. (1997). MeCP2 is a transcriptional repressor with abundant binding sites in genomic chromatin. Cell *88*, 471-481.

Nechiporuk, T., McGann, J., Mullendorff, K., Hsieh, J., Wurst, W., Floss, T., and Mandel, G. (2016). The REST remodeling complex protects genomic integrity during embryonic neurogenesis. Elife *5*, e09584.

Ohtsuka, T., Ishibashi, M., Gradwohl, G., Nakanishi, S., Guillemot, F., and Kageyama, R. (1999). Hes1 and Hes5 as notch effectors in mammalian neuronal differentiation. EMBO J *18*, 2196-2207.

Olins, A.L., and Olins, D.E. (1974). Spheroid chromatin units (v bodies). Science *183*, 330-332.

Osipovich, A.B., Long, Q., Manduchi, E., Gangula, R., Hipkens, S.B., Schneider, J., Okubo, T., Stoeckert, C.J., Jr., Takada, S., and Magnuson, M.A. (2014). Insm1 promotes endocrine cell differentiation by modulating the expression of a network of genes that includes Neurog3 and Ripply3. Development *141*, 2939-2949.

Otto, S.J., McCorkle, S.R., Hover, J., Conaco, C., Han, J.J., Impey, S., Yochum, G.S., Dunn, J.J., Goodman, R.H., and Mandel, G. (2007). A new binding motif for the transcriptional repressor REST uncovers large gene networks devoted to neuronal functions. J Neurosci *27*, 6729-6739.

Petryniak, M.A., Potter, G.B., Rowitch, D.H., and Rubenstein, J.L. (2007). Dlx1 and Dlx2 control neuronal versus oligodendroglial cell fate acquisition in the developing forebrain. Neuron *55*, 417-433.

Philips, A.K., Siren, A., Avela, K., Somer, M., Peippo, M., Ahvenainen, M., Doagu, F., Arvio, M., Kaariainen, H., Van Esch, H.*, et al.* (2014). X-exome sequencing in Finnish families with intellectual disability--four novel mutations and two novel syndromic phenotypes. Orphanet J Rare Dis *9*, 49.

Porteus, M.H., Bulfone, A., Ciaranello, R.D., and Rubenstein, J.L. (1991). Isolation and characterization of a novel cDNA clone encoding a homeodomain that is developmentally regulated in the ventral forebrain. Neuron *7*, 221-229.

Qureshi, I.A., Gokhan, S., and Mehler, M.F. (2010). REST and CoREST are transcriptional and epigenetic regulators of seminal neural fate decisions. Cell Cycle *9*, 4477-4486.

Ramachandran, R., Zhao, X.F., and Goldman, D. (2012). Insm1a-mediated gene repression is essential for the formation and differentiation of Muller glia-derived progenitors in the injured retina. Nat Cell Biol *14*, 1013-1023.

Rathgen, F.G., and Schachner, M. (1984). Immunocytological and biochemical characterization of a new neuronal cell surface component (L1 antigen) which is involved in cell adhesion. EMBO J. *3*, 1-10.

Robinson, M.D., McCarthy, D.J., and Smyth, G.K. (2010). edgeR: a Bioconductor package for differential expression analysis of digital gene expression data. Bioinformatics *26*, 139-140.

Rosenbaum, J.N., Duggan, A., and Garcia-Anoveros, J. (2011). Insm1 promotes the transition of olfactory progenitors from apical and proliferative to basal, terminally dividing and neuronogenic. Neural Dev *6*, 6.

Roy, K., Kuznicki, K., Wu, Q., Sun, Z., Bock, D., Schutz, G., Vranich, N., and Monaghan, A.P. (2004). The Tlx gene regulates the timing of neurogenesis in the cortex. J Neurosci *24*, 8333-8345.

Sachewsky, N., Leeder, R., Xu, W., Rose, K.L., Yu, F., van der Kooy, D., and Morshead, C.M. (2014). Primitive neural stem cells in the adult mammalian brain give rise to GFAP-expressing neural stem cells. Stem Cell Reports *2*, 810-824.

Saez, J.E., Gomez, A.V., Barrios, A.P., Parada, G.E., Galdames, L., Gonzalez, M., and Andres, M.E. (2015). Decreased Expression of CoREST1 and CoREST2 Together with LSD1 and HDAC1/2 during Neuronal Differentiation. PLoS One *10*, e0131760.

Sakaki-Yumoto, M., Kobayashi, C., Sato, A., Fujimura, S., Matsumoto, Y., Takasato, M., Kodama, T., Aburatani, H., Asashima, M., Yoshida, N.*, et al.* (2006). The murine homolog of SALL4, a causative gene in Okihiro syndrome, is essential for embryonic stem cell proliferation, and cooperates with Sall1 in anorectal, heart, brain and kidney development. Development *133*, 3005-3013.

Sakamoto, M., Hirata, H., Ohtsuka, T., Bessho, Y., and Kageyama, R. (2003). The basic helix-loop-helix genes Hesr1/Hey1 and Hesr2/Hey2 regulate

maintenance of neural precursor cells in the brain. J Biol Chem *278*, 44808-44815.

Saleque, S., Kim, J., Rooke, H.M., and Orkin, S.H. (2007). Epigenetic regulation of hematopoietic differentiation by Gfi-1 and Gfi-1b is mediated by the cofactors CoREST and LSD1. Mol Cell *27*, 562-572.

Sanes, D.H., Reh, T.A., and Harris, W.A. (2006). Development of the nervous system, 2nd edn (Amsterdam ; Boston: Elsevier).

Scheer, M.P., van der Maarel, S., Kubart, S., Schulz, A., Wirth, J., Schweiger, S., Ropers, H., and Nothwang, H.G. (2000). DXS6673E encodes a predominantly nuclear protein, and its mouse ortholog DXHXS6673E is alternatively spliced in a developmental- and tissue-specific manner. Genomics *63*, 123-132.

Schoenherr, C.J., and Anderson, D.J. (1995). The neuron-restrictive silencer factor (NRSF): a coordinate repressor of multiple neuron-specific genes. Science *267*, 1360-1363.

Sciavolino, P.J., Abrams, E.W., Yang, L., Austenberg, L.P., Shen, M.M., and Abate-Shen, C. (1997). Tissue-specific expression of murine Nkx3.1 in the male urogenital system. Dev Dyn *209*, 127-138.

Shen, J., and Walsh, C.A. (2005). Targeted disruption of Tgif, the mouse ortholog of a human holoprosencephaly gene, does not result in holoprosencephaly in mice. Mol Cell Biol *25*, 3639-3647.

Shi, Y., Lan, F., Matson, C., Mulligan, P., Whetstine, J.R., Cole, P.A., Casero, R.A., and Shi, Y. (2004). Histone demethylation mediated by the nuclear amine oxidase homolog LSD1. Cell *119*, 941-953.

Shi, Y.J., Matson, C., Lan, F., Iwase, S., Baba, T., and Shi, Y. (2005). Regulation of LSD1 histone demethylase activity by its associated factors. Mol Cell *19*, 857-864.

Shimojo, H., Ohtsuka, T., and Kageyama, R. (2011). Dynamic expression of notch signaling genes in neural stem/progenitor cells. Front Neurosci *5*, 78.

Singh, S., Howell, D., Trivedi, N., Kessler, K., Ong, T., Rosmaninho, P., Raposo, A.A., Robinson, G., Roussel, M.F., Castro, D.S.*, et al.* (2016). Zeb1 controls neuron differentiation and germinal zone exit by a mesenchymal-epithelial-like transition. Elife *5*.

Stenman, J.M., Wang, B., and Campbell, K. (2003). Tlx controls proliferation and patterning of lateral telencephalic progenitor domains. J Neurosci *23*, 10568-10576.

Su, X., Kameoka, S., Lentz, S., and Majumder, S. (2004). Activation of REST/NRSF target genes in neural stem cells is sufficient to cause neuronal differentiation. Mol Cell Biol *24*, 8018-8025.

Sun, G., Alzayady, K., Stewart, R., Ye, P., Yang, S., Li, W., and Shi, Y. (2010). Histone demethylase LSD1 regulates neural stem cell proliferation. Mol Cell Biol *30*, 1997-2005.

Tognatta, R., and Miller, R.H. (2016). Contribution of the oligodendrocyte lineage to CNS repair and neurodegenerative pathologies. Neuropharmacology *110*, 539-547.

Tontsch, S., Zach, O., and Bauer, H.C. (2001). Identification and localization of M-CoREST (1A13), a mouse homologue of the human transcriptional co-repressor CoREST, in the developing mouse CNS. Mech Dev *108*, 165-169.

Toresson, H., Potter, S.S., and Campbell, K. (2000). Genetic control of dorsal-ventral identity in the telencephalon: opposing roles for Pax6 and Gsh2. Development *127*, 4361-4371.

Tortorici, M., Borrello, M.T., Tardugno, M., Chiarelli, L.R., Pilotto, S., Ciossani, G., Vellore, N.A., Bailey, S.G., Cowan, J., O'Connell, M.*, et al.* (2013). Protein recognition by short peptide reversible inhibitors of the chromatin-modifying LSD1/CoREST lysine demethylase. ACS Chem Biol *8*, 1677-1682.

Towbin, H., Staehelin, T., and Gordon, J. (1979). Electrophoretic transfer of proteins from polyacrylamide gels to nitrocellulose sheets: procedure and some applications. Proc Natl Acad Sci U S A *76*, 4350-4354.

Tronche, F., Kellendonk, C., Kretz, O., Gass, P., Anlag, K., Orban, P.C., Bock, R., Klein, R., and Schutz, G. (1999). Disruption of the glucocorticoid receptor gene in the nervous system results in reduced anxiety. Nat Genet *23*, 99-103.

Tuoc, T.C., Boretius, S., Sansom, S.N., Pitulescu, M.E., Frahm, J., Livesey, F.J., and Stoykova, A. (2013). Chromatin regulation by BAF170 controls cerebral cortical size and thickness. Dev Cell *25*, 256-269.

UniProt UniProtKB - Q8C796 (RCOR2_MOUSE).

UniProt UniProtKB - Q8CFE3 (RCOR1_MOUSE).

Upadhyay, G., Chowdhury, A.H., Vaidyanathan, B., Kim, D., and Saleque, S. (2014). Antagonistic actions of Rcor proteins regulate LSD1 activity and cellular differentiation. Proc Natl Acad Sci U S A *111*, 8071-8076.

Vicent, G.P., Nacht, A.S., Zaurin, R., Font-Mateu, J., Soronellas, D., Le Dily, F., Reyes, D., and Beato, M. (2013). Unliganded progesterone receptor-mediated targeting of an RNA-containing repressive complex silences a subset of hormone-inducible genes. Genes Dev *27*, 1179-1197.

Vink, M., Kahn, R.S., Raemaekers, M., van den Heuvel, M., Boersma, M., and Ramsey, N.F. (2005). Function of striatum beyond inhibition and execution of motor responses. Hum Brain Mapp *25*, 336-344.

Walker, F.O. (2007). Huntington's disease. Lancet *369*, 218-228.

Wang, J., Scully, K., Zhu, X., Cai, L., Zhang, J., Prefontaine, G.G., Krones, A., Ohgi, K.A., Zhu, P., Garcia-Bassets, I.*, et al.* (2007). Opposing LSD1 complexes function in developmental gene activation and repression programmes. Nature *446*, 882-887.

Wang, J., Telese, F., Tan, Y., Li, W., Jin, C., He, X., Basnet, H., Ma, Q., Merkurjev, D., Zhu, X.*, et al.* (2015). LSD1n is an H4K20 demethylase regulating memory formation via transcriptional elongation control. Nat Neurosci *18*, 1256-1264.

Wang, Y., Wu, Q., Yang, P., Wang, C., Liu, J., Ding, W., Liu, W., Bai, Y., Yang, Y., Wang, H.*, et al.* (2016). LSD1 co-repressor Rcor2 orchestrates neurogenesis in the developing mouse brain. Nat Commun *7*, 10481.

Wang, Z.X., Teh, C.H., Chan, C.M., Chu, C., Rossbach, M., Kunarso, G., Allapitchay, T.B., Wong, K.Y., and Stanton, L.W. (2008). The transcription factor Zfp281 controls embryonic stem cell pluripotency by direct activation and repression of target genes. Stem Cells *26*, 2791-2799.

Weber, C.M., and Henikoff, S. (2014). Histone variants: dynamic punctuation in transcription. Genes Dev *28*, 672-682.

Welcker, J.E., Hernandez-Miranda, L.R., Paul, F.E., Jia, S., Ivanov, A., Selbach, M., and Birchmeier, C. (2013). Insm1 controls development of pituitary endocrine cells and requires a SNAG domain for function and for recruitment of histone-modifying factors. Development *140*, 4947-4958.

Whyte, W.A., Bilodeau, S., Orlando, D.A., Hoke, H.A., Frampton, G.M., Foster, C.T., Cowley, S.M., and Young, R.A. (2012). Enhancer decommissioning by LSD1 during embryonic stem cell differentiation. Nature *482*, 221-225.

Wildner, H., Gierl, M.S., Strehle, M., Pla, P., and Birchmeier, C. (2008). Insm1 (IA-1) is a crucial component of the transcriptional network that controls differentiation of the sympatho-adrenal lineage. Development *135*, 473-481.

Wu, J., Duggan, A., and Chalfie, M. (2001). Inhibition of touch cell fate by egl-44 and egl-46 in C. elegans. Genes Dev *15*, 789-802.

Xiao, S., Nalabolu, S.R., Aster, J.C., Ma, J., Abruzzo, L., Jaffe, E.S., Stone, R., Weissman, S.M., Hudson, T.J., and Fletcher, J.A. (1998). FGFR1 is fused with a novel zinc-finger gene, ZNF198, in the t(8;13) leukaemia/lymphoma syndrome. Nat Genet *18*, 84-87.

Yager, L.M., Garcia, A.F., Wunsch, A.M., and Ferguson, S.M. (2015). The ins and outs of the striatum: role in drug addiction. Neuroscience *301*, 529-541.

Yang, M., Gocke, C.B., Luo, X., Borek, D., Tomchick, D.R., Machius, M., Otwinowski, Z., and Yu, H. (2006). Structural basis for CoREST-dependent demethylation of nucleosomes by the human LSD1 histone demethylase. Mol Cell *23*, 377-387.

Yang, P., Wang, Y., Chen, J., Li, H., Kang, L., Zhang, Y., Chen, S., Zhu, B., and Gao, S. (2011). RCOR2 is a subunit of the LSD1 complex that regulates ESC property and substitutes for SOX2 in reprogramming somatic cells to pluripotency. Stem Cells *29*, 791-801.

Yao, H. (2014). Critical roles for the co-repressor, RCOR1, in lineage determination. In Department of Cell and Developmental Biology (Oregon Health & Science University).

Yao, H., Goldman, D.C., Nechiporuk, T., Kawane, S., McWeeney, S.K., Tyner, J.W., Fan, G., Kerenyi, M.A., Orkin, S.H., Fleming, W.H.*, et al.* (2014). Corepressor Rcor1 is essential for murine erythropoiesis. Blood *123*, 3175-3184.

Ying, G., Wu, S., Hou, R., Huang, W., Capecchi, M.R., and Wu, Q. (2009). The protocadherin gene Celsr3 is required for interneuron migration in the mouse forebrain. Mol Cell Biol *29*, 3045-3061.

You, A., Tong, J.K., Grozinger, C.M., and Schreiber, S.L. (2001). CoREST is an integral component of the CoREST- human histone deacetylase complex. Proc Natl Acad Sci U S A *98*, 1454-1458.

Yu, H.B., Johnson, R., Kunarso, G., and Stanton, L.W. (2011). Coassembly of REST and its cofactors at sites of gene repression in embryonic stem cells. Genome Res *21*, 1284-1293.

Yun, K., Garel, S., Fischman, S., and Rubenstein, J.L. (2003). Patterning of the lateral ganglionic eminence by the Gsh1 and Gsh2 homeobox genes regulates striatal and olfactory bulb histogenesis and the growth of axons through the basal ganglia. J Comp Neurol *461*, 151-165.

Yun, K., Potter, S., and Rubenstein, J.L. (2001). Gsh2 and Pax6 play complementary roles in dorsoventral patterning of the mammalian telencephalon. Development *128*, 193-205.

Zander, M.A., Cancino, G.I., Gridley, T., Kaplan, D.R., and Miller, F.D. (2014). The Snail transcription factor regulates the numbers of neural precursor cells and newborn neurons throughout mammalian life. PLoS One *9*, e104767.

Zeng, W., Kong, Q., Li, C., and Mao, B. (2010). Xenopus RCOR2 (REST corepressor 2) interacts with ZMYND8, which is involved in neural differentiation. Biochem Biophys Res Commun *394*, 1024-1029.

Zhang, F., Xu, D., Yuan, L., Sun, Y., and Xu, Z. (2014a). Epigenetic regulation of Atrophin1 by lysine-specific demethylase 1 is required for cortical progenitor maintenance. Nat Commun *5*, 5815.

Zhang, J., Bonasio, R., Strino, F., Kluger, Y., Holloway, J.K., Modzelewski, A.J., Cohen, P.E., and Reinberg, D. (2013). SFMBT1 functions with LSD1 to regulate expression of canonical histone genes and chromatin-related factors. Genes Dev *27*, 749-766.

Zhang, T., Liu, W.D., Saunee, N.A., Breslin, M.B., and Lan, M.S. (2009). Zinc finger transcription factor INSM1 interrupts cyclin D1 and CDK4 binding and induces cell cycle arrest. J Biol Chem *284*, 5574-5581.

Zhang, Y., Chen, K., Sloan, S.A., Bennett, M.L., Scholze, A.R., O'Keeffe, S., Phatnani, H.P., Guarnieri, P., Caneda, C., Ruderisch, N.*, et al.* (2014b). An RNA-

sequencing transcriptome and splicing database of glia, neurons, and vascular cells of the cerebral cortex. J Neurosci *34*, 11929-11947.